

The Eccentric Kozai-Lidov Effect and Its Applications

Smadar Naoz

Department of Physics and Astronomy, University of California, Los Angeles, CA 90095, USA;
snaoz@astro.ucla.edu

Annu. Rev. in Astronomy & Astrophysics
2016. AA:1–59
Copyright © 2016 by Annual Reviews.
All rights reserved

Keywords

Dynamics, binaries, triples, exoplanets, stellar systems, black holes

Abstract

The hierarchical triple body approximation has useful applications to a variety of systems from planetary and stellar scales to supermassive black holes. In this approximation, the energy of each orbit is separately conserved and therefore the two semi-major axes are constants. On timescales much larger than the orbital periods, the orbits exchange angular momentum which leads to eccentricity and orientation (i.e., inclination) oscillations. The orbits' eccentricity can reach extreme values leading to a nearly radial motion, which can further evolve into short orbit periods and merging binaries. Furthermore, the orbits' mutual inclination may change dramatically from pure prograde to pure retrograde leading to misalignment and a wide range of inclinations. This dynamical behavior is coined as the “eccentric Kozai-Lidov” mechanism. The behavior of such a system is exciting, rich and chaotic in nature. Furthermore, these dynamics are accessible from a large part of the triple body parameter space and can be applied to diverse range of astrophysical settings and used to gain insights to many puzzles.

Contents

1. Introduction	2
2. The hierarchical three body secular approximation	4
2.1. Physical picture	8
2.2. Circular outer body	8
2.3. Eccentric outer orbit	12
3. The validity of the approximation and the stability of the system	21
4. Short range forces and other astrophysical effects	24
4.1. General Relativity	24
4.2. Tides and rotation	27
5. Applications	30
5.1. Solar system	30
5.2. Planetary systems	32
5.3. Stellar systems	37
5.4. Compact objects	42
6. Beyond the three body secular approximation	44
7. Summary	44
8. Supplemental Material - The secular equations	45
9. Supplemental Material - Static tides equations	48

1. Introduction

Triple systems are common in the Universe. They are found in many different astrophysical settings covering a large range of mass and physical scales, such as triple stars (e.g., Tokovinin 1997; Eggleton et al. 2007; Tokovinin 2014b,a), and accreting compact binaries with a companion (such as companions to X-ray binaries e.g., Grindlay et al. 1988; Prodan and Murray 2012). In addition, it seems that supermassive black hole binaries and higher multiples are common and thus, any star in their vicinity forms a triple system (e.g., Valtonen 1996; Di Matteo et al. 2005; Khan et al. 2012; Kulkarni and Loeb 2012). Furthermore, considering the solar system, binaries composed of near earth objects, asteroids or dwarf planets (for which a substantial fraction seems to reside in a binary configuration, e.g., Polishook and Brosch 2006; Nesvorný et al. 2011; Margot et al. 2015) naturally form a triple system with our Sun. Lastly, it was shown that Hot Jupiters are likely to have a far away companion, forming a triple system of star-Hot Jupiter binary with a distant perturber (e.g., Knutson et al. 2014; Ngo et al. 2015; Wang et al. 2015). Stability requirements yield that most of these systems will be hierarchical in scale, with a tight inner binary orbited by a tertiary on a wider orbit, forming the outer binary. Therefore, in most cases the dynamical behavior of these systems takes place on timescales much longer than the orbital periods.

The study of secular perturbations (i.e., long term phase average evolution over timescales longer than the orbital periods) in triple systems can be dated back to Lagrange, Laplace and Poincare. Many years later, the study of secular *hierarchical* triple system was addressed by Lidov (1961, where the English translation version was published only in 1962). He studied the orbital evolution of artificial satellites due to gravitational perturbations from an axisymmetric outer potential. Short time after that, Kozai (1962) studied the effects of Jupiter’s gravitational perturbations on an inclined asteroid in our own solar system. In these settings a relatively tight inner binary composed of a primary

and a secondary (in these initial studies assumed to be a test particle), is orbited by a far away companion. We denote the inner (outer) orbit semi-major axis as a_1 (a_2). In this setting the secular approximation can be utilized. This implies that the energy of each orbit is conserved separately (as well as the energy of the entire system), thus a_1 and a_2 are constants during the evolution. The dynamical behavior is a result of angular momentum exchange between the two orbits. Kozai (1962), for example, expanded the 3-body Hamiltonian in semi-major axis ratio (since the outer orbit is far away, a_1/a_2 is a small parameter). He then averaged over the orbits and lastly truncated the expansion to the lowest order, called the quadrupole, which is proportional to $(a_1/a_2)^2$. Both Kozai (1962) and Lidov (1962) found that the inner test particle inclination and eccentricity oscillate on timescales much larger than its orbital period. In these studies the outer perturber was assumed to carry most of the angular momentum, and thus under the assumption of an axisymmetric outer potential the inner and outer orbits z-component of the angular momenta (along the total angular momentum) are conserved. This led to large variations between the eccentricity and inclination of the test particle orbit.

While the Kozai-Lidov¹ mechanism seemed interesting it was largely ignored for many years. However, about 15-20 years ago, probably correlating with the detection of the eccentric planet 6 Cyg B, (Cochran et al. 1996), or the close to perpendicular stellar Algol system (Eggleton et al. 1998; Baron et al. 2012), the Kozai-Lidov mechanism received its deserved attention. However, while the mechanism seemed very promising in addressing these astrophysical phenomena, it was limited to a narrow parts of the parameter space (favoring close to perpendicular initial orientation between the two orbits, e.g., Marchal 1990; Morbidelli 2002; Valtonen and Karttunen 2006; Fabrycky and Tremaine 2007) and produced only moderate eccentricity excitations. Most of the studies that investigated different astrophysical applications of the Kozai-Lidov mechanism used the Kozai (1962) and Lidov (1962) test particle, axisymmetric outer orbit quadrupole-level approximation.

This approximation has an analytical solution which describes (for initially highly inclined orbits $\sim 40^\circ - 140^\circ$, see below) the large amplitude oscillations between the inner orbit's eccentricity and inclination with respect to the outer orbit (e.g., Kinoshita and Nakai 1999; Morbidelli 2002). These oscillations have a well defined maximum and minimum eccentricity and inclination and limits the motion to either prograde ($\leq 90^\circ$) or retrograde ($\geq 90^\circ$) with respect to the outer orbit. The axisymmetric outer orbit quadrupole-level approximation is applicable for an ample amount of systems. For example, this approximation has appropriately described the motion of Earth's artificial satellites under the influence of gravitational perturbations from the moon (e.g Lidov 1962). Other astrophysical systems for which this approximation is applicable include (but are not limited to) the effects of the Sun's gravitational perturbation on planetary satellites, since in this case indeed the satellite mass is negligible compared to the other masses in the system, and the planet's orbit around the Sun is circular. Indeed it was shown that the axisymmetric outer orbit quadrupole-level approximation can successfully be used to study the inclination distribution of the Jovian irregular satellites (e.g., Carruba et al. 2002; Nesvorný et al. 2003) or in general the survival of planetary outer satellites (e.g., Kinoshita and Nakai 1991), as well as the dynamical evolution of the orbit of a Kuiper Belt object satellite due to perturbation from the sun (e.g., Perets and Naoz 2009; Naoz et al. 2010). Indeed this approximation is useful and can be applied in the limit of a circular outer orbit and a test

¹Although Lidov has published his work first, we are using here the alphabetical order for the name of the mechanism.

particle inner object.

Recently, Naoz et al. (2011, 2013a) showed that relaxing either one of these assumptions leads to qualitative different dynamical evolution. Considering systems beyond the test particle approximation, or a circular orbit, requires the next level of approximation, called the octupole-level of approximation (e.g. Harrington 1968, 1969; Ford et al. 2000b; Blaes et al. 2002). This level of approximation is proportional to $(a_1/a_2)^3$. In the octupole-level of approximation, the inner orbit eccentricity can reach extremely high values, and does not have a well defined value, as the system is chaotic in general (Ford et al. 2000b; Naoz et al. 2013a; Li et al. 2014b,a; Teyssandier et al. 2013). In addition, the inner orbit inclination can flip its orientation from prograde, with respect to the total angular momentum, to retrograde (Naoz et al. 2011). We refer to this process as the **eccentric Kozai-Lidov** (EKL) mechanism. We note that here we follow the literature coined acronym “EKL” as oppose to the more chronologically accurate acronym “ELK.”

As will be discussed below the EKL mechanism taps into larger parts of the parameter space (i.e., beyond the $\sim 40^\circ - 140^\circ$ range), and results in a richer and far more exciting dynamical evolution. As a consequence this mechanism is applicable to a wide range of systems that allow for eccentric orbits, or three massive bodies, from exoplanetary orbits over stellar interactions to black hole dynamics. The prospect of forming eccentric or short period planets through three body interactions was the source of many studies (e.g., Innanen et al. 1997; Wu and Murray 2003; Fabrycky and Tremaine 2007; Wu et al. 2007; Veras and Ford 2010; Correia et al. 2011; Batygin et al. 2011; Naoz et al. 2011, 2012; Petrovich 2015b,a). It also promoted many interesting application for stellar dynamics from stellar mergers (e.g., Perets and Fabrycky 2009; Naoz and Fabrycky 2014; Witzel et al. 2014; Stephan et al. 2016) to compact binary merger which may prompt supernova explosions for double white dwarf merger (e.g., Thompson 2011; Katz and Dong 2012), or gravitational wave emission for neutron star or black hole binary merger (e.g., Blaes et al. 2002; Seto 2013).

2. The hierarchical three body secular approximation

In the three-body approximation, dynamical stability requires that either the system has circular, concentric, coplanar orbits or a hierarchical configuration, in which the *inner binary* is orbited by a third body on a much wider orbit, the *outer binary* (Figure 1). In this case the secular approximation (i.e., phase averaged, long term evolution) can be applied, where the interactions between two non-resonant orbits is equivalent to treating the two orbits as massive wires (e.g., Marchal 1990). Here the line-density is inversely proportional to orbital velocity and the two orbits torque each other and exchange angular momentum, but not energy. Therefore the orbits can change shape and orientation (on timescales much longer than their orbital periods), but not semi-major axes of the orbits. The gravitational potential is then expanded in semi-major axis ratio of a_1/a_2 , where a_1 (a_2) is the semi-major axis of the inner (outer) body (Kozai 1962; Lidov 1962). This ratio is a small parameter due to the hierarchical configuration.

The hierarchical three body system consists of a tight binary (m_1 and m_2) and a third body (m_3). We define \mathbf{r}_{in} to be the relative position vector from m_1 to m_2 and \mathbf{r}_{out} the position vector of m_3 relative to the center of mass of the inner binary (see fig. 1). Using this coordinate system the dominant motion of the triple can be reduced into two separate Keplerian orbits: the first describing the relative tight orbit of bodies 1 and 2, and the second describes the wide orbit of body 3 around the center of mass of bodies 1

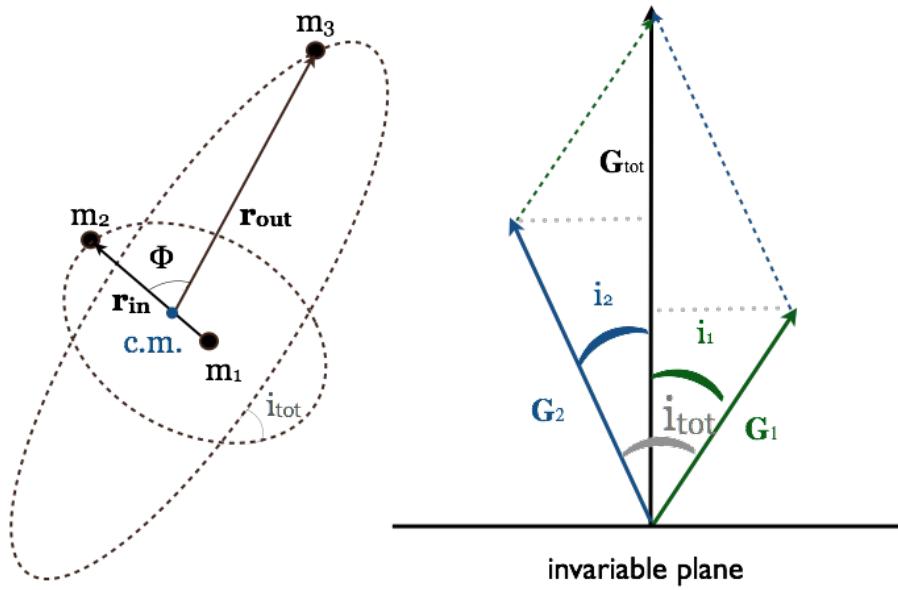


Figure 1

Schematic description of the coordinate system and the angles used (not to scale).

Left: The three bodies and the relative vectors. Here 'c.m.' denotes the center of mass of the inner binary, containing objects of masses m_1 and m_2 . The separation vector \mathbf{r}_in points from m_1 to m_2 ; \mathbf{r}_out points from 'c.m.' to m_3 . The angle between the vectors \mathbf{r}_in and \mathbf{r}_out is Φ . Right: Geometry of the angular momentum vectors and the definition of the relevant inclination angles. We show the total angular momentum vector (\mathbf{G}_tot), the angular momentum vector of the inner orbit (\mathbf{G}_1) with inclination i_1 with respect to \mathbf{G}_tot and the angular momentum vector of the outer orbit (\mathbf{G}_2) with inclination i_2 with respect to \mathbf{G}_tot . The angle between \mathbf{G}_1 and \mathbf{G}_2 defines the mutual inclination $i_\text{tot} = i_1 + i_2$. The invariable plane is perpendicular to \mathbf{G}_tot , in other words the z axis is parallel to \mathbf{G}_tot .

and 2. The Hamiltonian for the system can be decomposed accordingly into two Keplerian Hamiltonians plus a coupling term that describes the (weak) interaction between the two orbits. Let the semi-major axes (SMAs) of the inner and outer orbits be a_1 and a_2 , respectively. Then the coupling term in the complete Hamiltonian can be written as a power series in the ratio of the semi-major axes $\alpha = a_1/a_2$ (e.g., Harrington 1968). In a hierarchical system, by definition, this parameter α is small.

The complete Hamiltonian expanded in orders of α is (e.g., Harrington 1968),

$$\mathcal{H} = \frac{k^2 m_1 m_2}{2a_1} + \frac{k^2 m_3 (m_1 + m_2)}{2a_2} + \frac{k^2}{r_2} \sum_{n=2}^{n=\infty} \left(\frac{r_\text{in}}{r_\text{out}} \right)^n M_n P_n(\cos \Phi) \quad (1)$$

and in terms of the semi-major axes a_1 and a_2 :

$$\mathcal{H} = \frac{k^2 m_1 m_2}{2a_1} + \frac{k^2 m_3 (m_1 + m_2)}{2a_2} + \frac{k^2}{a_2} \sum_{n=2}^{\infty} \left(\frac{a_1}{a_2} \right)^n M_n \left(\frac{r_1}{a_1} \right)^n \left(\frac{a_2}{r_2} \right)^{n+1} P_n(\cos \Phi) \quad (2)$$

where k^2 is the gravitational constant, P_n are Legendre polynomials, Φ is the angle between

\mathbf{r}_{in} and \mathbf{r}_{out} (see Figure 1) and

$$M_n = m_1 m_2 m_3 \frac{m_1^{n-1} - (-m_2)^{n-1}}{(m_1 + m_2)^n} . \quad (3)$$

The right term is often called the perturbing function as it describes the gravitational perturbations between the two orbits. The left two terms in Equation (2) are simply the energy of the inner and outer Kepler orbits. Note that the sign convention for this Hamiltonian is positive .

The frame of reference chosen throughout this review is the *invariable plane* for which the z axis is set along the total angular momentum, which is conserved during the secular evolution of the system (see figure 1), (e.g., Lidov and Ziglin 1974). Another description used in the literature is the vectorial form (e.g. Katz et al. 2011; Boué and Fabrycky 2014a), which has been proven to be useful to address different astrophysical setting. Considering the invariable plane it is convenient to adopt the canonical variables known as Delaunay’s elements, (e.g. Valtonen and Karttunen 2006). These describe for each orbit three angles and three conjugate momenta.

The first set of angles are the mean anomalies, M_1 and M_2 (also often denote in the literature as l_1 and l_2), which describes the position of the object in their orbit. Their conjugate momenta are:

$$\begin{aligned} L_1 &= \frac{m_1 m_2}{m_1 + m_2} \sqrt{k^2 (m_1 + m_2) a_1} , \\ L_2 &= \frac{m_3 (m_1 + m_2)}{m_1 + m_2 + m_3} \sqrt{k^2 (m_1 + m_2 + m_3) a_2} , \end{aligned} \quad (4)$$

where subscripts 1, 2 denote the inner and outer orbits, respectively. The second set of angles are the arguments of periastron, ω_1 and ω_2 (g_1 and g_2), which describes the position of the eccentricity vector (in the plane of the ellipse). Their conjugate momenta are the magnitude of the angular momenta vector of each orbit G_1 and G_2 (often used as J_1 and J_2):

$$G_1 = L_1 \sqrt{1 - e_1^2} , \quad G_2 = L_2 \sqrt{1 - e_2^2} , \quad (5)$$

where e_1 (e_2) is the inner (outer) orbit eccentricity. The last set of angles are the longitudes of ascending nodes, Ω_1 and Ω_2 (h_1 and h_2). Their conjugate momenta are

$$H_1 = G_1 \cos i_1 , \quad H_2 = G_2 \cos i_2 , \quad (6)$$

(often denote as $J_{1,z}$ and $J_{2,z}$). Note that G_1 and G_2 are the magnitudes of the angular momentum vectors (\mathbf{G}_1 and \mathbf{G}_2), and H_1 and H_2 are the z -components of these vectors, (recall that the z -axis is chosen to be along the total angular momentum \mathbf{G}_{tot}). In Figure 1 we show the configuration of the angular momentum vectors of the inner and outer orbit (\mathbf{G}_1 and \mathbf{G}_2 , respectively) and H_1 and H_2 are the z -components of these vectors, where the z -axis is chosen to be along the total angular momentum \mathbf{G}_{tot} . This conservation of the total angular momentum G_{tot} yields a simple relation between the z component of the angular momenta and the total angular momentum magnitude:

$$G_{\text{tot}} = H_1 + H_2 . \quad (7)$$

The equations of motion are given by the canonical relations (for these equations we will use the l, g, h notation):

$$\frac{dL_j}{dt} = \frac{\partial \mathcal{H}}{\partial l_j} , \quad \frac{dl_j}{dt} = - \frac{\partial \mathcal{H}}{\partial L_j} , \quad (8)$$

$$\frac{dG_j}{dt} = \frac{\partial \mathcal{H}}{\partial g_j}, \quad \frac{dg_j}{dt} = -\frac{\partial \mathcal{H}}{\partial G_j}, \quad (9)$$

$$\frac{dH_j}{dt} = \frac{\partial \mathcal{H}}{\partial h_j}, \quad \frac{dh_j}{dt} = -\frac{\partial \mathcal{H}}{\partial H_j}, \quad (10)$$

where $j = 1, 2$. Note that these canonical relations have the opposite sign relative to the usual relations (e.g., Goldstein 1950) because of the sign convention typically chosen for this Hamiltonian.

As apparent from the Hamiltonian Eq. (2), if the semi-major axis ratio is indeed a small parameter then for the zeroth approximation each orbit can be described as a Keplerian orbit, for which its energy is conserved. Thus, we can average over the short timescale and focus on the long-term dynamics of the triple system. This process is known as the *secular approximation*, where the energy (semi-major axis) is conserved and the orbits exchange angular momentum. The short timescales terms in the Hamiltonian depend on l_1 and l_2 , and eliminating them needs to be done via a canonical transformation. The technique used is known as the Von Zeipel transformation (Brouwer 1959). In this canonical transformation, a time independent generating function is defined to be periodic in l_1 and l_2 , which allows the elimination of the short-period terms in the Hamiltonian and the details of this procedure are described in Naoz et al. (2013a) Appendix A2. Eliminating these angles from the Hamiltonian yields that their conjugate momenta L_1 and L_2 are conserved [see Eq. (8)], thus yielding $a_1 = \text{Const.}$ and $a_2 = \text{Const.}$, as expected. In the most general case of this three body secular approximation there are only two parameters which are conserved, i.e., the energy of the system (which also means that the energy of the inner and the outer orbits are conserved separately), and the total angular momentum G_{tot} .

The time evolution for the eccentricity and inclination of the system can be easily achieved from Equations (8)-(10)

$$\frac{de_j}{dt} = \frac{\partial e_j}{\partial G_j} \frac{\partial \mathcal{H}}{\partial g_j}, \quad (11)$$

and

$$\frac{d(\cos i_j)}{dt} = \frac{\dot{H}_j}{G_j} - \frac{\dot{G}_j}{G_j} \cos i_j, \quad (12)$$

where $j = 1, 2$ for the inner and outer orbit. See full set of equations of motions in Equations (73)-(84).

The lowest order of approximation, which is proportional to $(a_1/a_2)^2$ is called *quadrupole* level, and we find that an artifact of the averaging process results in conservation of the outer orbit angular momentum G_2 , in other words the system is symmetric for the rotation of the outer orbit. This was coined as the “happy coincidence” by Lidov and Ziglin (1976). Its significant consequence is that this approximation should be *only* used for an axisymmetric outer potential such as circular outer orbits (Naoz et al. 2013a).

The next level of approximation, the octupole, is proportional to $(a_1/a_2)e_2/(1-e_2^2)$ (see below) and thus the TPQ approximation can be successfully applied when this parameter is small for low inclinations (see below for numerical studies). However, close to perpendicular systems are extremely sensitive to this parameter.

A popular procedure which was done in earlier studies (e.g., Kozai 1962) used the “elimination of nodes” (e.g., Jefferys and Moser 1966). This describes the a simplification of the Hamiltonian by setting

$$h_1 - h_2 = \pi. \quad (13)$$

This relation holds in the invariable plane when the total angular momentum is conserved, such as in our case. Some studies that exploited explicitly this relation in the Hamiltonian incorrectly concluded [using Equation (10)] that the z -components of the orbital angular momenta are always constant. As showed in Naoz et al. (2011, 2013a), this leads to qualitatively different evolution for the triple body system. We can still use the Hamiltonian with the nodes eliminated as long as the equations of motions for the inclinations are derived from the total angular momentum conservation, instead of using the canonical relations (Naoz et al. 2013a).

2.1. Physical picture

Considering the quadrupole level of approximation (which is valid for axisymmetric outer orbit potential) for an inner test particle (either m_1 or m_2 goes to zero) the conserved quantities are the energy and the z -component of the angular momentum. In other words the Hamiltonian does not depend on longitude of ascending nodes (h_1) and thus the z -component of the inner orbit angular momentum, H_1 , is conserved and the system is integrable. In this case the equal precession rate of the inner orbit's longitude of ascending nodes (Ω_1) and the longitude of the periapsis ($\varpi = \Omega_1 + \omega_1$) means that an eccentric inner orbit feels an accumulating effect on the orbit. The the resonant angle $\omega_1 = \varpi_1 - \Omega_1$, will librate around 0° or 180° which cause large amplitude eccentricity oscillations of the inner orbit.

In that case (circular outer orbit, in the test particle approximation) the conservation of the z component of the angular momentum $j_z = \sqrt{1 - e_1^2} \cos i_{\text{tot}} = \text{Const.}$ yields oscillations between the eccentricity and inclination. The inner orbit will be more eccentric for smaller inclinations and less eccentric for larger inclinations.

2.2. Circular outer body

In this case the gravitational potential set by the outer orbit is axisymmetric, and thus the quadrupole level of approximation describes the behavior of the hierarchical system well. We will consider two possibility, in the first one of the members of the inner orbit is a test particle, (i.e., either m_1 or m_2 are zero). In the second we will allow for all three masses to be non-negligible.

2.2.1. Axisymmetric Potential and Inner Test Particle - TPQ. Following Lithwick and Naoz (2011) we call this case the test particle approximation quadrupole (TPQ). Without loss of generality we take $m_2 \rightarrow 0$, the Hamiltonian of this system is very simple and can be written as:

$$\mathcal{H} = \frac{3}{8} k^2 \frac{m_1 m_3}{a_2} \left(\frac{a_1}{a_2} \right)^2 \frac{1}{(1 - e_2^2)^{3/2}} F_{\text{quad}} , \quad (14)$$

where

$$F_{\text{quad}} = -\frac{e_1^2}{2} + \theta^2 + \frac{3}{2} e_1^2 \theta^2 + \frac{5}{2} e_1^2 (1 - \theta^2) \cos(2\omega_1) , \quad (15)$$

where $\theta = \cos i_{\text{tot}}$ (e.g., Yokoyama et al. 2003; Lithwick and Naoz 2011)².

At this physical setting the octupole level of approximation is zero and the inner orbit's angular momentum along the z axis is conserved ($H_1 \propto j_{z,1} = \sqrt{1 - e_1^2} \cos i_{\text{tot}} = \text{Const.}$),

²Note that unlike the Hamiltonian that will be presented in the next section [Equation (22)] this Hamiltonian only describes the test particle approximation.

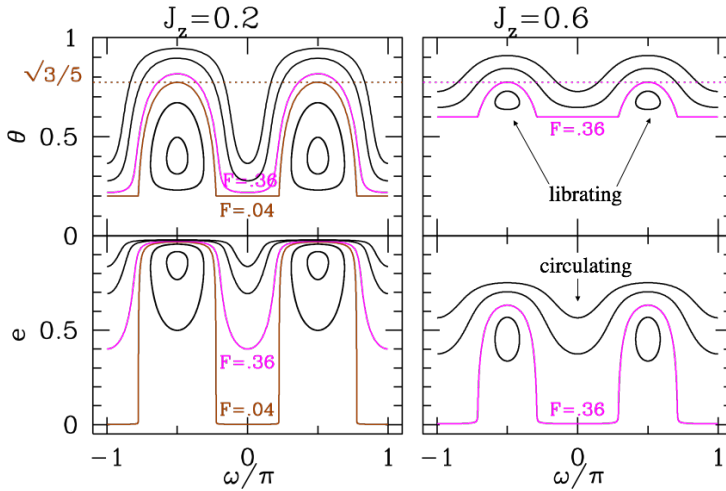


Figure 2

Cross section trajectory of the TPQ in the $\theta - \omega_1$ (top panels) and $e_1 - \omega_1$ (bottom panels) planes. We define $\theta = \cos i_{\text{tot}}$. The dashed horizontal lines in the top panels shows the critical inclination for which $\theta = \sqrt{3/5}$. The separatrix is associated with $e_1 = 0$ for $\omega_1 = 0$ and $\theta = \sqrt{3/5}$ for $\omega_1 = \pi/2$, as depicted in the Figure. *Left panels* shows the case for $J_z = 0.2$ and $F_{\text{quad}}^{\text{TP}} = -1.44$ and $-.64$ (librating) and $F_{\text{quad}}^{\text{TP}} = 0.04, 0.36, 1$ and 1.44 (circulating). *Right panels* shows the case for $J_z = 0.6$ and $F_{\text{quad}}^{\text{TP}} = 0.25$ (librating) and $F_{\text{quad}}^{\text{TP}} = 0.36, 0.64$ and 1 (circulating). Figure adopted from Lithwick and Naoz (2011).

where $j_{z,1}$ is the specific z component of the angular momentum. Since both H_1 and F_{quad} are conserved, a new constant of motion can be defined. It is convenient (for reasons that will be identified in Section 2.3.1) to define the following constant (Katz et al. 2011):

$$C_{KL} = \frac{F_{\text{quad}}}{2} - \frac{1}{2} j_{z,1}^2 = e^2 \left(1 - \frac{5}{2} \sin^2 i_{\text{tot}} \sin^2 \omega_1^2 \right), \quad (16)$$

which is a simple function of the initial conditions. The system is integrable and has a well defined maximum and minimum eccentricity and inclination. To find the extreme points we set $\dot{e}_1 = 0$ in the time evolution equation [see Equation (77), quadrupole part] and find that the values of the argument of periapsis that satisfy this condition are $\omega_1 = 0 + n\pi/2$, where $n = 0, 1, 2, \dots$. Thus, the resonant angle has two classes of trajectories, librating and circulating. On circulating trajectories, at $\omega_1 = 0$, the eccentricity is smallest and the inclination is largest, and visa versa for $\omega_1 = \pi/2$. In Figure 2, librating trajectories (or libration modes) are associated with bound oscillations of ω_1 and circulating trajectories (or circulation modes) are not constrained to a specific regime. The separatrix is the trajectory which separates the two modes of behavior, as we elaborate below.

The conservation of $j_{1,z}$ implies:

$$j_{z,1} = \sqrt{1 - e_{1,max/min}^2} \cos i_{1,min/max} = \sqrt{1 - e_{1,0}^2} \cos i_{1,0}, \quad (17)$$

where $e_{1,0}$ and $i_{1,0}$ are the initial values. Note that in this case (TPQ) $i_1 = i_{\text{tot}}$. Since the

energy is also conserved, plugging in $\omega_1 = 0$ for the circulating mode we find

$$E_0 = 2e_{1,min}^2 - 2 + (1 - e_{1,min}^2) \cos i_{max}^2, \quad (18)$$

and for $\omega_1 = \pm\pi/2$ in equation (15) we find:

$$E_0 = -3e_{1,max}^2 + (1 - 4e_{1,max}^2) \cos i_{min}^2, \quad (19)$$

where E_0 represents the initial conditions plugged in equation (15). From equations (17) and (18) one can easily find the minimum eccentricity and maximum inclination, and from equations (17) and (18) the maximum eccentricity and the minimum inclination. A special and useful case is found by setting initially $e_{1,0} = 0$ and $\omega_{1,0} = 0$, for this case the maximum eccentricity is

$$e_{max} = \sqrt{1 - \frac{5}{3} \cos^2 i_0}. \quad (20)$$

Solving the equations for $\cos i_{min}$ instead we can find

$$\cos i_{min} = \pm \sqrt{\frac{3}{5}}, \quad (21)$$

which gives $i_{min} = 39.2^\circ$ and $i_{min} = 140.77^\circ$, known as Kozai angles. These angles represent the regime where large eccentricity and inclination oscillations are expected to take place. The value $\cos i_{min} = \pm\sqrt{3/5}$ marks the seperatrix depicted in Figure 2.

2.2.2. Axisymmetric Potential Beyond the Test Particle Approximation. In this case we still keep the outer orbit circular, thus the quadrupole level of approximation still valid, but we will relax the test particle approximation. The quadrupole level hamiltonian can be written as:

$$\mathcal{H}_{quad} = C_2 \{ (2 + 3e_1^2) (3 \cos^2 i_{tot} - 1) + 15e_1^2 \sin^2 i_{tot} \cos(2\omega_1) \}, \quad (22)$$

where

$$C_2 = \frac{k^4}{16} \frac{(m_1 + m_2)^7}{(m_1 + m_2 + m_3)^3} \frac{m_3^7}{(m_1 m_2)^3} \frac{L_1^4}{L_2^3 G_2^3}. \quad (23)$$

Note that in this form of Hamiltonian the nodes (Ω_1 and Ω_2) have been eliminated, allowing for a cleaner format, however this does not mean that the z-component of the inner and outer angular momenta are constant of motion (as explained in Naoz et al. 2011, 2013a).

Relaxing the test particle approximation (i.e., none of the masses have insignificant mass) already allows for deviations from the nominal TPQ behavior. This is because now $j_{z,1}$ is no longer conserved and instead the total angular momentum is. Note that the outer potential is axisymmetric and $G_2 = \text{Const.}$ The system is still integrable and has well define maxima and minima for the eccentricity and inclination. The conservation of the total angular momentum, i.e., $\mathbf{G}_1 + \mathbf{G}_2 = \mathbf{G}_{tot}$ sets the relation between the maximum/minimum total inclination and inner orbit eccentricity.

$$L_1^2(1 - e_1^2) + 2L_1 L_2 \sqrt{1 - e_1^2} \sqrt{1 - e_2^2} \cos i_{tot} = G_{tot}^2 - G_2^2. \quad (24)$$

Note that in the quadrupole-level approximation G_2 , and thus e_2 , are constant. The right hand side of the above equation is set by the initial conditions. In addition, L_1 , and L_2 [see

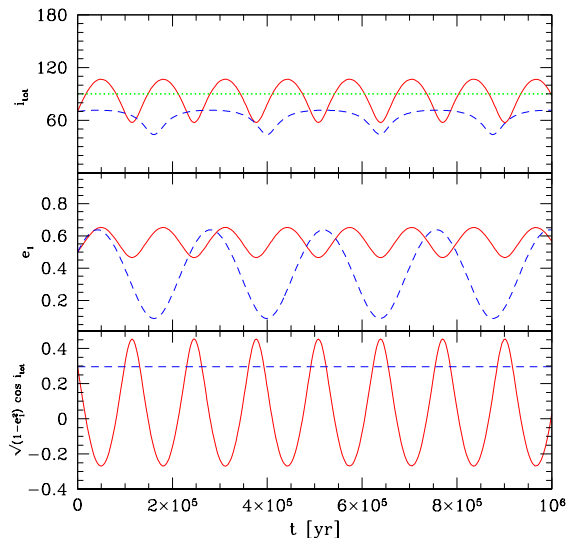


Figure 3

Comparison between the TPQ formalism (dashed blue lines) and the full quadrupole calculation (solid red lines). The system has an inner binary with $m_1 = 1.4 M_\odot$ and $m_2 = 0.3 M_\odot$, and the outer body has mass $m_3 = 0.01 M_\odot$. The orbit separations are $a_1 = 5$ AU and $a_2 = 50$ AU. The system was set initially with $e_1 = 0.5$ and $e_2 = 0$, $\omega_1 = 120^\circ$, $\omega_2 = 0$ and relative inclination $i_{\text{tot}} = 70^\circ$. The panels show from top to bottom, the mutual inclination i_{tot} , e_1 and $\sqrt{1 - e_1^2} \cos i_{\text{tot}}$, which in the TPQ formalism is constant (dashed line). Figure adopted from Naoz et al. (2013a).

eqs. (4) and (5)] are also set by the initial conditions. Using the conservation of energy we can write, for the minimum eccentricity/maximum inclination case (i.e., setting $\omega_1 = 0$)

$$\frac{\mathcal{H}_{\text{quad}}}{2C_2} = 3 \cos^2 i_{\text{tot},\text{max}} (1 - e_{1,\text{min}}^2) - 1 + 6e_{1,\text{min}}^2. \quad (25)$$

The left hand side of this equation, and the remainder of the parameters in Equation (24) are determined by the initial conditions. Thus solving equation (25) together with (24) gives the minimum eccentricity/maximum inclination during the system evolution as a function of the initial conditions. We find a similar equation if we set $\omega_1 = \pi/2$ for the maximum eccentricity/minimum inclination :

$$\frac{\mathcal{H}_{\text{quad}}}{2C_2} = 3 \cos^2 i_{\text{tot},\text{min}} (1 + 4e_{1,\text{max}}^2) - 1 - 9e_{1,\text{max}}^2. \quad (26)$$

Equations (24) and (26) give a simple relation between the total minimum inclination and the maximum inner eccentricity as a function of the initial conditions.

An interesting consequence of this physical picture is if the inner binary members are more massive than the third object. We adopt this example from Naoz et al. (2013a) and consider the triple system PSR B1620–26. The inner binary contains a millisecond radio pulsar of $m_1 = 1.4 M_\odot$ and a companion of $m_2 = 0.3 M_\odot$ (e.g., McKenna and Lyne 1988). We adopt parameters for the outer perturber of $m_3 = 0.01 M_\odot$ (Ford et al. 2000a) and

set $e_2 = 0$ (see the caption for a full description of the initial conditions). Note that Ford et al. (2000a) found $e_2 = 0.45$, which means that the quadrupole level of approximation is insufficient to represent the behavior of the system. We choose, however, to set $e_2 = 0$ to emphasize the point that even an axisymmetric outer potential may result in a qualitative different behavior if the TPQ approximation is assumed. For the same reason we also adopt a higher initial value for the inner orbit eccentricity ($e_1 = 0.5$ compared to the measured one $e_1 \sim 0.045$). The time evolution of the system is shown in Figure 3. In This Figure we compare the z-component of the angular momentum H_1 (solid red line) with $L_1 \sqrt{1 - e_1^2} \cos i_{\text{tot}}$ (dashed blue line), which is the angular momentum that would be inferred *if the outer orbit were instantaneously in the invariable plane*, as found in the TPQ formalism.

Taking the outer body to be much smaller than the inner binary (i.e., $m_3 < m_1, m_2$), as done in Figure 3, yields yet another interesting consequence for relaxing the test particle approximation. In some cases large eccentricity excitations can take place for inclinations that largely deviate from the nominal range of the Kozai angles of $39.2^\circ - 140.77^\circ$. The limiting mutual inclination that can result in large eccentricity excitations can be easily found when solving Equations (24) and (26), since they depend on mutual inclination, as noted by Martin and Triaud (2015b). This evolution is shown in Figure 4, where large eccentricity oscillation for the inner binary is achieved for an initial mutual inclination of 158° . This behavior, as expected from the Equations, is sensitive to the eccentricity of the outer orbit.

In the circular outer orbit case, the regular oscillations of the eccentricity and inclination yields a well defined associated timescale. This can be easily achieved by considering the equation of motion of the argument of periapsis ω_1 [see the part that is proportional to C_2 in Equation (73)]. More precisely, $t_{\text{quad}} \sim G_1/C_2$, where C_2 is given in Eq. (23). Integrating between the well defined maximum and minimum eccentricity Antognini (2015) found a numerical factor 16/15, and got

$$\begin{aligned} t_{\text{quad}} &\sim \frac{16}{15} \frac{a_2^3 (1 - e_2^2)^{3/2} \sqrt{m_1 + m_2}}{a_1^{3/2} m_3 k} \\ &= \frac{16}{30\pi} \frac{m_1 + m_2 + m_3}{m_3} \frac{P_2^2}{P_1} (1 - e_2^2)^{3/2}. \end{aligned} \quad (27)$$

This timescale is in a good agreement with the numerical evolution.

2.3. Eccentric outer orbit

2.3.1. Inner Orbit's Test Particle Approximation . In this approximation we will allow for an eccentric outer orbit but will restrict ourselves to take the mass of one of the inner members to zero, which yields $i_1 = i_{\text{tot}}$. In the test particle limit, the outer orbit is stationary and the system reduces to two degrees of freedom. The eccentric outer orbit yields the quadrupole level of approximation inadequate and thus we consider the test particle octupole (TPO) level here. This approximation is extremely useful in gaining an overall understanding of the general hierarchical system and the EKL mechanism. The hamiltonian H^{TP} of this system is very simple and can be written as (e.g., Lithwick and Naoz 2011),

$$\mathcal{H}^{TP} = \frac{3}{8} k^2 \frac{m_1 m_3}{a_2} \left(\frac{a_1}{a_2} \right)^2 \frac{1}{(1 - e_2^2)^{3/2}} (F_{\text{quad}} + \epsilon F_{\text{oct}}) , \quad (28)$$

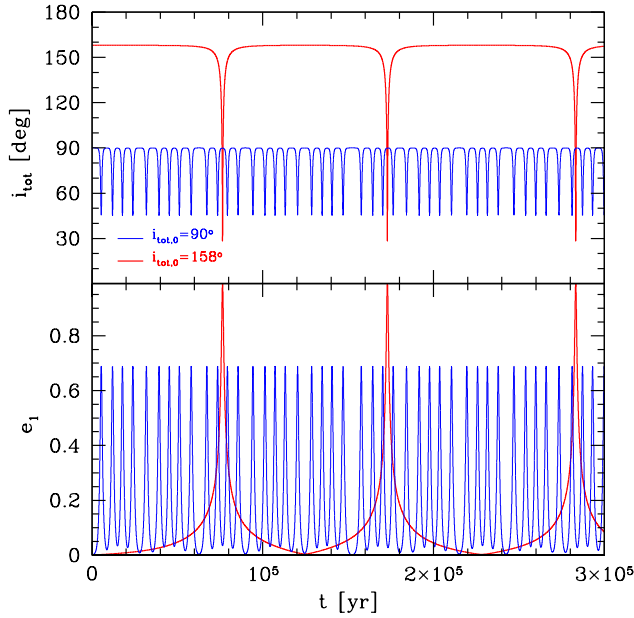


Figure 4

Small mass outer perturber that induces large eccentricity excitation away from the nominal range of the Kozai angles of $39.2^\circ - 140.77^\circ$. We consider $m_1 = 1 M_\odot$, $m_2 = 0.5 M_\odot$, $m_3 = 0.05 M_\odot$, $a_1 = 0.5 \text{ AU}$ and $a_2 = 5 \text{ AU}$. Both outer and inner eccentricities are set initially to zero, and also set initially $\omega_1 = 90^\circ$ and $\omega_2 = 0^\circ$. We show two examples, the first shows the eccentricity excitations for as expected initial mutual inclination of $i_{\text{tot}} = 90^\circ$, where in this case $i_1 = 25.01^\circ$ and $i_2 = 64.99^\circ$. This produces eccentricity excitation with $e_{1,\text{max}} = 0.689$. We also consider an example for which the mutual inclination is set initially to be $i_{\text{tot}} = 158^\circ$. In this case $i_1 = 17.12^\circ$ and $i_2 = 140.88^\circ$. The latter parameters are adopted from Martin and Triaud (2015b), which leads to maximum inner eccentricity of $e_{1,\text{max}} = 0.99$. Note that in both examples i_2 is close to the nominal Kozai angles range.

where

$$\epsilon = \frac{a_1}{a_2} \frac{e_2}{1 - e_2^2}, \quad (29)$$

F_{quad} is defined in Equation (15), and we reiterate it here for completeness,

$$F_{\text{quad}} = -\frac{e_1^2}{2} + \theta^2 + \frac{3}{2}e_1^2\theta^2 + \frac{5}{2}e_1^2(1 - \theta^2)\cos(2\omega_1), \quad (30)$$

and

$$F_{\text{oct}} = \frac{5}{16} \left(e_1 + \frac{3e_1^3}{4} \right) [(1 - 11\theta - 5\theta^2 + 15\theta^3)\cos(\omega_1 - \Omega_1) + (1 + 11\theta - 5\theta^2 - 15\theta^3)\cos(\omega_1 + \Omega_1)] \\ - \frac{175}{64} e_1^3 [(1 - \theta - \theta^2 + \theta^3)\cos(3\omega_1 - \Omega_1) + (1 + \theta - \theta^2 - \theta^3)\cos(3\omega_1 + \Omega_1)]. \quad (31)$$

In this case the z component of the outer orbit is not conserved and the system can flip from $i_{\text{tot}} < 90^\circ$ to $i_{\text{tot}} > 90^\circ$ (Naoz et al. 2011, 2013a). The flip is associated with

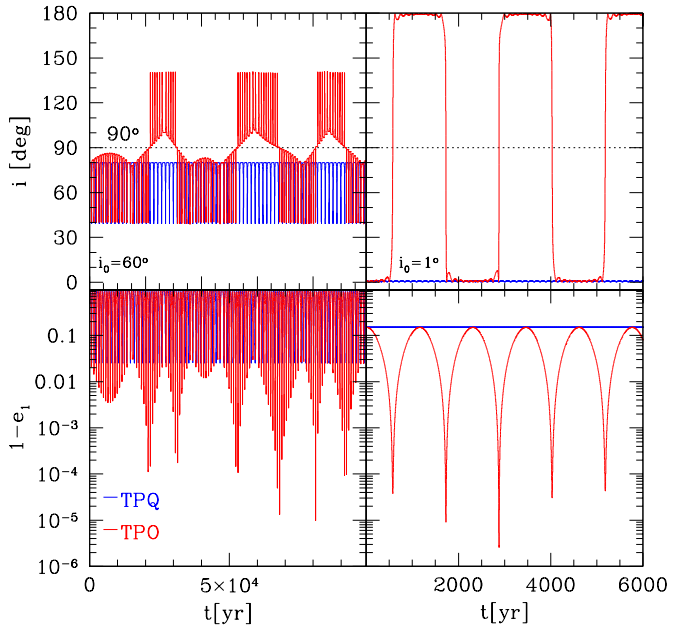


Figure 5

Time evolution example of the TPO (test partial octupole) approximation (red lines) and the TPQ (test particle quadrupole) approximation (blue lines). *Left panels* show high inclination flip while the *right panels* show the low inclination flip (see text). In this example we consider the time evolution of a test particle at 135 AU around a $10^4 M_{\odot}$ intermediate black hole located 0.03 pc from the massive black hole in the center of our galaxy ($4 \times 10^6 M_{\odot}$). In the left panels the system is initially set with $e_1 = 0.01$, $e_2 = 0.7$, $i = 60^\circ$, $\Omega_1 = 60^\circ$ and $\omega_1 = 0^\circ$. In the right panels the system is initially set with $e_1 = 0.85$, $e_2 = 0.85$, $i = 1^\circ$, $\Omega_1 = 180^\circ$ and $\omega_1 = 0^\circ$. In the top panels we show the inclination and in the bottom the inner orbit eccentricity as $1 - e_1$.

an extremely high eccentricity transition (see for example Figure 5). The octupole level of approximation introduces higher order resonances which overall render the system to be qualitatively different from a system at which the quadrupole level of approximation is applicable. We will begin by reviewing the different effects in the systems which can be divided into two main initial inclination regimes.

High initial inclination regime and chaos When the system begins with in a high inclination regime $39.2^\circ \leq i_{\text{tot}} \leq 140.7^\circ$ the resonance arises from the quadrupole level of approximation can cause large inclination and eccentricity amplitude modulations. Recall that this angle range is associated with the TPQ seperatrix. The octupole-level of approximation is associated with high order resonances that result in extremely large eccentricity peaks, flips (see Figure 5) as well as chaotic behavior (as explained below). As can be seen from equation (31) these resonances arise from higher order harmonics of the octupole-level Hamiltonian: $\omega_1 \pm \Omega_1$ and $3\omega_1 \pm \Omega_1$. A useful tool to analyze this system is in the form of surface of section (see fore example Figure 6). For a two-degrees of freedom system,

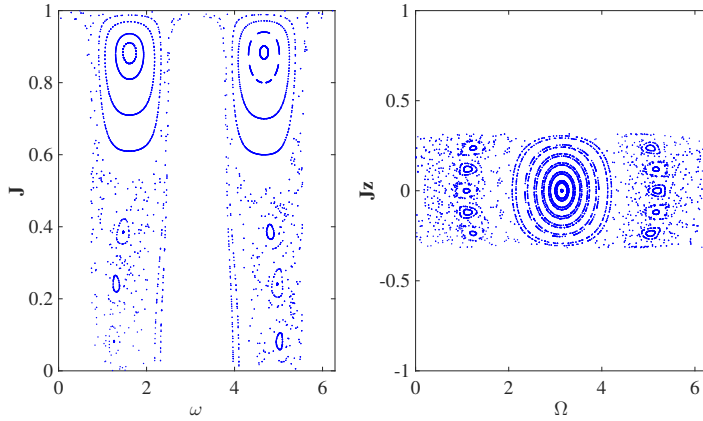


Figure 6

Surface of section for $F_{quad} + \epsilon F_{oct} = -0.1$ and $\epsilon = 0.1$. This initial configuration is associated with high initial inclination $i_{tot,0} > 39.2^\circ$. The quadrupole level resonances can clearly be seen (the big islands) as well as the emergence of high order resonances (the small islands). Figure adopted from Li et al. (2014a).

the surface of section projects a four-dimensional trajectory on a two-dimensional surface. The resonant regions are associated with fixed points and chaotic zones are a result of the overlap of the resonances between the quadrupole and the octupole resonances (Chirikov 1979; Murray and Holman 1997).

Figure 6 shows the surface of section for $\epsilon = 0.1$ and $F_{quad} + \epsilon F_{oct} = -0.1$, which is associated with high initial inclination $i_{tot,0} > 39.2^\circ$. In this Figure we can identify three distinct regions: resonant regions, circulation regions, and chaotic regions. The resonant regions are associated with trajectories of which the momenta (J and J_z) and the angles (ω_1 and Ω_1) undergo bound oscillations. The system is classified in a libration mode and the trajectories are quasi-periodic. The libration zones in the TPQ approximation are shown in Figure 2, and for the TPO in Figure 6. The circulation regions describes trajectories for which the coordinates are not constrained to a specific interval, and can take any value. Note that both resonant and circulatory trajectories map onto a one-dimensional manifold on the surface of section. On the contrary, chaotic trajectories map onto a two-dimensional manifold. In other words, while quasi-periodic trajectories form lines on the surface of section, chaotic trajectories are area-filling regimes. Embedded in the chaotic region, the small islands correspond to the higher, octupole order resonances, which are also quasi-periodic. The flip from $i_{tot} < 90^\circ$ to $i_{tot} > 90^\circ$ covers large parts of the parameter space as can be seen in Figure 7 right panel.

In some cases an analytical condition for the flip can be achieved by averaging over a quadrupole cycle (Katz et al. 2011). This averaging process yields a constant of motion

$$\chi = f(C_{KL}) + \epsilon \frac{\cos i_{tot} \sin \Omega_1 \sin \omega_1 - \cos \omega_1 \cos \Omega_1}{\sqrt{1 - \sin^2 i_{tot} \sin^2 \omega_1}} = \text{Const.} \quad , \quad (32)$$

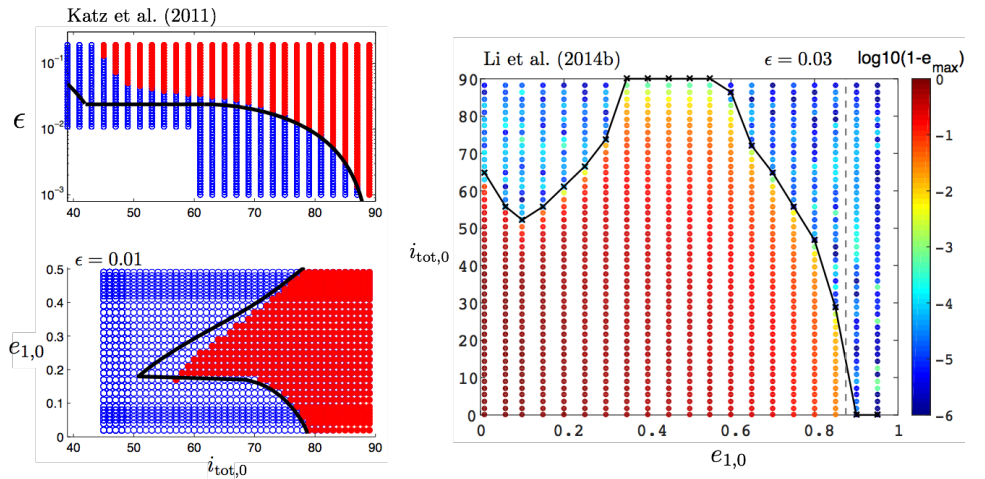


Figure 7

High inclination flip parameter space *Right panel* shows the results of numerical integrated systems associated maximum eccentricity (color coded as $1 - e_1$) in the $i_{\text{tot},0} - e_{1,0}$ parameter space for $\epsilon = 0.03$, after $30t_{\text{quad}}$. Systems above the black line flipped. *Left panel* shows the comparison with the analytical conditions derived by Katz et al. (2011). Open circles are the result of a numerical integration (red indicates systems that flipped and blue is for those that did not). Here the solid lines represent the flip conditions which for $e_{1,0} \sim 0$ and $i_{\text{tot},0} \gtrsim 61.7^\circ$ is reduced to equation (33). The bottom left panel shows the case of $\epsilon = 0.01$, and note that it shows only part of the parameter space. Left panels are adopted from Katz et al. (2011) and right panel is adopted from Li et al. (2014b).

where the function $f(C_{KL})$ is defined by:

$$f(C_{KL}) = \frac{32\sqrt{3}}{\pi} \int_{x_{\min}}^1 \frac{K(x) - 2E(x)}{(41x - 21)\sqrt{2x + 3}} dx \quad \text{and} \quad x_{\min} = \frac{3 - 3C_{KL}}{3 + 2C_{KL}}, \quad (33)$$

where $K(x)$ and $E(x)$ are the complete elliptic functions of the first and second kind, respectively. For initial high inclination a flipping critical value for the octupole pre-factor ϵ_c is a function of the initial inclination and the approximations takes a simple form

$$\epsilon_c = \frac{1}{2} \max |\Delta f(y)|, \quad (34)$$

where $\Delta f(y) = f(y) - f(C_{KL,0})$, C_{KL} was defined in Equation (16) and the subscript “0” marks the initial conditions. We note that C_{KL} in this TPO case is no longer constant (unlike the TPQ case). The parameter y has the range $C_{KL,0} < y < C_{KL,0} + (1 - e_{1,0}^2) \cos i_{\text{tot},0}/2$. For cases where $e_{1,0} \ll 1$, i.e., $C_{KL} \ll 1$ and $i_{\text{tot},0} \gtrsim 61.7^\circ$ Equation (34) takes a simple form:

$$\epsilon_c = \frac{1}{2} f\left(\frac{1}{2} \cos^2 i_{\text{tot},0}\right). \quad (35)$$

This approximation is valid for $\epsilon \lesssim 0.025$. The validity of this approximation for different initial values of e_1 and i_{tot} are shown in the left panels in Figure 7.

A timescale for the high inclination oscillation or flip is difficult to quantify since the evolution is chaotic. Furthermore, numerically it seems that the timescale for the first flip

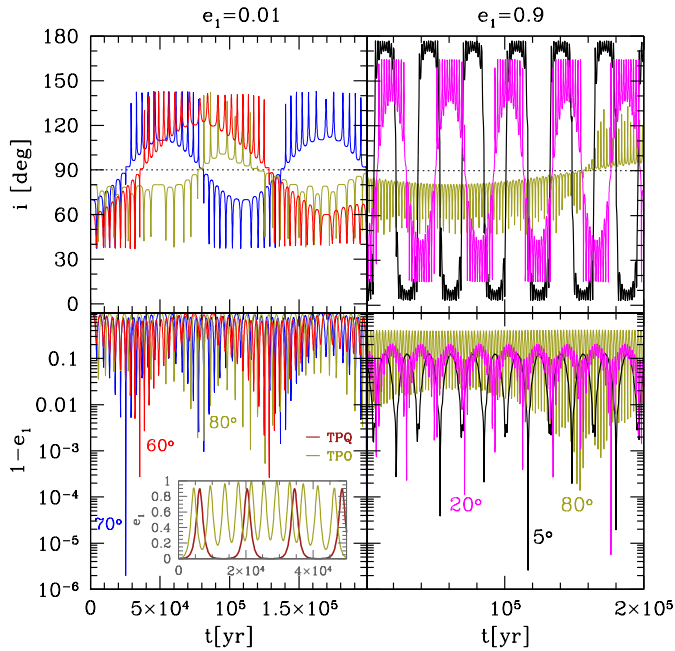


Figure 8

Flip timescales. We consider the following supermassive black hole binary system $m_1 = 10^7 M_\odot$, $m_3 = 10^9 M_\odot$ (note that in this case $m_2 \rightarrow 0$). The other parameters of this system are: $a_1 = 0.05$ pc $a_2 = 1$ pc and $e_2 = 0.7$. The system is sent initially with $\omega_1 = 51^\circ$, $\Omega_1 = 165.58^\circ$ and $e_1 = 0.01$ for the left panels and $e_1 = 0.9$ for the right panels. The initial inclinations considered are colored labeled in the Figure. Note the difference in flip timescale as a function of initial inclinations. In the inset we show the inner orbit eccentricity e_1 as a function of time for the TPQ (brown line) and TPO (green) for the initial setting of $e_1 = 0.01$ and $i_{\text{tot}} = 80^\circ$ case, which emphasizes the different short (quadruple) timescales between the TPQ and TPO level of approximation.

depends on the inclination (as can be seen in Figure 8). However, an approximate analytical condition, for the regular (none chaotic) mode was achieved recently by Antognini (2015), following Katz et al. (2011) formalism. This timescale has the following functional form:

$$t_{\text{flip}} = \frac{256\sqrt{10}}{15\pi\epsilon} \int_{C_{KL,\min}}^{C_{KL,\max}} \frac{dC_{KL}K(x)}{\sqrt{2(4\phi_{\text{quad}}/3 + 1/6 + C_{KL})(4 - 11C_{KL})\sqrt{6 + 4C_{KL}}}} \times \left(1 - \frac{(\chi - f(C_{KL}))^2}{\epsilon^2}\right)^{-1/2}, \quad (36)$$

where

$$\phi_{\text{quad}} = \frac{1}{8} (3F_{\text{quad}} - 1), \quad (37)$$

and note that ϕ_q defined in Antognini (2015) is simply $\phi_q = C_{KL} + j_{z,1}^2/2 = 4\phi_{\text{quad}}/3 - j_{z,1}^2/2 + 1/6$ in the notation used here. The upper limit of the integral in Equation (36) is

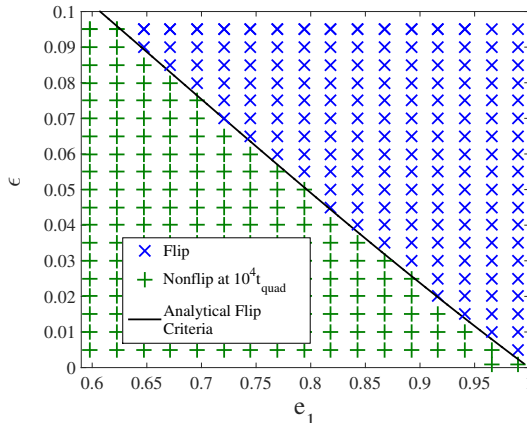


Figure 9

Surface of section for $F_{quad} + \epsilon F_{oct} = -2$ and $F_{quad} + \epsilon F_{oct} = -1$ for $\epsilon = 0.1$, this associated with low initial inclination $i_{tot,0} < 39.2^\circ$, Figure adopted from Li et al. (2014a). See similar plots in Petrovich (2015a), reproducing this analysis.

easy to find, since for $i_{tot} \rightarrow 90^\circ$ the z component of the angular momentum is zero, thus

$$C_{KL,max} = \frac{4}{3}\phi_{quad} + \frac{1}{6}, \quad (38)$$

and the minimum limit of the integral is found from solving $f(C_{KL,min}) = \chi \pm \epsilon$. This timescale takes a simple form, for setting initially $e_1 \rightarrow 0, \omega_1 \rightarrow 0$ and $i_{tot} \rightarrow 90^\circ$:

$$t_{flip} \sim \frac{128}{15\pi} \frac{a_2^3}{a_1^{3/2}} \frac{\sqrt{m_1}}{km_3} \sqrt{\frac{10}{\epsilon}} (1 - e_2)^{3/2} \quad \text{for } e_{1,0} \sim 0 \quad \text{and } i_{tot} \sim 90^\circ. \quad (39)$$

In the TPO level of approximation the short (quadrupole) timescales differ from the associated timescale at the TPQ level. In other words following the evolution of the same system, once by using the TPO and once using the TPQ yields different timescales, as depicted in the inset of Figure 8. This is because the Hamiltonian (i.e., the energy) is slightly different as the TPO includes the octupole term. Thus, the two calculations sample somewhat different values of the system energy. The difference is within a factor of a few as it represents the range of the phase space away from the separatrix (See Figure 2 for the different oscillation's amplitudes for given initial different energy).

Low initial inclination regime The octupole level of approximation yields an interesting behavior even beyond the Kozai angles. This is a result of the octupole level harmonics, i.e., $\omega \pm \Omega$ and $3\omega \pm \Omega$. Since the low order resonances are missing, the co-planer flip is not associated with chaotic behavior. Figure 9 shows the surface of section for two low inclination examples, specifically $F_{quad} + \epsilon F_{oct} = -2$ and $F_{quad} + \epsilon F_{oct} = -1$ for $\epsilon = 0.1$.

As can be seen from Figure 5 (as well as Figures 6 and 9) the two inclination regimes exhibit qualitative differences. The high inclination flip is driven by the quadrupole level resonance with the actual flip arises by accumulating effects from the high order resonates. Furthermore, this flip, many times, is associated with a chaotic behavior (Lithwick and

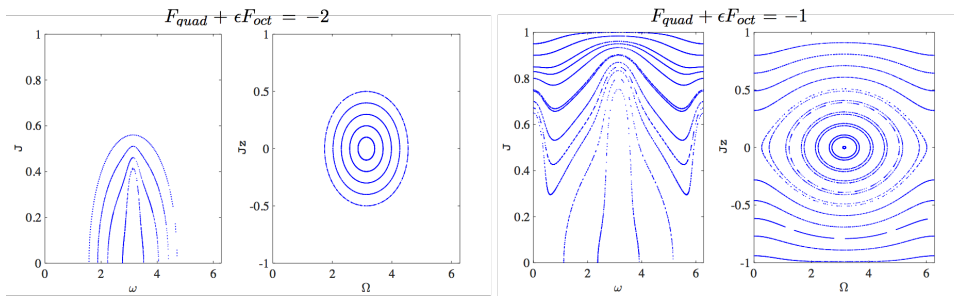


Figure 10

Low inclination flip criterion: Comparison between the analytical expression Equation (41), solid line, and numerical integration, (green crosses mark no flip after $10^4 t_{\text{quad}}$, and blue crosses systems that flipped). The system's parameters are: $m_1 = 1 M_{\odot}$, $m_2 \rightarrow 0$, $m_3 = 0.1 M_{\odot}$, $a_1 = 1 \text{ AU}$, $a_2 = 45.7 \text{ AU}$. The outer orbit eccentricity e_2 was changed to match the ϵ values indicated on the vertical axis. The system was initially set with $i_{\text{tot}} = 5^\circ$, $\omega_1 = 0^\circ$, $\Omega_1 = 180^\circ$ and e_1 as indicated in the figure. Figure adopted from Li et al. (2014b).

Naoz 2011; Li et al. 2014a). On the other hand, the low inclination flip is due to a regular trajectory. In addition, this flip takes place on a much shorter timescale than the high inclination flip.

Similarly to the analytical approximation for the high inclination flip conditions, Li et al. (2014b) achieved an analytical condition for the low inclination flip, after averaging over the flip timescale

$$\epsilon_c > \frac{8}{5} \frac{1 - e_1^2}{7 - e_1(4 + 3e_1^2) \cos(\omega_1 + \Omega_1)}. \quad (40)$$

Comparing this condition to the high inclination condition Equation (34), also emphasizes the qualitative difference between these two regimes.

The low inclination regime yields a flip timescale that can be easily found by setting $i_{\text{tot}} \rightarrow 0$. Li et al. (2014b) found an expression for the flip timescale:

$$t_{\text{flip}} = \left(\int_{e_{1,0}}^{e_{\min}} + \int_{e_{\min}}^{e_{\max}} \right) \frac{-8}{5(4 + 3e_1^2)} \left[\epsilon(1 - e_1^2) \left(1 - \frac{(F_{\text{quad}}^0 + \epsilon F_{\text{oct}}^0 - 8e_1^2)^2}{25e_1^2(4 + 3e_1^2)^2 \epsilon^2} \right) \right]^{-1/2}, \quad (41)$$

where $e_{1,0}$ is the initial inner orbit eccentricity and $F_{\text{quad}}^0 + \epsilon F_{\text{oct}}^0$ is the energy that corresponds to $i_{\text{tot}} = 0$ and the rest of the initial conditions. The reason for the two integrals is because if initially $\sin(\omega_1 + \Omega_1) > 1$, the inner orbit eccentricity, e_1 , decreases before it increases, otherwise if $\sin(\omega_1 + \Omega_1) < 1$ $e_{\min} = e_{1,0}$.

2.3.2. Beyond the Test Particle Approximation. Relaxing the test particle approximation leads to some qualitative differences. The first is that now one of the inner bodies can torque the outer body, and thus suppress the flip. This also causes a shift in the parameter space of the flip condition and the extreme eccentricity achieved compared to the TPQ case (see Figure 11). While the value of the maximum of e_1 is similar to that in the TPQ case, large eccentricity excitations may take place in different parts of the parameter space (compare Figure 11 to Figure 7). In particular, in the high inclination regime, the flips and the large eccentricity excitations of the TPQ case are concentrated around $i_{\text{tot}} = 90^\circ$

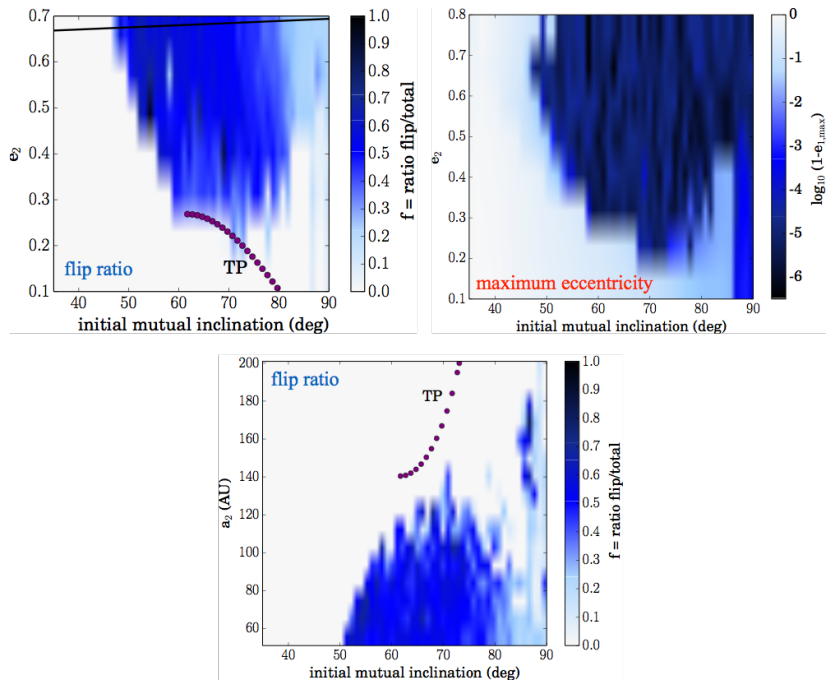


Figure 11

Flip and maximum eccentricity parameter space in two hierarchical planets configuration.

The color describes the maximum eccentricity reached over integration time of $\sim 5000t_{\text{quad}}$ (right top panel) and the flip ratio, defined as the time the total inclination spends over 90° from the entire integration time (the other two panels). The top two panels show the phase space corresponding to e_{max} (right) and the flip ratio (left) as a function of the initial outer orbit eccentricity (e_2) and the initial mutual inclination. Note that both follow exhibit interesting behavior at similar parts in the parameter space. However, for initial large inclination $80^\circ - 90^\circ$, the flip is suppressed. The system considered here has the following parameters: $m_1 = 1 M_\odot$, $m_2 = 1 M_J$, $m_3 = 6 M_J$, $a_1 = 5 \text{ AU}$, and $a_2 = 61 \text{ AU}$. The bottom panels shows the flip ratio in the initial a_2-i_{tot} phase space. The system considered in this panel has the same parameters as the top two panels, but with $e_2 = 0.5$ and varying a_2 . The flip condition for the TPQ, following the condition in Equation (35) is shown in purple dots. The TPQ analysis for the top left (bottom) panel suggests that all systems above (below) the “TP” dotted line are expected to flip. The solid line represents the stability condition, see Equation (51). Figure adopted from Teyssandier et al. (2013).

but in the full case they can shift to lower mutual inclinations and tap to larger range of inclinations (Figure 11). This is mainly because the outer orbit is being torqued by the inner orbit. Teyssandier et al. (2013) studied the effect of a similar mass companion and showed that if the outer body mass is reduced to below twice the smallest mass of the inner orbit, the flip and large eccentricity excitations are suppressed for large parts of the parameter space.

The system’s hamiltonian is (here again the nodes were eliminated for simplicity, but the z-component of the angular momenta are not conserved):

$$\mathcal{H} = \mathcal{H}_{\text{quad}} + \epsilon_M \mathcal{H}_{\text{oct}} , \tag{42}$$

where \mathcal{H}_{quad} is define in equation (22) and we copy it here for completeness

$$\mathcal{H}_{quad} = C_2 \{ (2 + 3e_1^2) (3 \cos^2 i_{tot} - 1) + 15e_1^2 \sin^2 i_{tot} \cos(2\omega_1) \} , \quad (43)$$

the octupole level approximation is:

$$\begin{aligned} \mathcal{H}_{oct} = & C_2 \{ (2 + 3e_1^2) (3 \cos^2 i_{tot} - 1) + 15e_1^2 \sin^2 i_{tot} \cos(2\omega_1) \} \\ & + C_3 e_1 e_2 \{ A \cos \phi + 10 \cos i_{tot} \sin^2 i_{tot} (1 - e_1^2) \sin \omega_1 \sin \omega_2 \} , \end{aligned}$$

where

$$\begin{aligned} C_3 = & -\frac{15 k^4}{16} \frac{4}{4} \frac{(m_1 + m_2)^9}{(m_1 + m_2 + m_3)^4} \frac{m_3^9 (m_1 - m_2)}{(m_1 m_2)^5} \frac{L_1^6}{L_2^3 G_2^5} \\ = & -C_2 \frac{15}{4} \frac{\epsilon_M}{e_2} \end{aligned} \quad (44)$$

and

$$\epsilon_M = \frac{m_1 - m_2}{m_1 + m_2} \frac{a_1}{a_2} \frac{e_2}{1 - e_2^2} . \quad (45)$$

and

$$A = 4 + 3e_1^2 - \frac{5}{2} B \sin i_{tot}^2 , \quad (46)$$

where

$$B = 2 + 5e_1^2 - 7e_1^2 \cos(2\omega_1) , \quad (47)$$

and

$$\cos \phi = -\cos \omega_1 \cos \omega_2 - \cos i_{tot} \sin \omega_1 \sin \omega_2 . \quad (48)$$

The latter equation emphasis one of the main difference that arise from relaxing the test particle approximation. In cases for which $m_1 \sim m_2$ the contribution from the octupole lever of approximation can be negligible. This can be seen in the example in Figure 12 for a system where the only difference between the left and right panels is setting $m_2 = 0$ in the left panels and $m_2 = 8 M_\odot$ in the right panels ($m_1 = 10 M_\odot$). In the pure Newtonian regime, (red lines) the EKL behavior is suppressed (no flips or eccentricity peaks). The complete set of equation of motions can be found in Section 8.

3. The validity of the approximation and the stability of the system

The secular approximation described here utilize averaging over the short orbital timescales, and thus any modulations over these times are washed out. Ivanov et al. (2005), Katz and Dong (2012), Antognini et al. (2014), Antonini et al. (2014) and Bode and Wegg (2014) showed that the inner orbit undergoes rapid eccentricity oscillations near the secular value (see for example Figure 13). Ivanov et al. (2005) found the change in angular momentum during an oscillation as

$$\frac{\Delta G_1}{\mu_1} = \frac{15}{4} \frac{m_3}{m_1 + m_2} \cos i_{\min} \left(\frac{a_1}{a_2} \right)^2 k \sqrt{m_3 a_2} , \quad (49)$$

where μ_1 is the reduced mass of the inner binary, and i_{\min} is the minimum inclination reached during the oscillation. These rapid eccentricity oscillations happen because the value of the inner orbit angular momentum goes to zero (i.e., extreme inner orbit eccentricity) on shorter timescale than the inner orbital period. In that case the averaging is not suffice and the secular approximation underestimates the maximum eccentricity that

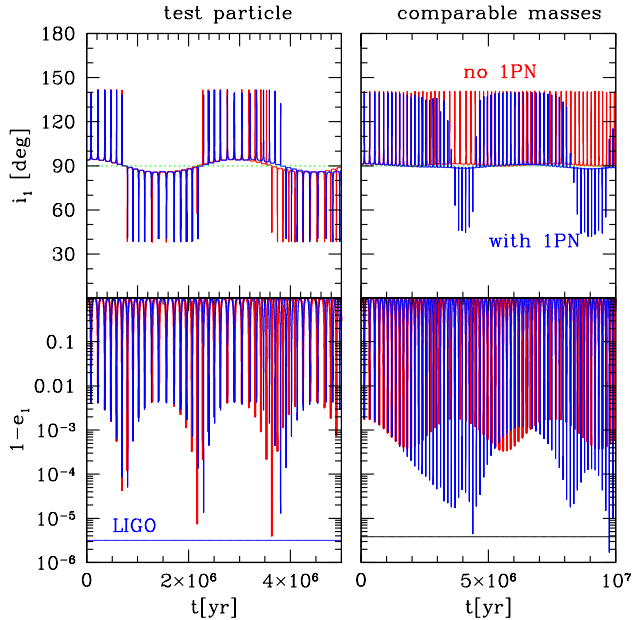


Figure 12

Comparison between test particle approximation and comparable mass system in the presence of general relativity. The systems in the right and left panel have same parameters and initial conditions apart from m_2 which is set to zero in the left panels and $m_2 = 8 M_\odot$ in the right panels. The other parameters are: $m_1 = 10 M_\odot$, $m_3 = 30 M_\odot$, $a_1 = 10$ AU, $a_2 = 502$ AU, $e_1 = 0.001$, $e_2 = 0.7$, $\omega_1 = \omega_2 = 240^\circ$ and $i_{\text{tot}} = 94^\circ$. Red lines corresponds to pure Newtonian evolution, and blue lines include general relativity effects (1st post newtonian expansion, to the inner and outer orbits). The horizontal lines are the minimum eccentricity corresponding to the detectable LIGO frequency range (horizontal lines in the bottom panels). General relativity corrections help to further increase the eccentricity and lead to orbital flips for the inner binary for comparable masses. Figure adopted from Naoz et al. (2013b)

the system can reach. Assuming a fixed outer perturber and adopting an instantaneous quadrupole torque, Antonini et al. (2014) took the limit of $e_1 \rightarrow 1$ and found a simple form to the condition for which the averaging is valid

$$\sqrt{1 - e_1} \gtrsim 5\pi \frac{m_3}{m_1 + m_2} \left(\frac{a_1}{a_2(1 - e_2)} \right)^3, \quad (50)$$

(using slightly different settings, Bode and Wegg (2014) found a similar condition). Thus, if during the evolution the specific angular momentum becomes smaller than the right hand side of this equation, the angular momentum goes to zero on shorter timescale than the inner orbital timescale. The immediate consequences of this is that the inner binary maximum eccentricity will be larger than the value the secular approximation predicts.

Recently, Luo et al. (2016) showed that these rapid short-timescale oscillations can accumulate over long timescales and lead also to deviations from the flip conditions discussed in §2.3.1, as described in Equation (34). They found that the double averaging procedure fails when the mass of the tertiary m_3 is large compared to the mass of the inner binary,

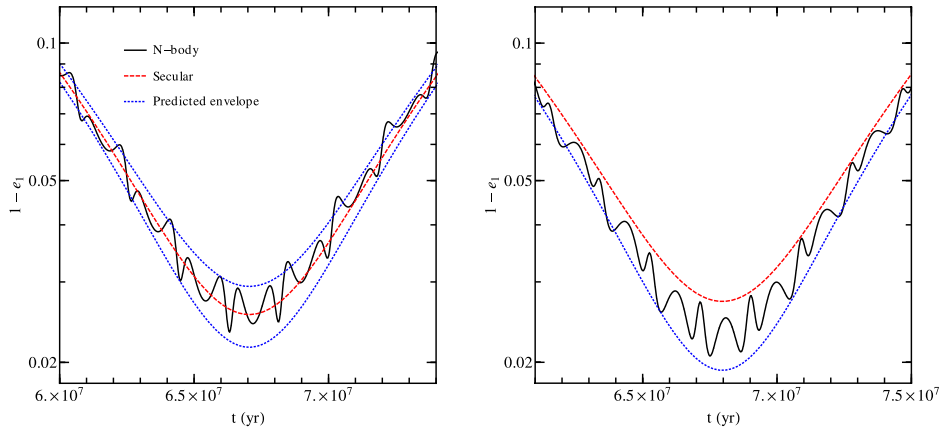


Figure 13

Comparison of the eccentricity excitations. The Figure considers the results from the secular approximation (red lines), and N-body (black lines) and the predicted change from Equation (49). The system considered has the following parameters: $m_1 = 10^7 M_\odot$, $m_2 = 10^5 M_\odot$, $m_3 = 10^7 M_\odot$, $a_1 = 1$ pc, $a_2 = 20$ pc, $e_1 = 0.1$, $e_2 = 0.2$, $i_{\text{tot}} = 80^\circ$. Left panel was initialized with $\omega_1 = \omega_2 = 0^\circ$ and the right panel was initialized with $\omega_1 - \omega_2 = 90^\circ$. Figure adopted from Antognini et al. (2014).

similarly to the condition in Equation (50).

Another consequence of large eccentricities is the stability of the system. A long term stability condition that is often used in the literature is the one give by Mardling and Aarseth (2001), which has the following form

$$\frac{a_2}{a_1} > 2.8 \left(1 + \frac{m_3}{m_1 + m_2}\right)^{2/5} \frac{(1 + e_2)^{2/5}}{(1 - e_2)^{6/5}} \left(1 - \frac{0.3i_{\text{tot}}}{180^\circ}\right). \quad (51)$$

Although this criterion was generated for similar mass binaries, and the inclination was added ad hock, it is often used for large range of masses. A criterion which takes into account both having the outer orbit be wider than the inner one, and the validity of secular approximation

$$\epsilon = \frac{a_1}{a_2} \frac{e_2}{1 - e_2^2} < 0.1. \quad (52)$$

This is numerically similar to the Mardling and Aarseth (2001) stability criterion [Equation (51)], for large range of mass system, (as shown in Naoz et al. 2013b).

The stability of a two planet system with low mutual inclination was studied in Petrovich (2015c), using N body integration. Assuming that m_1 is a stellar mass object and m_2 and m_3 are planetary mass objects he found a stability criterion of the form:

$$\frac{a_2(1 - e_2)}{a_1(1 + e_1)} > 2.4 \left[\max\left(\frac{m_2}{m_1}, \frac{m_3}{m_1}\right)\right]^{1/3} \sqrt{\frac{a_2}{a_1}} + 1.15. \quad (53)$$

Systems that do not satisfy this condition (by a margin factor of ~ 0.5) may become unstable. Specifically, Petrovich (2015c) found that systems for which $m_2/m_1 > m_3/m_1$ will most likely result in planetary ejections while systems for which $m_2/m_1 < m_3/m_1$ may slightly favor collisions with the host star.

The eccentricity excitations, both in the secular approximation and in its deviations, are extremely large (see Figures 7 and 11). This implies that in some cases the inner orbit can reach such a small pericenter distance R_{Lobe} so one of the objects may cross its Roche-limit (in the case where $m_2 < m_1$):

$$R_{Lobe} = \eta R_2 \left(\frac{m_2}{m_1 + m_2} \right)^{-1/3}, \quad (54)$$

where η is a numerical factor of order unity.

Considering the definition of the Roche limit, we can also ask when the eccentricity of the inner orbit becomes so large such that the tertiary captures a test particles that is orbiting around the primary ($m_1, m_3 \gg m_2$), which can be written as:

$$a_1(1 + e_1) = \tilde{\eta} a_2(1 - e_2) \left(\frac{m_1}{m_3} \right)^{1/3}, \quad (55)$$

where $\tilde{\eta}$ is of order of unity and is of different value from η in Equation (54). A test particle initially around m_1 with larger separations will feel a larger gravitational force from m_3 . Using the definition of ϵ , Naoz and Silk (2014) found the mass ratio that will result in a stable configuration as a function of the binary mass ratio, i.e.,

$$\frac{m_3}{m_1} = \left(\tilde{\eta} \frac{e_2}{\epsilon(1 + e_1)(1 + e_2)} \right)^3. \quad (56)$$

Thus for mass ratios for that are larger than the right hand side the approximation breaks down and the test particle may be captured by m_3 (some consequences are discussed at Li et al. 2015).

4. Short range forces and other astrophysical effects

The Newtonian evolution of the secular hierarchical three body system has proven to be very useful in modeling and analyzing many astrophysical systems. In realistic systems there are several short range forces and astrophysical affects that can significantly alter the evolution of the system. For example, some short range forces, such as tides and general relativity induce precession of the periape which strongly depends on the orbital eccentricity. If the orbit precesses due to the short range force to the opposite direction than the one induced by the Kozai-Lidov mechanism, further excitations of the eccentricity can be suppressed. In the limiting case, the precession is so fast compared to quadrupole-level precession that the inner orbit initial eccentricity remains constant. In fact, as will be discussed below, in some cases, the eccentricity excitation in the presence of short range force can be estimated analytically. Since in the Kozai-Lidov mechanism eccentricity is being traded for inclination, once the eccentricity can not be excited, the oscillations in the inclination are limited in a similar way.

4.1. General Relativity

The fast precession of the perihelion of the inner orbit due to GR effects takes place on the opposite direction of the quadrupole precession. Therefore, as mentioned before, the inner orbit extremely high eccentricity excitations are suppressed, and thus are the inclination flips as well.. For example, in the current location of most hot Jupiters, further eccentricity excitations are suppressed due to fast general relativity precession (and tides) compared

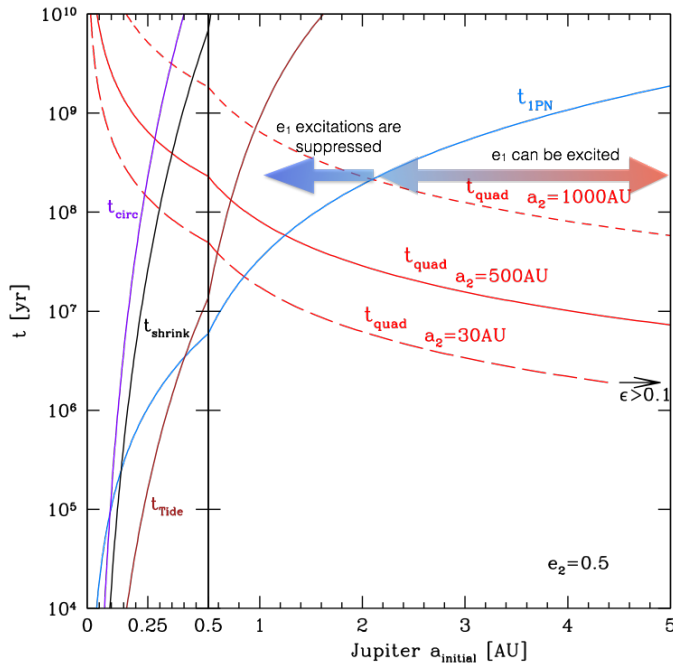


Figure 14

Relevant timescales for a Jupiter system. The system considered here is a Jupiter mass planet at different initial separations a_{initial} from a $1 M_{\odot}$ star. We consider the quadrupole timescale [Equation (27)] for a stellar perturber ($m_3 = 1 M_{\odot}$) at $a_2 = 1000$ AU and $a_2 = 500$ AU (short-dash and solid red lines, respectively), as well as the case of a Jupiter perturber at 30 AU (long-dashed red line). $e_2 = 0.5$ in all these cases. We also consider the precession of the inner orbit due to general relativity, according to Equation (58), blue line. The crossing point between the blue and red lines roughly separates between the different behaviors, as depicted by the arrows. We also consider the precession due to oblate objects from static tides (Equation (61), brown line), and the typical timescales to circularize and shrink the orbit (purple and black lines, respectively) according to the equations in Section 9 while adopting $T_{V,1} = 50$ yr and $T_{V,2} = 1.5$ yr.

to the quadrupole precession. Thus, Hot Jupiters have decoupled from their potential perturbers, and do not flip anymore. On the other hand, the t_{quad} timescale is much shorter compared to the general relativity precession in asteroid and Kuiper belt binaries.

The precession of the inner orbit due to general relativity has a simple form

$$\left. \frac{d\omega_1}{dt} \right|_{1PN, \text{inner}} = \frac{3k^3(m_1 + m_2)^{3/2}}{a_1^{5/2}c^2(1 - e_1^2)}, \quad (57)$$

where the subscript $1PN, \text{inner}$ indicates that precession is due to first Post Newtonian (PN) expansion for the inner orbit (see Misner et al. 1973, for a general derivation). A similar expression can be written to outer orbit general relativity precession, although this, typically, has little effect. Expanding the 1st PN three body Hamiltonian in semi-major axes ratio up to the octupole level of approximation reveals another term which describes

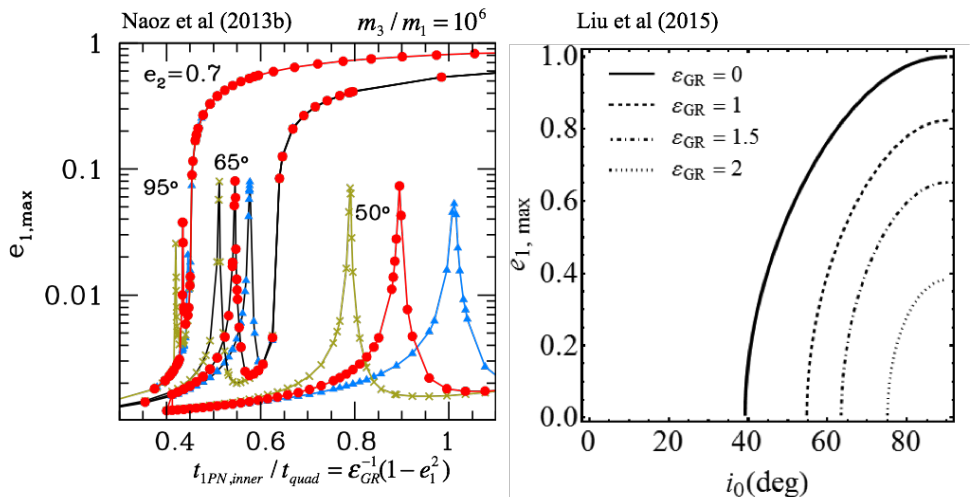


Figure 15

General relativity (1PN) effects on the hierarchical three body system. *Left panel:* shows the emergence of resonant-like eccentricity excitations in the $e_{1,max} - \epsilon_{GR}^{-1}$ plane for different initial inclinations. We consider the secular Newtonian evolution and the PN evolution including terms only up to $\mathcal{O}(a_1^{-2})$ (inner orbit precession, blue triangles), $\mathcal{O}(a_2^{-2})$ (outer orbit precession, green crosses) and the interaction term (red squares). The location of the resonance shift when including additional 3-body 1st PN terms. The system is initialized with $e_1 = 0.001$, $\omega_2 = 0^\circ$ and $\omega_1 = 240^\circ$ and with mutual inclination corresponding to (from left to right) 95° , 65° and 50° . The other parameters are $m_3/m_1 = 10^6$, $m_2 \rightarrow 0$ and $e_2 = 0.7$. Figure adopted from Naoz et al. (2013b). *Right panel:* shows the analytical solution for the maximum eccentricity in the $e_{1,max} - i_0$ plane for different values of ϵ_{GR} (note that $\epsilon_{GR} \rightarrow 0$ means no PN contribution). This calculation considers only the inner orbit precession for small ϵ_{GR} and high inclination test particle orbit. Figure adopted from Liu et al. (2015).

the general relativity interaction between the inner and outer orbits (Naoz et al. 2013b). In many cases, where the leading Newtonian terms are important, this interaction term can be neglected. The inner orbit GR precession timescale can be estimated simply as (Naoz et al. 2013b):

$$t_{1PN,inner} \sim 2\pi \frac{a_1^{5/2} c^2 (1 - e_1^2)}{3k^3 (m_1 + m_2)^{3/2}}. \quad (58)$$

If this timescale is shorter than the quadrupole timescale Equation (27) eccentricity excitations are suppressed (this was noted in many studies before, e.g., Ford et al. 2000b; Fabrycky and Tremaine 2007; Naoz et al. 2013b). For example, Figure 14, depicts the relevant timescales for a Jupiter around a $1 M_\odot$ star. Different perturbers induce quadrupole precessions which are compared to the general relativity precession, Equation (58). For example a planetary companion at 30 AU cannot excite the eccentricity of a Jupiter that formed at 0.5 AU (a closer companion can), however, a companion can excite the eccentricity of a 1 AU Jupiter which may result in the formation of a Hot Jupiter (see below).

The relation between the timescales can be estimated by (e.g., Naoz et al. 2013b)

$$\frac{t_{1PN,inner}}{t_{quad}} = \frac{a_1^4}{3a_2^3} \frac{(1 - e_1^2) m_3 c^2}{(1 - e_2^2)^{3/2} (m_1 + m_2)^2 k^2} = \epsilon_{GR}^{-1} (1 - e_1^2), \quad (59)$$

where we also introduced the parameter ε_{GR}^{-1} defined in Liu et al. (2015). When the two timescales are similar to one another a resonant like behavior emerges (Ford et al. 2000b; Naoz et al. 2013b). An example for this behavior is shown in the left panel of Figure 15 for different initial mutual inclination and setting initially $e_1 \rightarrow 0$. The value of this eccentricity can be estimated analytically, and have a simplified equation for large eccentricity excitations (Liu et al. 2015)

$$\left(\frac{\varepsilon_{GR}}{\sqrt{1-e_1^2}} \right)_{e_1=e_{1,max}} \approx \frac{9}{8} e_{1,max}^2 \frac{j_{1,min}^2 - 5 \cos^2 i_0 / 3}{j_{1,min}^2}, \quad (60)$$

where we remind the reader that $j_{1,min} = \sqrt{1-e_{1,max}^2} \ll 1$. This behavior is shown in the right panel of Figure 15 (see also Fabrycky and Tremaine 2007). The general expression of Equation (60), which is valid for all values of $e_{1,max}$, can be found in Eq. 50 in Liu et al. (2015)³. As shown in this latter study, given an extra short range force, such as ε_{GR} , the maximum eccentricity can be predicted for the octupole level of approximation, by considering the perpendicular case of the quadrupole level of approximation.

Interestingly, even if the GR precession timescale is longer than the quadrupole timescale $t_{1PN,inner} > t_{quad}$ general relativity can have significant implications on the dynamical evolution. Specifically, if $t_{quad} < t_{1PN,inner} \lesssim t_{oct}$ general relativity precession can re-trigger the EKL behavior for similar mass inner binaries. This can be seen in the right hand side example of Figure 12, where we compare between the pure Newtonian case (red lines) and the case which includes general relativity precession for the inner orbit (blue lines). As depicted, including general relativity effects re-trigger the EKL behavior.

In the secular approximation general relativity effects are typically being taking into account by only including the *inner* body precession [Equation (57)]. Sometimes the outer orbit precession is also being taken into account (simply replace 1 with 2 in Equation (57)), this mainly affects the position of the $t_{quad} \sim t_{1PN,inner}$ resonance (e.g., Naoz et al. 2013b, and see left panel of Figure 15).

In some astrophysical settings higher PN orders of the inner orbit are important (e.g., Miller and Hamilton 2002; Blaes et al. 2002; Wen 2003; Seto 2013; Antognini et al. 2014). In some cases the general relativity (1PN) term that describes the interactions between the inner and outer orbits may have some effects (Naoz et al. 2013b). However, as shown by Will (2014b,a) when GR effects between the two orbits become more important, the gravitational weak field approximation is no longer valid, which results in deviations of the dynamics compared to the double averaging process.

4.2. Tides and rotation

Similarly to the suppression of eccentricity excitations due to general relativity precession, precession of the nodes due to oblate objects from static tides, or rotating objects, can cause similar affect. Mazeh and Shaham (1979) first included tidal effects to the hierarchical triple dynamical evolution (in the TPQ case and assuming small mutual inclinations). This was then generalized in a series of papers by Kiseleva et al. (1998), Eggleton et al. (1998) and Eggleton and Kiseleva-Eggleton (2001), based on Hut (1980) equilibrium and static tides formalism. The strength of the equilibrium tide recipe presented here is that it

³Note that it has a typo and the 3/5 in that equation should be 5/3, Liu et al private communication.

is self consistent with the secular approach. Furthermore, assuming polytropic stars this recipe has only one dissipation parameter for each member of the binary. In other words, tides can be considered for both members of the inner orbit. Using this description one is able to follow the precession of the spin of the star and the planet due to oblateness and tidal torques. We provide the set of equations in Section 9. Different choices of the tidal model can result in quantitatively different results, such as the relevant separations at which eccentricity excitations are suppressed, and the time evolution of the circularization and orbital shrinking process.

During the system evolution, the EKL mechanism can cause large eccentricity excitations for the inner orbit (for example, see Figures 7 and 11). Thus, on one hand, the nearly radial motion of the binary drives the two inner binary members to merge, while on the other hand, the tidal forces tend to shrink and circularize the orbit, see Figure 16 right and left panels, respectively. If during the evolution the tidal precession timescale (or the GR timescale) is similar to that of the quadrupole timescale (which is the shortest secular timescale, Equation (27)), further eccentricity excitations are suppressed. In this case tides can shrink the binary semi-major axis and form a tight binary decoupled from the tertiary companion. In other words, the precession timescale associated with the gravitational perturbations from the tertiary is slower than the short range precession timescales. The final separation may remain on a stable orbit⁴. An example of this behavior is shown in the left panels of Figure 16. However, if the eccentricity is excited on a much shorter timescale than the typical tidal (or GR) precession timescale (but, of course still long enough so the secular approximation is valid), the orbit becomes almost radial and tidal precession does not have enough time to affect the evolution. In this case the peri-center distance may be shorter than the Roche limit of at least one of the binary members (see Eq. (54)). An example of this behavior is shown in the right panels of Figure 16.

The typical timescales associated with these precessions are (see equations (86)-(90) for the source of these timescales)

$$t_{\text{Tide}} \sim \frac{a_1^{13/2} m_2 (1 - e_1^2)^5}{\sqrt{k} k_{L,2} f_T(e) m_1 (m_1 + m_2) R_2^5} \quad (61)$$

and

$$t_{\text{Rot}} \sim \frac{\sqrt{k} a_1^{7/2} m_2 (1 - e_1^2)^2}{k_{q,2} \Omega_{s,2}^2 \sqrt{1 + m_2} R_2^5} \quad (62)$$

for tidal and rotational precessions respectively. We define

$$f_T(e_1) = 1 + \frac{3}{2} e_1^2 + \frac{1}{8} e_1^4 \quad (63)$$

and R_1 and $\Omega_{s,2}$ are the radius and spin rate of m_2 . Furthermore, $k_{L,2}$ is its Love parameter and $k_{q,2}$ the apsidal motion constant. Similarly to the GR case, Liu et al. (2015) defined $\varepsilon_{\text{Rot}} = t_{\text{quad}}/t_{\text{Rot}}(1 - e_1^2)^2$ and $\varepsilon_{\text{Tide}} = t_{\text{quad}}(1 - e_1^2)^5/(t_{\text{Tide}} f_T(e_1))$. With these definitions, Equation (60) can be generalized (Liu et al. 2015)

$$\left(\frac{\varepsilon_{GR}}{\sqrt{1 - e_1^2}} + \frac{1}{15} \frac{\varepsilon_{\text{Tide}}}{(1 - e_1^2)^{9/2}} \tilde{f}(e_1) + \frac{1}{3} \frac{\varepsilon_{\text{Rot}}}{(1 - e_1^2)^{3/2}} \right)_{e_1=e_{1,max}} \approx \frac{9}{8} e_{1,max}^2 \frac{j_{1,min}^2 - 5 \cos^2 i_0/3}{j_{1,min}^2}, \quad (64)$$

⁴Note that tides always tend to shrink the binary separation, but this happens on much longer timescale.

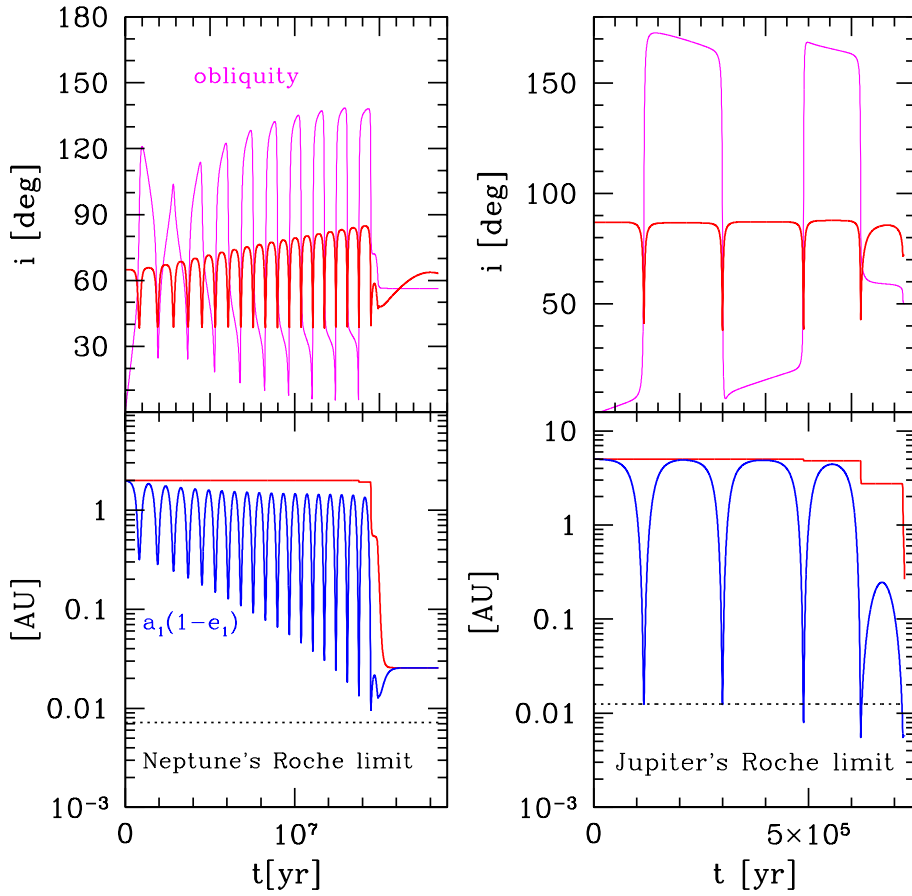


Figure 16

Tidal disruption (right panel) and circularization and shrinking the orbits due to tides (left panel). Top panels show the systems' mutual inclination (red line), and obliquity (magenta lines). Bottom panels show the semi-major axes (red lines) and pericenter distances (blue lines) in AU. Also shown in dashed lines are the pericenter at which tidal disruption takes place according to Equation (54), adopting $\eta = 2.7$ (e.g., Guillochon et al. 2011; Liu et al. 2013). Left panels consider a Neptune around a $0.32 M_{\odot}$ M dwarf star, initially set at $a_1 = 2$ AU, and $e_1 = 0.01$. The third object is a brown dwarf with $m_3 = 10 M_j$ at 50 AU, with $e_2 = 0.52$. The orbits have initially $\omega_1 = \omega_2 = 0^\circ$ and mutual inclination of 65° . The spin periods of the star and planet were assumed to be 4.6 days and 1 day, respectively. Right panels consider a Jupiter mass planet at a 5 AU separation from a $1 M_{\odot}$ star with a $1 M_{\odot}$ stellar companion at 200 AU. The system initially sets with $e_1 = 0.001$, $e_2 = 0.75$, $\omega_1 = \omega_2 = 0^\circ$ and $i = 87^\circ$. The spin periods of the star and planet were assumed to be 24 days and 10 days, respectively. Both systems start initially aligned (i.e., zero obliquity for both the planet and the star) and $T_{V,1} = 50$ yr and $T_{V,2} = 1.5$ yr.

where

$$\tilde{f}(e_1) = 1 + 3e_1^2 + \frac{3}{8}e_1^4. \quad (65)$$

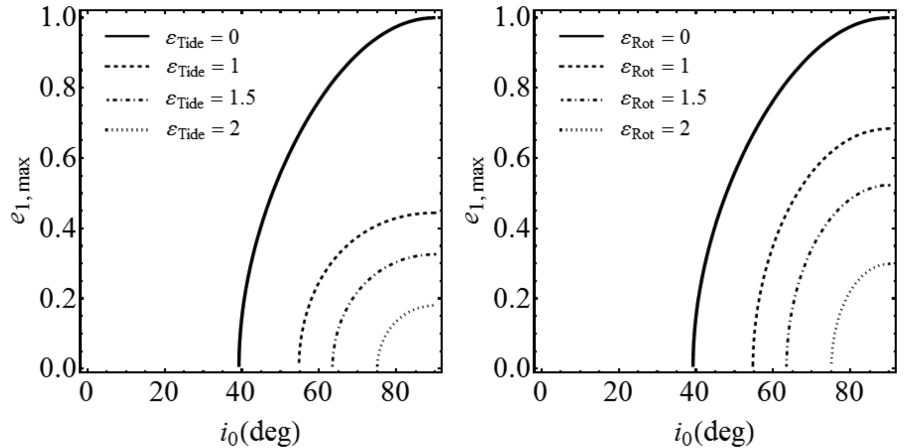


Figure 17

Maximum eccentricity in the presence of rotation (right panel) and tides (left panel). Figure adopted from Liu et al. (2015).

Note that here we used the ε notation introduced in Liu et al. (2015), to avoid confusion with their definition of $\dot{\omega}$ which is different than the one used in this review. In Figure 14 we show the tidal precession timescale compared to the other relevant timescales for a Jupiter around a Sun like star. The maximum eccentricity that can be achieved as a function of inclination for a test particle approximation, and $e_{1,0} \sim 0$ is shown in Figure 17.

5. Applications

There are a few main general commonalities between all applications discussed below. The first is the possible outcome due to eccentricity excitation of the inner orbit. As shown in Figure 16, these high eccentricities can result in tidal evolution which will lead to tight inner binary, or it will result in Roche limit crossing. For a different astrophysical setting this can result in mergers, collisions, tidal disruption events, supernova etc. Another general outcome is that an initial isotropic distribution of inclination of triple systems is not conserved. In the following we review a few examples of these applications to different astrophysical systems.

5.1. Solar system

Kozai (1962) studied the secular dynamical evolution of an asteroid, at 2 AU, due to Jupiter’s gravitational perturbations in the framework of the TPQ approximation. He showed that the asteroid undergoes large eccentricity and inclination oscillations. Considering the hierarchical nature of the approximation, we note that the system is in fact not valid to be addressed by secular approximation. The semi-major axes ratio between the asteroid (2 AU) and Jupiter (5 AU) yields rather large value ($a_1/a_2 = 0.6$), which suggests that the hierarchical approximation is not valid. Furthermore, Kozai (1962) assumed the Jupiter’s eccentricity is strictly zero. Taking into account Jupiter’s eccentricity ~ 0.05

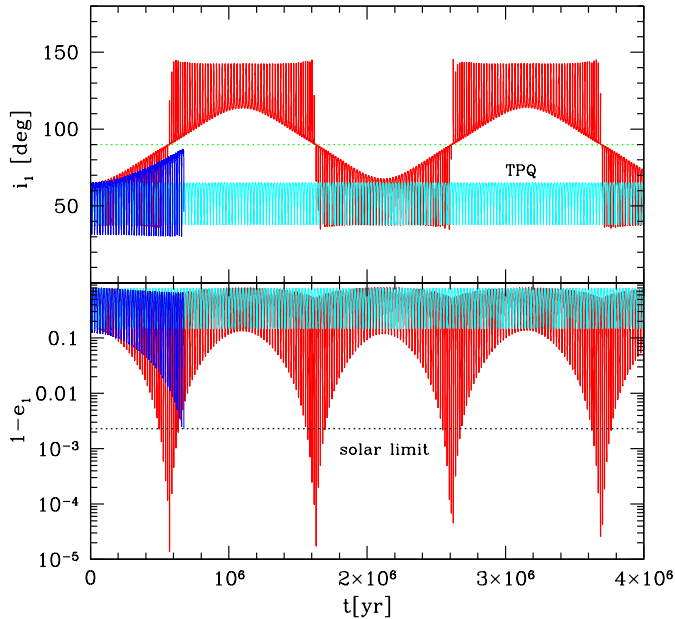


Figure 18

Kozai's (1962) study of secular evolution of an asteroid due to Jupiter's gravitational perturbations. The system is set with $m_1 = 1 M_\odot$, $m_2 \rightarrow 0$ and $m_3 = 1 M_J$, with $a_1 = 2$ AU and $a_2 = 5$ AU. We initialize the system with $e_1 = 0.2$, $e_2 = 0.05$, $\omega_1 = \omega_2 = 0^\circ$ and $i_{\text{tot}} = 65^\circ$. We consider the TPQ evolution (cyan lines) and the EKL evolution (red lines). The thin horizontal dotted line in the top panel marks the 90° boundary. The result of an N -body simulation (blue lines) is also shown. The thin horizontal dotted line in the bottom panel marks the eccentricity corresponding to a collision with the solar surface, $1 - e_1 = R_\odot/a_1$. At this instance we have stopped the numerical integration. Figure adopted from Naoz et al. (2013a).

leads to non-negligible contribution from the octupole level of approximation $\epsilon = 0.03$, this suggest that the EKL mechanism may significantly alters the evolution of the asteroid. This is shown in Figure 18 which considers the TPQ approximation (cyan lines) but also consider the EKL evolution (red lines). The latter show that the TPQ approximation is rather inadequate to address this problem. Furthermore, as mentioned, Jupiter is not far away enough to unitize the hierarchical approximation for this problem, which can be seen from the N -body simulation result, using the *Mercury* software package (Chambers and Migliorini 1997). We used both Bulirsch-Stoer and symplectic integrators (Wisdom and Holman 1991). This calculation shows that indeed the asteroid may impact the sun, and that the actual evolution of the system is closer in behavior to the EKL (TPO in this case) than the TPQ approximation.

As mentioned above, the TPQ approximation can successfully describe the evolution for a verity of test particle systems in the solar system. For example, it was used to explain the inclinations of gas giant satellites and Jovian irregular satellites (e.g., Kinoshita and Nakai 1991; Vashkov'yak 1999; Carruba et al. 2002; Nesvorný et al. 2003; Čuk and Burns 2004; Kinoshita and Nakai 2007). Furthermore, the importance of secular interactions for

the dynamics of comets and other test particles in the solar system was noted in several studies (e.g., Kozai 1979; Quinn et al. 1990; Bailey et al. 1992; Thomas and Morbidelli 1996; Duncan and Levison 1997; Gronchi and Milani 1999; Gomes et al. 2005; Tamayo et al. 2013). Another interesting example of the application of three body dynamics relates to binary minor planets. Observations suggests that Near Earth asteroid binaries are common (about 15% $r_{NEA} > 300\text{m}$ (Pravec et al. 2006; Margot et al. 2015) and perhaps as high as 63%, for a larger range of sizes (Polishook and Brosh 2006)). Furthermore, about 15% of asteroids and high multiples reside in binaries (Pravec et al. 2006) and Nesvorný et al. (2011) suggested that the binary fraction in the Kuiper belt can be as high as 40%. In all of these cases a natural third body is simply the Sun, which gravitationally perturb the binary orbit. Perets and Naoz (2009) and Naoz et al. (2010) have studied the evolution of binary minor planets, in the frame work of TPQ, and showed that the dynamical evolution largely affects the observed orbital distribution of these objects. Specifically they showed that in the inclination–separation phase space there is a regime associated with high mutual inclination which is devoid of eccentric wide binaries. Eccentricity excitations in this regime, due to the Sun’s gravitational perturbation, can lead to shrinking, and circularizing of the binary’s orbit, or even lead to binary coalescence’s. Furthermore, Kinoshita and Nakai (1991), Vashkov’yak (1999), Carruba et al. (2002), Nesvorný et al. (2003), Ćuk and Burns (2004) and Kinoshita and Nakai (2007) suggested that secular interactions and Kozai oscillations may explain the significant inclinations of gas giant satellites and Jovian irregular satellites. Binaries that are closer to the sun, such as binary asteroids and near Earth binaries will be sensitive to a wider range of physical effects, and specifically the induced precession of the binary due to an oblate object may suppress eccentricity excitations (Fang and Margot 2012). Another, potentially important mechanism, is the YORP effect which can significantly alter the spin of asteroids and near earth objects (e.g., Polishook and Brosh 2009). This in turn can result in even larger effects on the precession due to rotation.

5.2. Planetary systems

Recent ground and space based observations have transformed our understanding of the properties of exoplanetary systems. The detection of several thousand planets and planet candidates have revealed many puzzles that challenge traditional planet formation theories and generated many new ideas. One of the greatest mysteries in the last two decades lays in a class of giant planets called “Hot Jupiters.” These are a Jupiter size planets that are found in extremely short period orbits around their host stars (i.e. periods of a few days or less). Most theories posit that these planets still form on larger ($> AU$) scales, like in the solar system, but move inwards to short orbital periods. Thus, a migration mechanism is needed to reduce the angular momentum of these planets by two orders of magnitude (from few AUs to about few percent of an AU). Broadly speaking, there are two main channels considered in the literature to achieve this. In the first channel, planets form in the disk, and in some cases, angular momentum exchange between the planets and the protoplanetary disk can produce inward migration (e.g., Lin and Papaloizou 1986; Masset and Papaloizou 2003). In the second channel, planets also formed in the disk, but dynamical interactions between multiple planets or a stellar companion greatly affect the final orbital configuration of the system, through a variety of mechanisms such as planet-planet scattering (e.g., Rasio and Ford 1996a), EKL (see below), or secular chaos (Lithwick and Wu 2012; Hansen and Zink 2015). The role of planet or stellar dynamical interactions

is motivated by the presence of substantial eccentricities amongst the more distant Jovian population, and the discovery of high obliquities (misalignments between planetary orbital and host star spin directions, e.g., Albrecht et al. 2012b). Both of these features would tend to be damped by the dissipative interactions with a protoplanetary disk and have spawned an interest in processes that can lead to migration through predominantly dynamical interactions.

The first application of three body secular interaction to a planetary system began with the detection of 16 Cyg B (Cochran et al. 1996), where Holman et al. (1997) and Mazeh et al. (1997) attributed its high eccentricity ($e \sim 0.63$) to the Kozai-Lidov mechanism (in the framework of the TPQ approximation). They also showed that the planet spends about $\sim 35\%$ of its lifetime in a high eccentric orbit $e > 0.6$. In subsequent nominal studies by Wu and Murray (2003), Wu et al. (2007) and Fabrycky and Tremaine (2007) the consequences of the TPQ approximation in forming Hot Jupiters in stellar binaries was investigated in greater detail including GR and tides. As the orbit evolves dynamically due to gravitational perturbation from the outer orbit the planet's orbit becomes eccentric and the planet spends long times around the host star. At these intervals tides on the planet and on the star affect the orbit, which tends to circularize and shrink it. This scenario was suggested as a possible formation channel for Hot Jupiter without the need for disk migration (Lin and Papaloizou 1986).

As an aftermath of using the TPQ approximation these studies found that in order to form Hot Jupiters the initial mutual inclination needs to be rather close to perpendicular ($90^\circ \pm 3^\circ$ e.g., Fabrycky and Tremaine 2007). An important outcome from these calculations was the prediction of retrograde Hot Jupiters (i.e., obliquities larger than 90°) (Fabrycky and Tremaine 2007; Wu et al. 2007). The recent detections of retrograde Hot Jupiters (e.g., Triaud et al. 2010; Winn et al. 2010; Albrecht et al. 2012b) resulted in a new interest in the possibility that secular three body interactions presented in this field.

The formation of Hot Jupiters via the EKL mechanism, including GR and tides for two planet systems was studied in Naoz et al. (2011), see Figure 19. A simplified Monte-Carlo for initially an aligned Jupiter in a two planet system resulted in a nearly uniform obliquity distribution, as well as nearly uniform mutual inclination distribution. Similar results for the inclination and obliquity distributions were achieved for the formation of Hot Jupiters in stellar binary systems (effectively repeating the analysis by Fabrycky and Tremaine (2007) but for the EKL mechanism and exploring larger range of orbital parameters). The obliquity distribution is shown in Figure 20 left panel. Projecting the resulted obliquity angles on the sky (see right panel of Figure 20) allows for direct comparison with observations (e.g., Morton and Johnson 2011). Naoz et al. (2012) performed a bayesian analysis that treats the complete obliquity distribution as a sum of contributions from an aligned component, an EKL component, and planet-planet scattering component (adopting Nagasawa and Ida 2011). They found that the EKL most likely accounts for $\sim 30\%$ of the observed systems and planet-planet scattering contributes about $\sim 10\% - 20\%$, independently of the formation rate. That analysis also showed that EKL produces between 60% to 80% of large obliquity angles. These values are consistent with complementary analyses that showed that Hot Jupiters are likely to have a far away companion (e.g., Knutson et al. 2014; Ngo et al. 2015; Wang et al. 2015).

It was later shown, in the frame work of hierarchical triple system, that the behavior of the obliquity angle is chaotic in nature (Storch et al. 2014; Storch and Lai 2015). The planetary orbital angular momentum vector precesses around the total angular momentum at a rate which is inversely proportional to the quadrupole timescale $\sim t_{\text{quad}}^{-1}$. Due to the

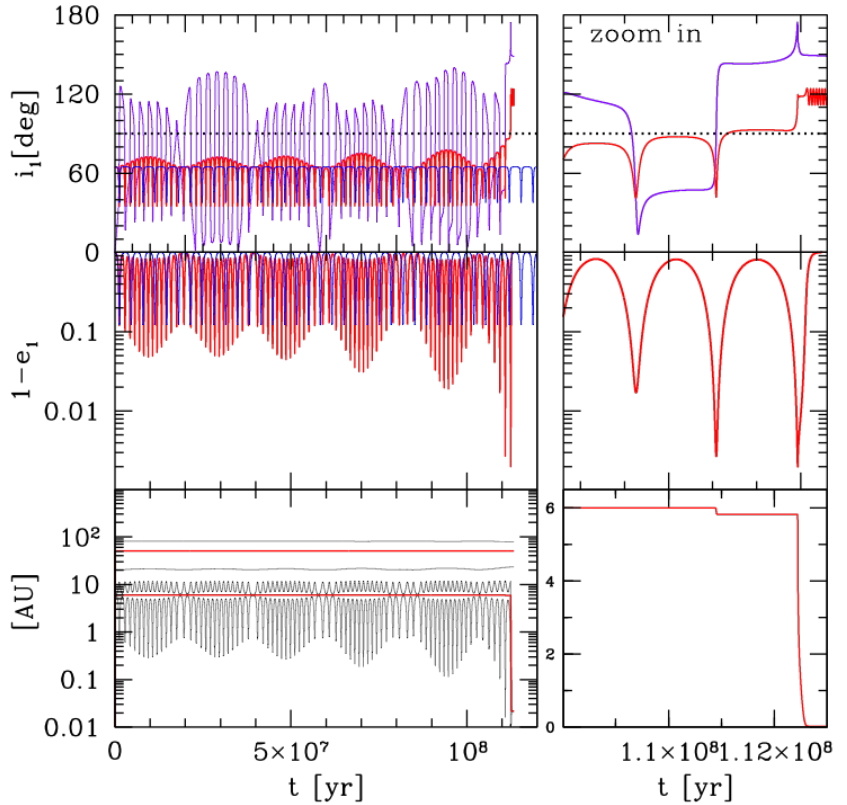


Figure 19

Hot Jupiter formation in a two planet system Left panels show the full evolution and the right panel show a zoom in on the final three quadrupole cycles. We consider the full, octupole level evolution which includes GR and tides evolution (red lines), the quadrupole level, including GR and tides (blue lines). Top panels show the inclination of the system of the full, up to the octupole level evolution which includes GR and tides (red line), and the inclination for the quadrupole level, including GR and tides (blue lines). In purple we show the obliquity. Middle panels show the eccentricity as $1 - e_1$ (again red lines are for the octupole and the blue lines are for the quadrupole). Bottom panels show the semi-major axes for the outer (top) and inner (bottom) binaries (red lines) and their apo- and peri-centers (grey lines). Note that the left bottom panel is log scale while the right bottom panel is linear scaled. The system parameters are: $m_1 = 1 M_\odot$, $m_2 = 1 M_j$, $m_3 = 3 M_j$, $a_1 = 6$ AU, $a_2 = 61$ AU, $e_1 = 0.001$, $e_2 = 0.6$, $\omega_1 = 45^\circ$, $\omega_2 = 0^\circ$ and $i_{\text{tot}} = 71.5^\circ$. The system started with zero obliquity and the spin periods of the star and the planet are 25 days and 10 days, respectively. The viscous times here are $t_{V,1} = 5$ yr and $t_{V,2} = 1.5$ yr, the spin period of the star was assumed to be 25 d. Figure adopted from Naoz et al. (2011), but shows the evolution of the obliquity.

rotation-induced stellar quadrupole, the planet induces precession in the stellar spin axis which is proportional to the stellar spin's angular momentum. As shown by Storch et al. (2014), when the latter precession spin is larger than the orbital precession rate, the stellar spin axis follows \mathbf{G}_1 adiabatically, while maintaining an approximately constant obliquity.

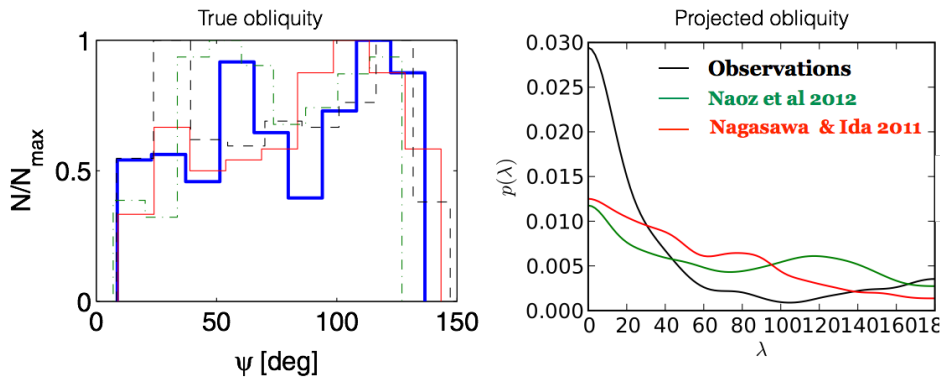


Figure 20

Hot Jupiter obliquity distribution in stellar binaries. Left panel shows the true obliquity (ψ) distribution, as a result from fiducial Monte Carlo simulations by Naoz et al. (2012) (blue line), for wide range of companion initial separations and setting planetary viscous tides to be $t_{V,2} = 1.5$ yr. This distribution has a characteristic cut-off near 140° . This limit arises from the Kozai angles (the separatrix $\sim 140^\circ$) for which the large oscillations take place. Also shown are the results from the Monte Carlo simulations with different settings. In particular, the dashed black line represents a companion at $a_2 = 1000$ AU, and thin solid red line represents a companion with $a_2 = 500$ AU. In both cases the planetary viscous tides is set to be: $t_{V,2} = 1.5$ yr. Also over-plotted is a Monte-Carlo simulation for a companion separation of $a_2 = 500$ AU with $t_{V,2} = 0.015$ yr, dot-dashed green line. Right panel shows the projected obliquity from (Naoz et al. 2012) Monte-Carlo simulations, as well as the observations (as for 2012) *exoplanets.org*, and the projected obliquity of Nagasawa and Ida (2011). The stellar spin-period assumed for these figures was 25 d. Different Roche-limit estimates do not change this result (e.g., Petrovich 2015b), however, different stellar spin-periods or evolution of the spin period may result in deviation from this distribution (Storch et al. 2014). Figure adopted from Naoz et al. (2012).

In the other extreme case, when the maximal spin precession rate is always smaller than the orbital precession rate the spin axis effectively precesses around the total angular momentum (about which \mathbf{G}_1 is precessing). In the intermediate regime, Storch et al. (2014) showed that a secular resonance occurs, which leads to complex and chaotic spin evolution. Short range forces can further complicate the obliquity evolution, and affect the formation of Hot Jupiters (Storch et al. 2014; Storch and Lai 2015).

The large eccentricity excitations induced via the EKL mechanism can result in a nearly radial motion and drive the planet into the star (as illustrated in Figure 16, right panel). Thus, the formation fraction of Hot Jupiters is highly sensitive to the disruption distance (as shown in Figure 21, vertical lines are based on Eq. (54)). For lower mass planets, such as rocky planets, tides (or GR, or quadrupole moments from fast rotating stars) are largely ineffective to stop the EKL's nearly radial motion, resulting in high probability of tidal disruption (e.g. Lanza and Shkolnik 2014; Rice 2015). Apart from tidally disrupting the planet, binary companions can also lead to large instabilities, which may result in swapping planets between the stars (e.g., Kratter and Perets 2012; Moeckel and Veras 2012). In addition, as the star evolve beyond the main sequence, the existence of a companion (either a star, brown dwarf or a planet) can lead to ejection of planets (e.g., Veras and Tout 2012; Veras et al. 2013, 2014) or engulfment of the inner most planet (e.g., Li et al. 2014c; Frewen and Hansen 2015).

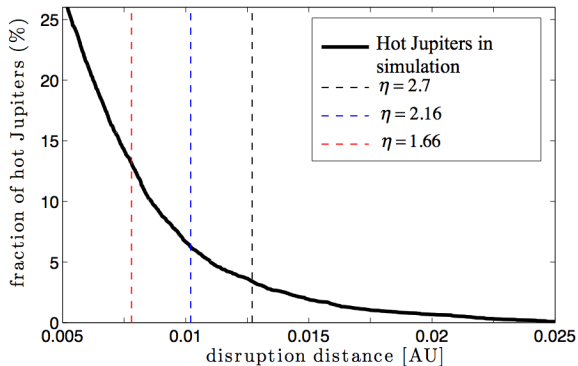


Figure 21

Fraction of Hot Jupiters in stellar binaries The fraction of hot Jupiters formed in the fiducial Monte Carlo simulation by Petrovich (2015b) as a function of the disruption distance. The vertical lines indicate different disruptions distances parametrized by η in Equation (54). The different values ($\eta = 1.66, 2.16$ and 2.7) correspond to the values adopted in three different studies: Naoz et al. (2012), Wu et al. (2007) and Petrovich (2015b), respectively. Figure adopted from Petrovich (2015b).

The observational studies that showed that Hot Jupiters are likely to have far away companion (e.g., Knutson et al. 2014; Ngo et al. 2015; Wang et al. 2015) promoted further investigations of two planet systems. As shown in Figure 11, a similar mass perturber yields large eccentricity excitations with suppression of large eccentricities for large mutual inclinations (Teyssandier et al. 2013). Therefore an inclined planetary perturber can lead to short period oblique planets (Naoz et al. 2011; Li et al. 2014c). If large eccentricities are generated, according to the stability criterion in Equation (53) the inner planet can either be ejected from the system or collide with the host star. In some cases, when the forced eccentricity from the perturber causes the orbit to shrink, the orbit reaches a semi-major axis for which tidal precession is comparable to the quadrupole timescale (as noted in Section 9). This suppresses further circularization and shrinking of the orbit, which may lead to the formation of eccentric warm Jupiters (Dawson and Chiang 2014).

Recently, the Kepler mission detected several circumbinary planetary systems (Doyle et al. 2011; Orosz et al. 2012b,a; Welsh et al. 2012, 2015; Kostov et al. 2013, 2014; Schwamb et al. 2013). These systems are composed of a stellar binary on an orbit with a typical period of 7.5 to 41 days orbited by a planetary companion on a much longer period ($\sim 50 - 250$ days). Interestingly, no transiting planets have been found around more compact stellar binaries ($\lesssim 7$ days period), although these binaries are abundant in nature and in Kepler eclipsing binary data (Raghavan et al. 2006, 2010; Tokovinin 2014b). Two main questions about circumbinary planets were addressed recently in the literature. One considered the apparent absence of circumbinary planets around compact stellar binary, and the other was about the configuration of the planetary orbit. Starting with the former, the formation of compact stellar binaries is often associated with dynamical evolution, which involves a tertiary (e.g., Naoz and Fabrycky 2014, and see below). In the context of this channel, it was suggested that the outer perturber that drives the two stars into a tight orbit may also impact the planetary companion around the inner two stars and may result

in a large eccentricity planetary orbit leading to ejection or colliding with the inner stars. However, circumbinary planets around compact binaries may still exist but they probably will end up to be misaligned with the inner stellar orbit (e.g. Hamers et al. 2015b; Martin et al. 2015; Muñoz and Lai 2015). In fact the misalignment can be generated simply due to eccentricity and inclination oscillations on the inner orbit, from a test particle as shown in Figure 4, (e.g., Martin and Triaud 2015b). Therefore, since many of the Kepler binary detections are eclipsing binaries, if a misaligned systems around the stellar systems were to exist, they are presently hidden from the current Kepler detection methods. This may imply that circumbinary planets are rather abundant, perhaps even more than planets around single stars (e.g., Armstrong et al. (2014); Martin et al. (2015); Martin and Triaud (2015a,b) but see, Deacon et al. (2015)).

5.3. Stellar systems

Most massive stars reside in a binary configuration ($\gtrsim 70\%$ for massive stars; see Raghavan et al. 2010). It seems that stellar binaries are responsible for diverse astrophysical phenomena, from Type Ia supernovae to X-ray binaries. However, observational campaigns have suggested that probably many of these binaries are in fact triples (e.g., Tokovinin 1997, 2008; Eggleton et al. 2007). Tokovinin (1997) showed that 40% of binary stars with period < 10 d in which the primary is a dwarf ($0.5 - 1.5 M_{\odot}$) have at least one additional companion. He found that the fraction of triples and higher multiples among binaries with period (10 – 100 d) is $\sim 10\%$. Moreover, Pribulla and Rucinski (2006) surveyed a sample of contact binaries, and noted that among 151 contact binaries brighter than 10 mag., $42 \pm 5\%$ are at least triple. Furthermore, a recent analysis of eclipse time variation curves of *Kepler* binaries showed that indeed a substantial fraction of these binaries have a third body (Borkovits et al. 2016). Thus, it seems that triple stars are abundant in our galaxy. From dynamical stability arguments these must be hierarchical triples, in which the (inner) binary is orbited by a third body on a much wider orbit.

Application of the secular hierarchical triple body system to triple stellar system was first considered by Harrington (1968, 1969). His work was motivated by Heintz (1967) that observed triple stellar systems with possible perturbations from the outer orbit. In this early work he already recognize the importance of the octupole level of approximation and expanded the Hamiltonian up to the octupole level of approximation. From the equations of motion he estimated a distribution for the inner orbit specific angular momentum $\sqrt{1 - e_1^2}$ to match the observed distribution of triples. Later, Mazeh and Shaham (1979) showed that tidal effects during eccentricity excitations of the Kozai-Lidov cycle can circularize and shrink the orbit.

During the system evolution, the their star can cause large eccentricity excitations for the inner orbit. Therefore, the nearly radial motion of the binary drives the two stars to merge, however, tidal forces tend to shrink and circularize the orbit. If during the evolution the quadrupole-level of approximation precession timescale is longer than the precession timescale associated with short range forces (such as tides, e.g., Eq. (61) or GR, e.g., Eq. (58)) further eccentricity excitations are suppressed. In this channel, tidal forces can shrink and circularize the inner orbit, forming a tight inner stellar binary decoupled from the tertiary. This process was studied in great length in the literature as a promising channel to explain triples and close binaries observations (e.g., Söderhjelm 1975; Soderhjelm 1982; Söderhjelm 1984; Kiseleva et al. 1998; Eggleton et al. 1998; Eggleton and Kiseleva-Eggleton 2001; Ford et al. 2000a; Fabrycky and Tremaine 2007; Perets

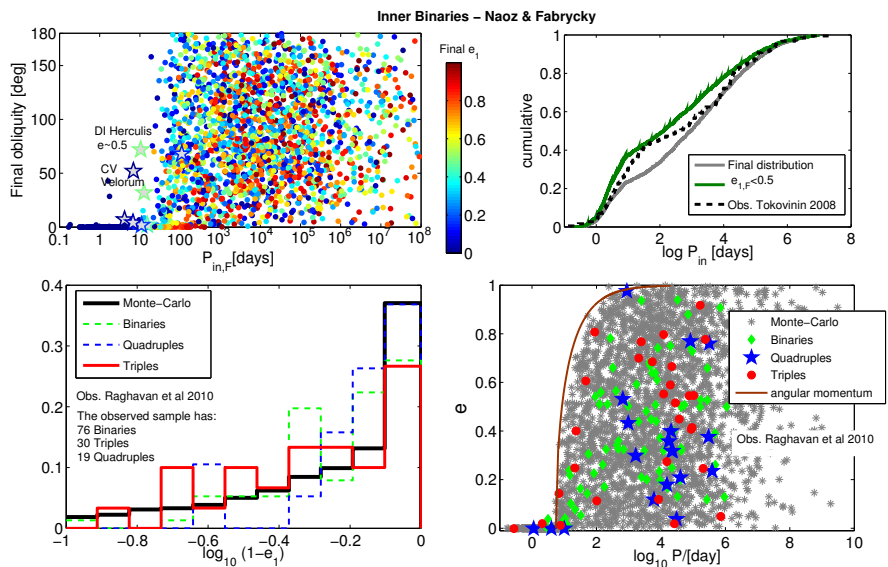


Figure 22

Simulated inner binary orbital configuration compared to observations. **Top right panel** the cumulative distribution of the observations distribution taken from Tokovinin (2008) public catalog (black dashed line), compared to the final distribution (grey solid line). Since the public catalog has typical inner orbital eccentricity of 0.5, the final distribution is also shown for system with $e_{1,F} < 0.5$ (green solid line). **Top left panel:** Final distribution of the spin orbit angle (i.e., the obliquity) of the primary Vs the final period of the inner orbit, the color code is the final eccentricity of the inner binary. We also plot the observations (Albrecht et al. 2009, 2011, 2013, 2014; Triaud et al. 2013; Harding et al. 2013; Zhou and Huang 2013). **Bottom left panel:** shows the inner orbit final eccentricity as a function of the final period. Over-plotted are observations adopted from Raghavan et al. (2010) public catalog. The solid line represents a constant angular momentum curve with a final binary period of 5.5 days. **Bottom right panel:** reproduction of the inner orbit specific angular momentum distribution considered first by Harrington (1968), compared to Raghavan et al. (2010) observations. The top two panels and the Monte-Carlo simulations are adopted from Naoz and Fabrycky (2014).

and Fabrycky 2009; Thompson 2011; Shappee and Thompson 2013; Naoz and Fabrycky 2014). We show here the updated inner orbit specific angular momentum simulated distribution compared to observations in Figure 22 bottom left panel, reproducing Harrington (1968, 1969) figure. Observations are taken from Raghavan et al. (2010) and Monte-Carlo simulations are adopted from Naoz and Fabrycky (2014) EKL triple star simulations.

Naoz and Fabrycky (2014) ran a large Monte-Carlo simulations, including the EKL mechanism, tides (as described in section 9) and general relativity, for 10Gyr of evolution producing the distribution for semi-major axis, eccentricity, inclination, and obliquity. The observed bimodal distribution of the inner orbit reported by Tokovinin (2008) public catalog (see Figure 22, top left panel) is reproduced by Naoz and Fabrycky (2014) simulations. Their Kolmogorov-Smirnov test does not reject the null hypothesis that the observed inner orbit period's distribution and the simulated one are from the same continuous distribution. Furthermore, they found that the simulated outer orbit distribution of the close binaries is consistent with the one from Tokovinin (2008) catalog of observed triples (e.g.,

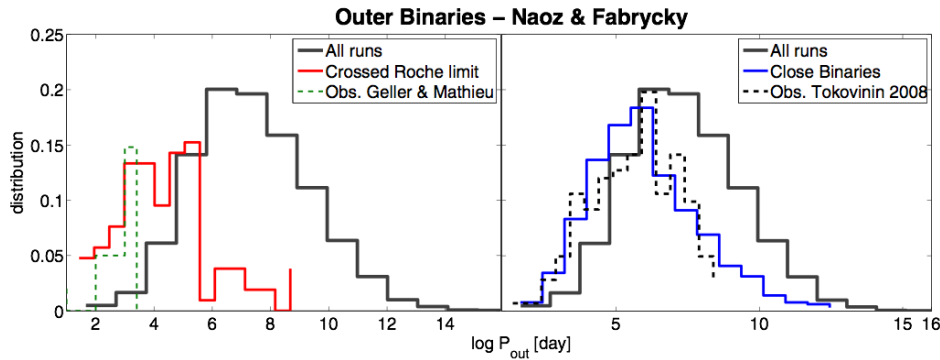


Figure 23

Simulated outer binary period compared to observations. *Right panel:* shows the period distribution of the companion of the close binaries (blue line), the latter defined to have periods shorter than ~ 16 days. Over-plotted is the observed distribution, scaled to match the theory lines, adopted from (Tokovinin 2008) public catalog. *Left panel:* shows the period of companions for the merged stellar population (red line) and the observed blue stragglers binary distribution of NGC 188 (Geller and Mathieu 2012), also scaled to match the theory lines. In both panels, grey lines represent the period distribution at the final stage of all of the outer companions in the Monte-Carlo runs. Figure adopted from Naoz and Fabrycky (2014).

Figure 23). Thus, they concluded that secular evolution in triple's plays an important role in shaping the distribution of these systems.

Tokovinin and Smekhov (2002) reported that wide binaries are more likely to have non-negligible eccentricity (see also Tokovinin & Kiyaveva 2015). For wide binaries in triple systems this seems to be in agreement with the dynamical eccentricity excitation from an outer perturber where tidal shrinking and circularization are less efficient (as can be seen in Figure 22 bottom left, adopted from Naoz and Fabrycky 2014). The systems near the constant angular momentum line (solid line in the Figure), may represent a population of migrating binaries due to tidal dissipation (as also seen in the *Kepler* binary stellar population, e.g., Dong et al. 2013). Furthermore, The formation channel of close stellar binaries via EKL and tides was suggested to somewhat suppress the likelihood of finding aligned circumbinary planets around tight stellar binaries (e.g. Hamers et al. 2015b; Martin et al. 2015; Muñoz and Lai 2015).

An interesting and promising observable for triple stellar dynamics may be the obliquity angle. As more binary stars obliquities are being observed, e.g., the BANANA survey (Albrecht et al. 2012a), and by other individual endeavors, the obliquity distribution may provide a key observable. During the tidal evolution the obliquity of the tight binaries will most likely decay to zero faster than the eccentricity. This results in systems that are close to the angular momentum line to have typically low obliquities (Naoz and Fabrycky 2014). This behavior is depicted in Figure 22 top left panel that shows that the final obliquity distribution of close binaries with moderate eccentricities (blue to yellow color) have moderate obliquities. Close circular inner binaries with non-negligible obliquities (> 10 deg) are found to have smaller spin periods (see also Levrard et al. 2007; Fabrycky et al. 2007). The simulated stellar obliquities shown in Figure 22 are consistent with the current available observations.

Strong gravitational perturbations can lead to mergers of the inner members, if the

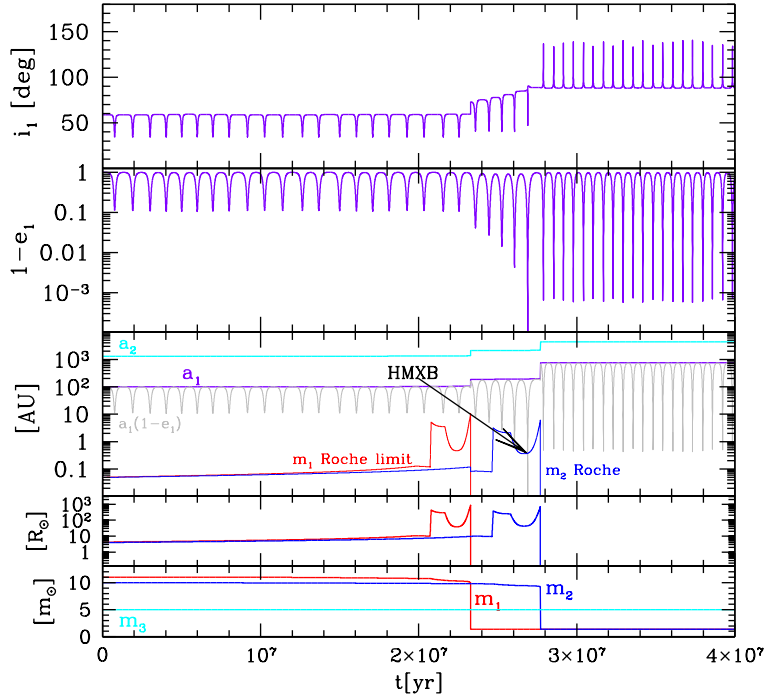


Figure 24

Re-triggering EKL by mass loss. This example produces a High Mass X-ray Binary (HMXB) or a supernova impostor. We show (top to bottom) the inner orbit inclination i_1 , the inner orbit eccentricity (depicted as $1 - e_1$), the semi-major axis of the inner (purple) and outer (cyan) orbit as well as the inner orbit peri-center and the two masses disruption distances (see Eq. (54) for a popular definition), the stellar radii and finally the bottom panel shows the masses of all three stars. This calculation includes solving the equations of the octupole-level of approximation, GR for both the inner and outer orbit, and stellar evolution according to SSE (Hurley et al. 2000), which includes mass loss and staler inflation. For simplicity the supernova was modeled here as a simple mass loss and assuming no kicks. Tidal evolutions were turned off for illustration purposes. A consequence of the first mass loss episode and the formation of a neutron star is that the initially small ϵ_M increased. This yields eccentricity excitations leading to Roche limit crossing as the m_2 star's radius inflates. This may result in a HMXB, or even a supernova impostor. The system parameters are set initially: $m_1 = 11 M_\odot$, $m_2 = 10 M_\odot$, $m_3 = 5 M_\odot$, $a_1 = 100$ AU, $a_2 = 1300$ AU, $e_1 = 0.001$, $e_2 = 0.6$, $\omega_1 = \omega_2 = 0$ and $i_{\text{tot}} = 79^\circ$. These parameters yield initial $\epsilon_M = 0.0034$. Naoz et al. (2015) discussed the formation scenario of low mass X-ray binaries via triple body evolution similarly to the example illustrated here.

tidal forces cannot react fast enough to stabilize the system (see for example Figure 16 right panel). In the previous section we discussed tidal disruptions of Hot Jupiters due to large eccentricity excitations. In the context of triple stellar systems, extreme values of the eccentricity which take place on shorter timescales than the short range forces (such as GR and tides, but still long to allow the system to remain secular), may lead to the merger of stellar binary. If sufficient time has past from the merger time (perhaps

at the order of Kelvin-Helmholtz timescale) this merger product may be identified as a blue straggler. Perets and Fabrycky (2009) envisioned a two-step process for which triple body interactions can form blue stragglers. In their study, three-body dynamics plus tidal dissipation created a close binary, and that binary subsequently merged by magnetic breaking or had unstable or efficient mass transfer. Naoz and Fabrycky (2014) suggested that large eccentricity excitation during the EKL evolution can lead to mergers. They found that their simulated outer orbital period distribution is consistent with observations for the companion of the merged population, adopted from Geller and Mathieu (2012), as depicted in Figure 23. This further emphasizes the notion that three body secular interactions may be the main channel for merged systems like blue stragglers.

Another interesting evidence for a merged system via perturbations from a distant perturber was recently found in the Galactic Center. Specifically, it seems that the object known as G2 (Gillessen et al. 2012) is a binary star in disguise (Witzel et al. 2014). Therefore, a similar mechanism to that of the formation of blue stragglers may operate in the Galactic center, where the massive black hole in the center of the galaxy causes large eccentricity excitations on a stellar binary in its vicinity (e.g., Antonini and Perets 2012; Prodan et al. 2015, Stephan et al. in Prep.).

The secular approximation allows for very long integration times where stellar evolution may play an important role (e.g. Perets and Kratter 2012; Shappee and Thompson 2013). In particular, systems that have inner binary members with close mass values (i.e., $m_1 \approx m_2$), the octupole level is suppressed (recall the definition of ϵ_M , Eq. (45), and Figure 12). However, stellar mass loss during post main sequence evolution can dramatically change the mass balance and re-trigger the EKL behavior (Shappee and Thompson 2013). This is because the semi-major axis changes proportional to the mass loss ratio, i.e., $a_f/a_i = m_f/m_i$, where the subscripts “f” and “i” refer to the final and initial values. Note that adiabatic mass loss conserves the value of the orbital eccentricity. Thus, the ϵ_M due to mass loss can change compared to the initial value (e.g., Shappee and Thompson 2013; Michaely and Perets 2014; Naoz et al. 2015)

$$\frac{\epsilon_{M,f}}{\epsilon_{M,i}} = \frac{m_{1,f} + m_2 + m_3}{m_{1,i} + m_2 + m_3} \left(\frac{m_{1,f} - m_2}{m_{1,i} - m_2} \right) \left(\frac{m_{1,i} + m_2}{m_{1,f} + m_2} \right)^2, \quad (66)$$

where for simplicity, for this equation, we assumed that only one mass will undergo mass loss ($m_{1,i} \rightarrow m_{1,f}$). Overall the absolute value of ϵ_M via this process increases. An example of this evolution is shown in Figure 24. The system is set initially with an inner binary composed with two similar mass stars. As the more massive star loses mass the new ϵ_M increased, according to Eq. (66) allowing for larger eccentricity excitations. When the stars inflate in radius as they leave the main sequence, the disruption distance associated with their Roche limit increases as well (e.g., Eq. (54)). The eccentricity excitations were too small to affect the orbit before the first neutron star was born. However, during the large eccentricities excitation after ϵ_M increased, the inflation in radius of the less massive star resulted in having this star crossing its Roche limit. This may form a high mass X-ray binary which may be associated with a supernova impostor (as suggested for a binary interaction for supernova 2010d a, e.g., Binder et al. 2011). Another possible outcome for this system is a Thorne-Żytkow object (e.g., Thorne and Zytkow 1975), which has distinct observational signatures (e.g., Levesque et al. 2014). Recently, Naoz et al. (2015) showed that triple dynamics can offer a possible formation channel to low mass X-ray binaries, while skipping the common envelope phase, and by that overcoming the challenges that arise with the standard formation scenario (for more details about the challenges in the

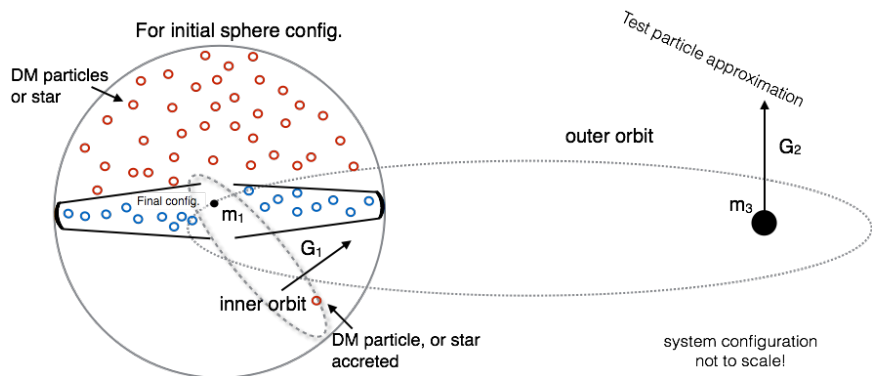


Figure 25

Cartoon description of the resulted torus-like configuration from EKL in

supermassive black hole binaries. The particles in a near-polar orbit, with respect to the black hole binary orbit, will undergo large eccentricity and inclination oscillations. This leads to such large eccentricities that will result in either tidal disruption events for stars (Li et al. 2015), or accretion of dark matter particles which may orbit the black hole (Naoz and Silk 2014).

standard formation see Podsiadlowski et al. 2003).

Shappee and Thompson (2013) suggested that re-triggering the EKL behavior via mass loss may facilitate the formation of close neutron star (NS)–white dwarf (WD) binaries (or other combination such as NS-NS, or WD-WD) without an initial common envelope phase. If compact objects such as double white dwarfs in triples find themselves in the right part of the parameter space, the above process may trigger large eccentricities, that can lead to grazing interactions or even collisions (recall that the approximation may break, yielding even larger eccentricities), which may promote Type Ia supernovae (e.g., Thompson 2011; Hamers et al. 2013; Prodan et al. 2013; Katz and Dong 2012; Kushnir et al. 2013; Dong et al. 2014).

5.4. Compact objects

With in the hierarchical galaxy formation paradigm, and the strong observational evidence that a high abundance of the local galaxies host supermassive black holes, one expects that major galaxy mergers should inevitably result in the formation of supermassive black hole binaries or multiples (e.g., Valtonen 1996; Di Matteo et al. 2005; Hoffman and Loeb 2007; Callegari et al. 2009; Dotti et al. 2012; Khan et al. 2012; Kulkarni and Loeb 2012). The evolution of these binaries highly depends on the conditions of the host galaxy. Numerical studies of spheroidal gas-poor galaxies suggest that these binaries can reach about a parsec separation and may stall there (e.g., Begelman et al. 1980; Milosavljević and Merritt 2001; Yu 2002). The effect of gravitational perturbations of supermassive black hole binaries on an ambient star cluster has been discussed in length in the literature (e.g., Wen 2003; Miller and Hamilton 2002; Blaes et al. 2002; Ivanov et al. 2005; Chen et al. 2009, 2011; Gualandris and Merritt 2009; Iwasawa et al. 2011; Sesana et al. 2011; Gualandris and Merritt 2012; Madigan and Levin 2012; Meiron and Laor 2013; Antonini et al. 2014; Bode and Wegg 2014; Wang et al. 2014; Naoz and Silk 2014; Li et al. 2015). In particular, it was suggested that the three body interactions may play an important role in both the growth of black

holes at the centers of dense star clusters by increasing the tidal directions event rate of stars. It was also shown that interactions with the surrounding stars can either increase or decrease the eccentricity of the supermassive black hole binaries depending on the fraction of counter-rotating to co-rotating stars. Furthermore, the presence of supermassive black holes may increase the stellar tidal disruption event rate and even lead to a torus-like configuration of stars (or dark matter particles) around one of the black holes (see Figure 25). The supermassive black hole binary can also lead to an eccentric or ejected population of stars from the cluster.

For a supermassive black hole binaries embedded in a dense stellar environment, such as the one in the Galactic Center, other physical processes may affect the precession of a star around the primary black hole. Similarly to the short range forces discussed in Section 4, if the extra precession takes place in an opposite direction to that induced due to the EKL mechanism, and it takes place on shorter timescale than t_{quad} eccentricity excitations may be suppressed. These physical processes may include (but not limited to) precession caused by the stellar potential, scalar resonant relaxation or reorientation of the orbital plane due to vector resonant relaxation (Kocsis and Tremaine 2011, 2015) or Lense-Thirring precession (Merritt et al. 2010; Merritt and Vasiliev 2012). For the EKL mechanism of supermassive black hole binaries embedded in a dense stellar environment, Li et al. (2015) found that precession caused by the stellar potential and GR may have large effects on the dynamics while the others (such as tidal effects, scalar and vector resonant relaxation, and LenseThirring precession) are typically less important.

A dissipation mechanism which may play an important role when black holes (or other compact objects) are involved is gravitational wave (GW) emission. In this scenario, black hole binary high orbital eccentricity induced by the outer perturber can lead to a more efficient merger rate, due to GW emission (e.g., Blaes et al. 2002). GW emission can also lead to the formation of extreme mass ratio binaries, such as supermassive black hole and a stellar mass black hole, or any other test particle, on a tight orbit (e.g., Bode and Wegg 2014). Considering the dynamical evolution of compact objects in the presence of an outer perturber, large eccentricities induced by the perturber can lead to a close approach between the two compact objects such that GW emission will decay their orbital separation (e.g., Wen 2003; Miller and Hamilton 2002; Antonini and Perets 2012; Seto 2013). This perhaps can lead to a detectable signal using LIGO5 and VIRGO6 (e.g., Wen (2003) and Naoz et al. (2013b), but see Mandel et al. (2008) and O’Leary et al. (2006)). Since GW emission associated with eccentric orbits is stronger and have a very different spectrum relative to their circular counterparts, it was suggested that using the GW information emitted by the close binary, it might be possible to constrain the mass or distance of the third body (e.g., Yunes et al. 2011; Galaviz and Brügmann 2011).

Recently it was also suggested that black hole -low-mass X-ray binaries (BH-LMXBs) may form via EKL mechanism (Naoz et al. 2015). During the dynamical evolution of the triple system, the EKL mechanism can cause large eccentricity excitations on the LMXB progenitor, resulting BH-LMXB candidate, while skipping the common-envelope phase. Interestingly, a substantial number of close binaries with an accreting compact object, e.g., LMXBs and their descendants (e.g., millisecond radio pulsars), are known or suspected triples (Grindlay et al. 1988; Thorsett et al. 1999; Rasio 2001; Sigurdsson et al. 2003; Chou and Grindlay 2001; Zdziarski et al. 2007; Prodan and Murray 2012; Prodan et al. 2015).

6. Beyond the three body secular approximation

There are different channels to consider when going beyond the secular approximation. The first is to consider the validity of the approximation discussed in Section 3. In other words allowing for more compact systems (e.g., $\epsilon > 0.1$, Equation (52)) which means considering the implications of having changes in the angular momentum on short timescale compared to the orbital timescale (e.g., Equation (49)). The second is to allow for higher multiples.

Considering compact systems, a popular application of the three body interaction is the merger of two white dwarfs to prompt the so called double degenerate type Ia supernova. It was suggested that double degenerate type Ia supernova may represents a substantial fraction (if not all) of the type Ia supernovae. Observational evidences for this may lay in distribution of times between star formation and the type Ia supernova explosion, usually called the delay-time distribution, that seems to favor the double degenerate scenario (e.g., Maoz et al. 2014) or in the lack of hydrogen lines that are expected in the single degenerated (white dwarf with a stellar companion) scenario (e.g., Shappee et al. 2013). There are different theoretical models that address the double degenerate type Ia supernova formation. In the context of triple body interactions it was suggested that the large eccentricities associated with the EKL mechanism can lead to double degenerate type Ia supernova (e.g., Thompson 2011; Hamers et al. 2013; Prodan et al. 2013). Considering more compact systems, the inner orbit specific angular momentum is likely to reach almost zero (i.e., an almost radial motion) on timescales at the order of the inner orbit period (see Section 3) causing the collision of two white dwarfs and resulting in type Ia supernova (e.g., Katz and Dong 2012; Kushnir et al. 2013; Dong et al. 2014).

Another interesting astrophysical application for the insight gained in the triple study is by considering higher multiples. There are of course many ways to address high multiple interaction. The first is to consider a scattering, short time scale, event, which has been discussed in length in the literature (e.g., Hut and Bahcall 1983; Rasio and Ford 1996b; Chatterjee et al. 2008; Nagasawa et al. 2008; Antognini and Thompson 2015). In a stable system, which does not undergo a scattering event, the additional fourth (or more) companion can have large effects on the eccentricity and inclination evolution. In particular it can help tapping into large parts of the parameter space (e.g., Takeda et al. 2008; Touma et al. 2009; Pejcha et al. 2013; Boué and Fabrycky 2014a; Hamers et al. 2015a), and affect the spin orbit evolution (e.g., Li et al. 2014c; Boué and Fabrycky 2014b). A consequence of the latter effect is that circumbinary planets may be misaligned (e.g. Hamers et al. 2015b; Martin et al. 2015; Muñoz and Lai 2015). In the context of the secular approximation, the Gauss averaging method can be utilized for N number of stable orbits (e.g. Touma et al. 2009). This method is a phase-averaged calculation for which the gravitational interactions between non-resonant orbits are equivalent in treating the orbits as massive wires interacting with each other, where the line-density is inversely proportional to the orbital velocity. As explained above, a consequence of the secular approximation is that the semi-major axes of the wires are constants of motion (e.g., Murray and Dermott 2000). In general this method can be used to explore different many body secular effects, for example the evolution of a particle disk in the presence of a perturber (Batygin 2012).

7. Summary

The high abundance of hierarchical triple systems in nature motivates the investigation of their dynamics. Furthermore, this approximation seems to be very useful in addressing a variety of puzzles and systems that are observe, such as retrograde Hot Jupiters, blue

stragglers, low and high mass X-ray binaries, compact object binaries, double degenerate type Ia supernova etc. Building on the physical understandings gained in the past years in this subject, motivates us to go beyond the approximation for an even wider range of applications.

The recent theoretical developments can be summarized by the following:

- The z-component of the angular momentum of the inner and outer orbits (i.e., the nominal $\sqrt{1 - e_{1,2}^2} \cos i_{1,2}$) are only conserved if one of the binary members is a test particle and the outer orbit is axisymmetric ($e_2 = 0$).
- Relaxing any of these assumptions may lead to high order resonances characterized by large eccentricity excitations and flips of the orbital orientation as well as chaotic behavior.
- These high order resonances allow the system to tap into larger parts of the initial parameter space for which the EKL mechanism is triggered.
- Short range forces and other physical processes (such as GR and stellar mass loss) can also re-trigger the EKL mechanism for systems that did not exhibit these dynamics in the point mass approximation.

The field continues to developed and to go beyond three body systems and the secular or hierarchical approximations. These improvements allow for the application to, and the understanding of, a larger variety of systems. The intuition and insight that the Eccentric Kozai-Lidov mechanism has provided is utilized for these approaches.

DISCLOSURE STATEMENT

The author is not aware of any affiliations, memberships, funding, or financial holdings that might be perceived as affecting the objectivity of this review.

ACKNOWLEDGMENTS

I greatly thank Fred Rasio, Brad Hansen, Gongjie Li and Diego Munoz for useful comments. I also thank the referee Ruth Murray-Clay, for reading the review thoroughly and providing useful suggestions. Furthermore, I deeply thank Alexander Stephan for reading the draft in great details. I thank J. Antognini, B. Katz, G. Li, B. Liu, C. Petrovich, J. Teyssandier, for sharing figures. I acknowledge the partial support from the Sloan Foundation Research Fellowships as well as the Annie Jump Cannon Prize.

8. Supplemental Material - The secular equations

The full octupole-order equations of motion for the most general case (i.e., relaxing the test particle and axisymmetric potential approximations) presented in Naoz et al. (2013a) are reiterated here for completeness. We begin with reminding the reader of the definitions of a few useful parameters:

$$\begin{aligned} C_3 &= -\frac{15}{16} \frac{k^4}{4} \frac{(m_1 + m_2)^9}{(m_1 + m_2 + m_3)^4} \frac{m_3^9 (m_1 - m_2)}{(m_1 m_2)^5} \frac{L_1^6}{L_2^3 G_2^5} \\ &= -C_2 \frac{15}{4} \frac{\epsilon_M}{e_2} \end{aligned} \quad (67)$$

where

$$\epsilon_M = \frac{m_1 - m_2}{m_1 + m_2} \frac{a_1}{a_2} \frac{e_2}{1 - e_2^2} \quad (68)$$

and

$$A = 4 + 3e_1^2 - \frac{5}{2}B \sin i_{\text{tot}}^2, \quad (69)$$

where

$$B = 2 + 5e_1^2 - 7e_1^2 \cos(2\omega_1), \quad (70)$$

and

$$\cos \phi = -\cos \omega_1 \cos \omega_2 - \cos i_{\text{tot}} \sin \omega_1 \sin \omega_2. \quad (71)$$

As shown in Naoz et al. (2013a) elimination of the nodes (i.e., setting $\Omega_1 - \Omega_2 = \pi$) can be done as long as one does not conclude that the conjugate z-component of the angular momenta (H_1 and H_2) are constant of motion. The partial derivatives with respect to the other coordinates and momenta are not affected by the substitution $\Omega_1 - \Omega_2 = \pi$. In that case, the time evolution of H_1 and H_2 (and thus i_1 and i_2) can be derived from the total angular momentum conservation. The doubly averaged Hamiltonian after eliminating the nodes:

$$\begin{aligned} \mathcal{H}(\Delta h \rightarrow \pi) = & C_2 \{ (2 + 3e_1^2) (3 \cos^2 i_{\text{tot}} - 1) \\ & + 15e_1^2 \sin^2 i_{\text{tot}} \cos(2\omega_1) \} \\ & + C_3 e_1 e_2 \{ A \cos \phi \\ & + 10 \cos i_{\text{tot}} \sin^2 i_{\text{tot}} (1 - e_1^2) \sin \omega_1 \sin \omega_2 \}. \end{aligned} \quad (72)$$

The time evolution of the argument of periapse for the inner and outer orbits are given by:

$$\begin{aligned} \dot{\omega}_1 = & 6C_2 \left\{ \frac{1}{G_1} [4 \cos^2 i_{\text{tot}} + (5 \cos(2\omega_1) - 1)] \right. \\ & \times (1 - e_1^2 - \cos^2 i_{\text{tot}}) + \frac{\cos i_{\text{tot}}}{G_2} [2 + e_1^2 (3 - 5 \cos(2\omega_1))] \left. \right\} \\ & - C_3 e_2 \left\{ e_1 \left(\frac{1}{G_2} + \frac{\cos i_{\text{tot}}}{G_1} \right) \right. \\ & \times [\sin \omega_1 \sin \omega_2 (10(3 \cos^2 i_{\text{tot}} - 1)(1 - e_1^2) + A) \\ & - 5B \cos i_{\text{tot}} \cos \phi] - \frac{1 - e_1^2}{e_1 G_1} \times [\sin \omega_1 \sin \omega_2 \\ & \times 10 \cos i_{\text{tot}} \sin i_{\text{tot}}^2 (1 - 3e_1^2) \\ & \left. + \cos \phi (3A - 10 \cos i_{\text{tot}}^2 + 2)] \right\}, \end{aligned} \quad (73)$$

and

$$\begin{aligned} \dot{\omega}_2 = & 3C_2 \left\{ \frac{2 \cos i_{\text{tot}}}{G_1} [2 + e_1^2 (3 - 5 \cos(2\omega_1))] \right. \\ & \left. + \frac{1}{G_2} [4 + 6e_1^2 + (5 \cos^2 i_{\text{tot}} - 3)(2 + e_1^2 (3 - 5 \cos(2\omega_1)))] \right\} \\ & + C_3 e_1 \left\{ \sin \omega_1 \sin \omega_2 \left(\frac{4e_2^2 + 1}{e_2 G_2} 10 \cos i_{\text{tot}} \sin^2 i_{\text{tot}} (1 - e_1^2) \right. \right. \\ & \left. \left. - e_2 \left(\frac{1}{G_1} + \frac{\cos i_{\text{tot}}}{G_2} \right) [A + 10(3 \cos^2 i_{\text{tot}} - 1)(1 - e_1^2)] \right) \right. \\ & \left. + \cos \phi \left[5B \cos i_{\text{tot}} e_2 \left(\frac{1}{G_1} + \frac{\cos i_{\text{tot}}}{G_2} \right) + \frac{4e_2^2 + 1}{e_2 G_2} A \right] \right\} \end{aligned} \quad (74)$$

The time evolution of the longitude of ascending nodes is given by:

$$\begin{aligned}\dot{\Omega}_1 = & -\frac{3C_2}{G_1 \sin i_1} (2 + 3e_1^2 - 5e_1^2 \cos(2\omega_1)) \sin(2i_{\text{tot}}) \\ & - C_3 e_1 e_2 [5B \cos i_{\text{tot}} \cos \phi \\ & - A \sin \omega_1 \sin \omega_2 + 10(1 - 3 \cos^2 i_{\text{tot}}) \\ & \times (1 - e_1^2) \sin \omega_1 \sin \omega_2] \frac{\sin i_{\text{tot}}}{G_1 \sin i_1},\end{aligned}\quad (75)$$

where in the last part we have used again the law of sines for which $\sin i_1 = G_2 \sin i_{\text{tot}}/G_{\text{tot}}$. The evolution of the longitude of ascending nodes for the outer orbit can be easily obtained using:

$$\dot{\Omega}_2 = \dot{\Omega}_1 . \quad (76)$$

The evolution of the inner and outer eccentricities is:

$$\begin{aligned}\dot{e}_1 = & C_2 \frac{1 - e_1^2}{G_1} [30e_1 \sin^2 i_{\text{tot}} \sin(2\omega_1)] \\ & + C_3 e_2 \frac{1 - e_1^2}{G_1} [35 \cos \phi \sin^2 i_{\text{tot}} e_1^2 \sin(2\omega_1) \\ & - 10 \cos i_{\text{tot}} \sin^2 i_{\text{tot}} \cos \omega_1 \sin \omega_2 (1 - e_1^2) \\ & - A(\sin \omega_1 \cos \omega_2 - \cos i_{\text{tot}} \cos \omega_1 \sin \omega_2)] ,\end{aligned}\quad (77)$$

and

$$\begin{aligned}\dot{e}_2 = & -C_3 e_1 \frac{1 - e_2^2}{G_2} [10 \cos(i_{\text{tot}}) \sin^2(i_{\text{tot}}) (1 - e_1^2) \sin \omega_1 \cos \omega_2 \\ & + A(\cos \omega_1 \sin \omega_2 - \cos(i_{\text{tot}}) \sin \omega_1 \cos \omega_2)] .\end{aligned}\quad (78)$$

The angular momenta derivatives of the inner and outer orbits as a function of time can be easily calculated, where for the inner orbit we write:

$$\begin{aligned}\dot{G}_1 = & -C_2 30e_1^2 \sin(2\omega_1) \sin^2(i_{\text{tot}}) + C_3 e_1 e_2 (\\ & - 35e_1^2 \sin^2(i_{\text{tot}}) \sin(2\omega_1) \cos \phi + A[\sin \omega_1 \cos \omega_2 \\ & - \cos(i_{\text{tot}}) \cos \omega_1 \sin \omega_2] \\ & + 10 \cos(i_{\text{tot}}) \sin^2(i_{\text{tot}}) [1 - e_1^2] \cos \omega_1 \sin \omega_2) ,\end{aligned}\quad (79)$$

and for the outer orbit (where the quadrupole term is zero)

$$\begin{aligned}\dot{G}_2 = & C_3 e_1 e_2 [A\{\cos \omega_1 \sin \omega_2 - \cos(i_{\text{tot}}) \sin \omega_1 \cos \omega_2\} \\ & + 10 \cos(i_{\text{tot}}) \sin^2(i_{\text{tot}}) [1 - e_1^2] \sin \omega_1 \cos \omega_2] .\end{aligned}\quad (80)$$

Also the z-component of the inner orbit angular momentum is

$$\dot{H}_1 = \frac{G_1}{G_{\text{tot}}} \dot{G}_1 - \frac{G_2}{G_{\text{tot}}} \dot{G}_2 , \quad (81)$$

where using the law of sines we write:

$$\dot{H}_1 = \frac{\sin i_2}{\sin i_{\text{tot}}} \dot{G}_1 - \frac{\sin i_1}{\sin i_{\text{tot}}} \dot{G}_2 . \quad (82)$$

Because the total angular momentum is conserved $G_{\text{tot}} = \text{Const.} = H_1 + H_2$ the outer orbit z-component time evolution is simply $\dot{H}_2 = -\dot{H}_1$. The inclinations equation of motion is

$$(\cos i_1) = \frac{\dot{H}_1}{G_1} - \frac{\dot{G}_1}{G_1} \cos i_1 , \quad (83)$$

and

$$(\cos i_2) = \frac{\dot{H}_2}{G_2} - \frac{\dot{G}_2}{G_2} \cos i_2 . \quad (84)$$

9. Supplemental Material - Static tides equations

Tidal interaction considered in this review are limited to the inner orbit members equilibrium and static tides formalism (e.g., Hut 1980; Eggleton et al. 1998; Kiseleva et al. 1998; Eggleton and Kiseleva-Eggleton 2001). A compact representation of the tidal interactions equation can be found when using the Laplace- Runge-Lenz vector system. In this system the three vector base is composed from the inner orbit eccentricity vector \mathbf{e}_1 the specific angular momentum vector

$$\mathbf{J}_1 = \sqrt{K^2(m_1 + m_2)a_1(1 - e_1^2)}\hat{\mathbf{J}}_1 = \mathbf{G}_1(m_1 + m_2)/(m_1m_2) . \quad (85)$$

The vector $\hat{\mathbf{q}} = \hat{\mathbf{J}}_1 \times \hat{\mathbf{e}}_1$ completes the right-hand triad of unit vectors $(\hat{\mathbf{q}}, \hat{\mathbf{J}}_1, \hat{\mathbf{e}}_1)$. Each of the inner member masses have a spin vector $\boldsymbol{\Omega}_{s1}$ and $\boldsymbol{\Omega}_{s2}$, respectively. The time evolution equations are (where subscript 1 and 2 refer to masses m_1 and m_2):

$$\frac{1}{e_1} \frac{d\mathbf{e}_1}{dt} = (Z_1 + Z_2)\hat{\mathbf{q}} - (Y_1 + Y_2)\hat{\mathbf{J}}_1 - (V_1 + V_2)\hat{\mathbf{e}}_1 , \quad (86)$$

$$\frac{1}{J_1} \frac{d\mathbf{J}_1}{dt} = -(X_1 + X_2)\hat{\mathbf{q}} - (W_1 + W_2)\hat{\mathbf{J}}_1 + (Y_1 + Y_2)\hat{\mathbf{e}}_1 , \quad (87)$$

$$I_1 \frac{d\boldsymbol{\Omega}_{s1}}{dt} = \mu J_1 (X_1 \hat{\mathbf{q}} + W_1 \hat{\mathbf{J}}_1 - Y_1 \hat{\mathbf{e}}_1) , \quad (88)$$

$$I_2 \frac{d\boldsymbol{\Omega}_{s2}}{dt} = \mu J_1 (X_2 \hat{\mathbf{q}} + W_2 \hat{\mathbf{J}}_1 - Y_2 \hat{\mathbf{e}}_1) , \quad (89)$$

where $\mu = m_1 m_2 / (m_1 + m_2)$ is the reduced mass, I_1 (I_2) is the moment of inertia of mass m_1 (m_2). The vector (X, Y, Z) is the angular velocity of the $(\hat{\mathbf{q}}, \hat{\mathbf{J}}_1, \hat{\mathbf{e}}_1)$ frame and can be easily related to the Delaunay's elements in the invariable plan as (Eggleton et al. 1998):

$$X = \frac{di_1}{dt} \cos \omega_1 + \frac{d\Omega_1}{dt} \sin \omega_1 \sin i_1 , \quad (90)$$

$$Y = -\frac{di_1}{dt} \sin \omega_1 + \frac{d\Omega_1}{dt} \cos \omega_1 \sin i_1 , \quad (91)$$

$$Z = \frac{d\omega_1}{dt} + \frac{d\Omega_1}{dt} \cos i_1 \quad (92)$$

This set of equations gives the precession rate due to tides $d\omega_1/dt$ as well as how the other Delaunay's elements vary with time. We note that these equations (86)-(89) are identical to that of Eggleton and Kiseleva-Eggleton (2001) and Fabrycky and Tremaine (2007), up to the gravitational influence of the third body which they described by the tensor \mathbf{S} . In our formalism its redundant. The functional form of W, V, X, Y and Z were given in Eggleton and Kiseleva-Eggleton (2001) and are simply:

$$V_1 = \frac{9}{t_{F1}} \left(\frac{1 + 15e_1^2/4 + 15e_1^4/8 + 5e_1^6/64}{(1 - e_1^2)^{13/2}} - \frac{11\Omega_{s1,J}}{18n} \frac{1 + 3e_1^2/2 + e_1^4/8}{(1 - e_1^2)^5} \right) , \quad (93)$$

$$W_1 = \frac{1}{t_{F1}} \left(\frac{1 + 15e_1^2/2 + 45e_1^4/8 + 5e_1^6/16}{(1 - e_1^2)^{13/2}} - \frac{11\Omega_{s1,J}}{n} \frac{1 + 3e_1^2 + 3e_1^4/8}{(1 - e_1^2)^5} \right), \quad (94)$$

$$X_1 = -\frac{m_2 k_1 R_1^5}{\mu n a_1^5} \frac{\Omega_{s1,J} \Omega_{s1,e}}{(1 - e_1^2)^2} - \frac{\Omega_{s1,q}}{2n t_{F1}} \frac{1 + 9e_1^2/2 + 5e_1^4/8}{(1 - e_1^2)^5}, \quad (95)$$

$$Y_1 = -\frac{m_2 k_1 R_1^5}{\mu n a_1^5} \frac{\Omega_{s1,J} \Omega_{s1,q}}{(1 - e_1^2)^2} + \frac{\Omega_{s1,e}}{2n t_{F1}} \frac{1 + 3e_1^2/2 + e_1^4/8}{(1 - e_1^2)^5}, \quad (96)$$

$$Z_1 = \frac{m_2 k_1 R_1^5}{\mu n a_1^5} \left(\frac{2\Omega_{s1,J}^2 - \Omega_{s1,q}^2 - \Omega_{1s,e}^2}{2(1 - e_1^2)^2} + \frac{15k^2 m_2}{a_1^3} \frac{1 + 3e_1^2/2 + e_1/8}{(1 - e_1^2)^5} \right), \quad (97)$$

where the expression for mass m_2 can be easily found by replacing subscript 1 with 2. The mean motion is

$$n = \frac{2\pi}{P_1} = \sqrt{\frac{k^2(m_1 + m_2)}{a_1^3}}. \quad (98)$$

also, k_1 is classical apsidal motion constant, which is a measure of quadrupolar deformability, and related to the Love parameter of mass m_1 by $k_L = 2k_1$. It also related to Eggleton and Kiseleva-Eggleton (2001) coefficient Q_E by

$$k_1 = \frac{1}{2} \frac{Q_E}{1 - Q_E}. \quad (99)$$

The tidal friction timescale can be expressed in terms of the viscous timescale t_{V1} (which is assume dot be constant in the tides applications in this review):

$$t_{F1} = \frac{t_{V1}}{9} \left(\frac{a_1}{R_1} \right)^8 \frac{m_1^2}{(m_1 + m_2)m_2} \frac{1}{(1 + 2k_1)^2}, \quad (100)$$

and similar equation for t_{F2} can be found by replacing 1 with 2. This formalism describes viscosity that causes the tidal bulge to lag the instantaneous direction of the companion by a constant angle $1/(2Q)$ at constant time interval. The quality factor Q can be expressed as a function of viscous timescale as well by (e.g., Fabrycky and Tremaine 2007; Hansen 2010)

$$Q = \frac{4}{3} \frac{k_1}{(1 + 2k_1)^2} \frac{k^2 m_1}{R_1^3} \frac{t_{V1}}{n}. \quad (101)$$

LITERATURE CITED

- Albrecht, S., S. Reffert, I. A. G. Snellen, and J. N. Winn, 2009: Misaligned spin and orbital axes cause the anomalous precession of DIHerculis. *Nature*, **461**, 373–376.
- Albrecht, S., J. Setiawan, G. Torres, D. C. Fabrycky, and J. N. Winn, 2013: The BANANA Project. IV. Two Aligned Stellar Rotation Axes in the Young Eccentric Binary System EPCrucis: Primordial Orientation and Tidal Alignment. *ApJ*, **767**, 32.
- Albrecht, S., J. N. Winn, J. A. Carter, I. A. G. Snellen, and E. J. W. de Mooij, 2011: The Banana Project. III. Spin-Orbit Alignment in the Long-period Eclipsing Binary NY Cephei. *ApJ*, **726**, 68.
- Albrecht, S., J. N. Winn, D. C. Fabrycky, G. Torres, and J. Setiawan, 2012a: The BANANA Survey: Spin-Orbit Alignment in Binary Stars. In Richards, M. T. and I. Hubeny, eds., *IAU Symposium*, vol. 282 of *IAU Symposium*, pp. 397–398.
- Albrecht, S., J. N. Winn, J. A. Johnson, A. W. Howard, G. W. Marcy, R. P. Butler, P. Arriagada, J. D. Crane, S. A. Shectman, I. B. Thompson, T. Hirano, G. Bakos, and J. D. Hartman, 2012b: Obliquities of Hot Jupiter host stars: Evidence for tidal interactions and primordial misalignments. *ArXiv e-prints*.

- Albrecht, S., J. N. Winn, G. Torres, D. C. Fabrycky, J. Setiawan, M. Gillon, E. Jehin, A. Triaud, D. Queloz, I. Snellen, and P. Eggleton, 2014: The BANANA project. V. Misaligned and precessing stellar rotation axes in CV Velorum. *ArXiv e-prints*.
- Antognini, J. M., B. J. Shappee, T. A. Thompson, and P. Amaro-Seoane, 2014: Rapid eccentricity oscillations and the mergers of compact objects in hierarchical triples. *MNRAS*, **439**, 1079–1091.
- Antognini, J. M. O., 2015: Timescales of Kozai-Lidov oscillations at quadrupole and octupole order in the test particle limit. *ArXiv e-prints*.
- Antognini, J. M. O. and T. A. Thompson, 2015: Dynamical formation - scattering of hierarchical triples: Cross sections, Kozai-Lidov oscillations, and collisions. *ArXiv e-prints*.
- Antonini, F., N. Murray, and S. Mikkola, 2014: Black Hole Triple Dynamics: A Breakdown of the Orbit Average Approximation and Implications for Gravitational Wave Detections. *ApJ*, **781**, 45.
- Antonini, F. and H. B. Perets, 2012: Secular Evolution of Compact Binaries near Massive Black Holes: Gravitational Wave Sources and Other Exotica. *ApJ*, **757**, 27.
- Armstrong, D. J., H. P. Osborn, D. J. A. Brown, F. Faedi, Y. Gómez Maqueo Chew, D. V. Martin, D. Pollacco, and S. Udry, 2014: On the abundance of circumbinary planets. *MNRAS*, **444**, 1873–1883.
- Bailey, M. E., J. E. Chambers, and G. Hahn, 1992: Origin of sungrazers - A frequent cometary end-state. *A&A*, **257**, 315–322.
- Baron, F., J. D. Monnier, E. Pedretti, M. Zhao, G. Schaefer, R. Parks, X. Che, N. Thureau, T. A. ten Brummelaar, H. A. McAlister, S. T. Ridgway, C. Farrington, J. Sturmann, L. Sturmann, and N. Turner, 2012: Imaging the Algol Triple System in the H Band with the CHARA Interferometer. *ApJ*, **752**, 20.
- Batygin, K., 2012: A primordial origin for misalignments between stellar spin axes and planetary orbits. *Nature*, **491**, 418–420.
- Batygin, K., A. Morbidelli, and K. Tsiganis, 2011: Formation and evolution of planetary systems in presence of highly inclined stellar perturbers. *A&A*, **533**, A7.
- Begelman, M. C., R. D. Blandford, and M. J. Rees, 1980: Massive black hole binaries in active galactic nuclei. *Nature*, **287**, 307–309.
- Binder, B., B. F. Williams, A. K. H. Kong, T. J. Gaetz, P. P. Plucinsky, J. J. Dalcanton, and D. R. Weisz, 2011: Chandra Detection of SN 2010da Four Months After Outburst: Evidence for a High-mass X-Ray Binary in NGC 300. *ApJ*, **739**, L51.
- Blaes, O., M. H. Lee, and A. Socrates, 2002: The Kozai Mechanism and the Evolution of Binary Supermassive Black Holes. *ApJ*, **578**, 775–786.
- Bode, J. N. and C. Wegg, 2014: Production of EMRIs in supermassive black hole binaries. *MNRAS*, **438**, 573–589.
- Borkovits, T., T. Hajdu, J. Sztakovics, S. Rappaport, A. Levine, I. B. Bíró, and P. Klagyivik, 2016: A comprehensive study of the Kepler triples via eclipse timing. *MNRAS*, **455**, 4136–4165.
- Boué, G. and D. C. Fabrycky, 2014a: Compact Planetary Systems Perturbed by an Inclined Companion. I. Vectorial Representation of the Secular Model. *ApJ*, **789**, 110.
- , 2014b: Compact Planetary Systems Perturbed by an Inclined Companion. II. Stellar Spin-Orbit Evolution. *ApJ*, **789**, 111.
- Brouwer, D., 1959: Solution of the problem of artificial satellite theory without drag. *AJ*, **64**, 378–+.
- Callegari, S., L. Mayer, S. Kazantzidis, M. Colpi, F. Governato, T. Quinn, and J. Wadsley, 2009: Pairing of Supermassive Black Holes in Unequal-Mass Galaxy Mergers. *ApJ*, **696**, L89–L92.
- Carruba, V., J. A. Burns, P. D. Nicholson, and B. J. Gladman, 2002: On the Inclination Distribution of the Jovian Irregular Satellites. *Icarus*, **158**, 434–449.
- Chambers, J. E. and F. Migliorini, 1997: Mercury - A New Software Package for Orbital Integrations. In *AAS/Division for Planetary Sciences Meeting Abstracts #29*, vol. 29 of *Bulletin of the American Astronomical Society*, pp. 1024–+.
- Chatterjee, S., E. B. Ford, S. Matsumura, and F. A. Rasio, 2008: Dynamical Outcomes of Planet-

- Planet Scattering. *ApJ*, **686**, 580–602.
- Chen, X., P. Madau, A. Sesana, and F. K. Liu, 2009: Enhanced Tidal Disruption Rates from Massive Black Hole Binaries. *ApJ*, **697**, L149–L152.
- Chen, X., A. Sesana, P. Madau, and F. K. Liu, 2011: Tidal Stellar Disruptions by Massive Black Hole Pairs. II. Decaying Binaries. *ApJ*, **729**, 13.
- Chirikov, B. V., 1979: A universal instability of many-dimensional oscillator systems. *Phys. Rep.*, **52**, 263–379.
- Chou, Y. and J. E. Grindlay, 2001: Binary and Long-Term (Triple?) Modulations of 4U 1820-30 in NGC 6624. *The Astrophysical Journal*, **563(2)**, 934–940.
- Cochran, W. D., A. P. Hatzes, R. P. Butler, and G. W. Marcy, 1996: Detection of a planetary companion to 16 Cygni B. In *Bulletin of the American Astronomical Society*, vol. 28 of *Bulletin of the American Astronomical Society*, p. 1111.
- Correia, A. C. M., J. Laskar, F. Farago, and G. Boué, 2011: Tidal evolution of hierarchical and inclined systems. *ArXiv e-prints*.
- Ćuk, M. and J. A. Burns, 2004: On the Secular Behavior of Irregular Satellites. *AJ*, **128**, 2518–2541.
- Dawson, R. I. and E. Chiang, 2014: A class of warm Jupiters with mutually inclined, apsidally misaligned close friends. *Science*, **346**, 212–216.
- Deacon, N. R., A. L. Kraus, A. W. Mann, E. A. Magnier, K. C. Chambers, R. J. Wainscoat, J. L. Tonry, N. Kaiser, C. Waters, H. Flewelling, K. W. Hodapp, and W. S. Burgett, 2015: A Pan-STARRS1 study of the relationship between wide binarity and planet occurrence in the Kepler field. *ArXiv e-prints*.
- Di Matteo, T., V. Springel, and L. Hernquist, 2005: Energy input from quasars regulates the growth and activity of black holes and their host galaxies. *Nature*, **433**, 604–607.
- Dong, S., B. Katz, D. Kushnir, and J. L. Prieto, 2014: Type Ia Supernovae with Bi-Modal Explosions Are Common – Possible Smoking Gun for Direct Collisions of White-Dwarfs. *ArXiv e-prints*.
- Dong, S., B. Katz, and A. Socrates, 2013: Exploring a “Flow” of Highly Eccentric Binaries with Kepler. *ApJ*, **763**, L2.
- Dotti, M., A. Sesana, and R. Decarli, 2012: Massive Black Hole Binaries: Dynamical Evolution and Observational Signatures. *Advances in Astronomy*, **2012**, 3.
- Doyle, L. R., J. A. Carter, D. C. Fabrycky, R. W. Slawson, S. B. Howell, J. N. Winn, J. A. Orosz, A. Prsa, W. F. Welsh, S. N. Quinn, D. Latham, G. Torres, L. A. Buchhave, G. W. Marcy, J. J. Fortney, A. Shporer, E. B. Ford, J. J. Lissauer, D. Ragozzine, M. Rucker, N. Batalha, J. M. Jenkins, W. J. Borucki, D. Koch, C. K. Middour, J. R. Hall, S. McCauliff, M. N. Fanelli, E. V. Quintana, M. J. Holman, D. A. Caldwell, M. Still, R. P. Stefanik, W. R. Brown, G. A. Esquerdo, S. Tang, G. Furesz, J. C. Geary, P. Berlind, M. L. Calkins, D. R. Short, J. H. Steffen, D. Sasselov, E. W. Dunham, W. D. Cochran, A. Boss, M. R. Haas, D. Buzasi, and D. Fischer, 2011: Kepler-16: A Transiting Circumbinary Planet. *Science*, **333**, 1602–.
- Duncan, M. J. and H. F. Levison, 1997: A scattered comet disk and the origin of Jupiter family comets. *Science*, **276**, 1670–1672.
- Eggleton, P. P., L. G. Kiseleva, and P. Hut, 1998: The Equilibrium Tide Model for Tidal Friction. *ApJ*, **499**, 853–+.
- Eggleton, P. P. and L. Kiseleva-Eggleton, 2001: Orbital Evolution in Binary and Triple Stars, with an Application to SS Lacertae. *ApJ*, **562**, 1012–1030.
- Eggleton, P. P., L. Kiseleva-Eggleton, and X. Dearborn, 2007: The Incidence of Multiplicity Among Bright Stellar Systems. In W. I. Hartkopf, E. F. Guinan, & P. Harmanec, ed., *IAU Symposium*, vol. 240 of *IAU Symposium*, pp. 347–355.
- Fabrycky, D. and S. Tremaine, 2007: Shrinking Binary and Planetary Orbits by Kozai Cycles with Tidal Friction. *ApJ*, **669**, 1298–1315.
- Fabrycky, D. C., E. T. Johnson, and J. Goodman, 2007: Cassini States with Dissipation: Why Obliquity Tides Cannot Inflate Hot Jupiters. *ApJ*, **665**, 754–766.

- Fang, J. and J.-L. Margot, 2012: The Role of Kozai Cycles in Near-Earth Binary Asteroids. *AJ*, **143**, 59.
- Ford, E. B., K. J. Joshi, F. A. Rasio, and B. Zbarsky, 2000a: Theoretical Implications of the PSR B1620-26 Triple System and Its Planet. *ApJ*, **528**, 336–350.
- Ford, E. B., B. Kozinsky, and F. A. Rasio, 2000b: Secular Evolution of Hierarchical Triple Star Systems. *ApJ*, **535**, 385–401.
- Frewen, S. and B. M. S. Hansen, 2015: The Effect of Stellar Evolution on Migrating Warm Jupiters. *ApJ*.
- Galaviz, P. and B. Brügmann, 2011: Characterization of the gravitational wave emission of three black holes. *Phys. Rev. D*, **83(8)**, 084013.
- Geller, A. M. and R. D. Mathieu, 2012: WIYN Open Cluster Study. XLVIII. The Hard-binary Population of NGC 188. *AJ*, **144**, 54.
- Gillessen, S., R. Genzel, T. K. Fritz, E. Quataert, C. Alig, A. Burkert, J. Cuadra, F. Eisenhauer, O. Pfuhl, K. Dodds-Eden, C. F. Gammie, and T. Ott, 2012: A gas cloud on its way towards the supermassive black hole at the Galactic Centre. *Nature*, **481**, 51–54.
- Goldstein, H., 1950: *Classical mechanics*.
- Gomes, R. S., T. Gallardo, J. A. Fernández, and A. Brunini, 2005: On The Origin of The High-Perihelion Scattered Disk: The Role of The Kozai Mechanism And Mean Motion Resonances. *Celestial Mechanics and Dynamical Astronomy*, **91**, 109–129.
- Grindlay, J. E., C. D. Bailyn, H. Cohn, P. M. Lugger, J. R. Thorstensen, and G. Wegner, 1988: Discovery of a possible X-ray triple - 4U 1915-05. *Astrophysical Journal*, **334**, L25–L29.
- Gronchi, G. F. and A. Milani, 1999: The stable Kozai state for asteroids and comets. With arbitrary semimajor axis and inclination. *A&A*, **341**, 928–935.
- Gualandris, A. and D. Merritt, 2009: Perturbations of Intermediate-mass Black Holes on Stellar Orbits in the Galactic Center. *ApJ*, **705**, 361–371.
- , 2012: Long-term Evolution of Massive Black Hole Binaries. IV. Mergers of Galaxies with Collisionally Relaxed Nuclei. *ApJ*, **744**, 74.
- Guillochon, J., E. Ramirez-Ruiz, and D. Lin, 2011: Consequences of the Ejection and Disruption of Giant Planets. *ApJ*, **732**, 74.
- Hamers, A. S., H. B. Perets, F. Antonini, and S. F. Portegies Zwart, 2015a: Secular dynamics of hierarchical quadruple systems: the case of a triple system orbited by a fourth body. *MNRAS*, **449**, 4221–4245.
- Hamers, A. S., H. B. Perets, and S. F. Portegies Zwart, 2015b: A triple origin for the lack of tight coplanar circumbinary planets around short-period binaries. *ArXiv e-prints*.
- Hamers, A. S., O. R. Pols, J. S. W. Claeys, and G. Nelemans, 2013: Population synthesis of triple systems in the context of mergers of carbon-oxygen white dwarfs. *MNRAS*, **430**, 2262–2280.
- Hansen, B. M. S., 2010: Calibration of Equilibrium Tide Theory for Extrasolar Planet Systems. *ApJ*, **723**, 285–299.
- Hansen, B. M. S. and J. Zink, 2015: On the potentially dramatic history of the super-Earth ρ 55 Cancri e. *MNRAS*, **450**, 4505–4520.
- Harding, L. K., G. Hallinan, Q. M. Konopacky, K. M. Kratter, R. P. Boyle, R. F. Butler, and A. Golden, 2013: Spin-orbit alignment in the very low mass binary regime. The L dwarf tight binary 2MASSW J0746425+200032AB. *A&A*, **554**, A113.
- Harrington, R. S., 1968: Dynamical evolution of triple stars. *AJ*, **73**, 190–194.
- , 1969: The Stellar Three-Body Problem. *Celestial Mechanics*, **1**, 200–209.
- Heintz, W. D., 1967: Störungen und Bahnelemente im System ξ Ursae Maioris. *Astronomische Nachrichten*, **289**, 269.
- Hoffman, L. and A. Loeb, 2007: Dynamics of triple black hole systems in hierarchically merging massive galaxies. *MNRAS*, **377**, 957–976.
- Holman, M., J. Touma, and S. Tremaine, 1997: Chaotic variations in the eccentricity of the planet orbiting 16 Cygni B. *Nature*, **386**, 254–256.
- Hurley, J. R., O. R. Pols, and C. A. Tout, 2000: Comprehensive analytic formulae for stellar

- evolution as a function of mass and metallicity. *MNRAS*, **315**, 543–569.
- Hut, P., 1980: Stability of tidal equilibrium. *A&A*, **92**, 167–170.
- Hut, P. and J. N. Bahcall, 1983: Binary-single star scattering. I - Numerical experiments for equal masses. *ApJ*, **268**, 319–341.
- Innanen, K. A., J. Q. Zheng, S. Mikkola, and M. J. Valtonen, 1997: The Kozai Mechanism and the Stability of Planetary Orbits in Binary Star Systems. *AJ*, **113**, 1915–+.
- Ivanov, P. B., A. G. Polnarev, and P. Saha, 2005: The tidal disruption rate in dense galactic cusps containing a supermassive binary black hole. *MNRAS*, **358**, 1361–1378.
- Iwasawa, M., S. An, T. Matsubayashi, Y. Funato, and J. Makino, 2011: Eccentric Evolution of Supermassive Black Hole Binaries. *ApJ*, **731**, L9.
- Jefferys, W. H. and J. Moser, 1966: Quasi-periodic Solutions for the three-body problem. *AJ*, **71**, 568–+.
- Katz, B. and S. Dong, 2012: The rate of WD-WD head-on collisions may be as high as the SNe Ia rate. *ArXiv e-prints*.
- Katz, B., S. Dong, and R. Malhotra, 2011: Long-Term Cycling of Kozai-Lidov Cycles: Extreme Eccentricities and Inclinations Excited by a Distant Eccentric Perturber. *ArXiv e-prints*.
- Khan, F. M., I. Berentzen, P. Berczik, A. Just, L. Mayer, K. Nitadori, and S. Callegari, 2012: Formation and Hardening of Supermassive Black Hole Binaries in Minor Mergers of Disk Galaxies. *ApJ*, **756**, 30.
- Kinoshita, H. and H. Nakai, 1991: Secular perturbations of fictitious satellites of Uranus. *Celestial Mechanics and Dynamical Astronomy*, **52**, 293–303.
- , 1999: Analytical Solution of the Kozai Resonance and its Application. *Celestial Mechanics and Dynamical Astronomy*, **75**, 125–147.
- , 2007: General solution of the Kozai mechanism. *Celestial Mechanics and Dynamical Astronomy*, **98**, 67–74.
- Kiseleva, L. G., P. P. Eggleton, and S. Mikkola, 1998: Tidal friction in triple stars. *MNRAS*, **300**, 292–302.
- Knutson, H. A., B. J. Fulton, B. T. Montet, M. Kao, H. Ngo, A. W. Howard, J. R. Crepp, S. Hinkley, G. Á. Bakos, K. Batygin, J. A. Johnson, T. D. Morton, and P. S. Muirhead, 2014: Friends of Hot Jupiters. I. A Radial Velocity Search for Massive, Long-period Companions to Close-in Gas Giant Planets. *ApJ*, **785**, 126.
- Kocsis, B. and S. Tremaine, 2011: Resonant relaxation and the warp of the stellar disc in the Galactic Centre. *MNRAS*, **412**, 187–207.
- , 2015: A numerical study of vector resonant relaxation. *MNRAS*, **448**, 3265–3296.
- Kostov, V. B., P. R. McCullough, J. A. Carter, M. Deleuil, R. F. Díaz, D. C. Fabrycky, G. Hébrard, T. C. Hinse, T. Mazeh, J. A. Orosz, Z. I. Tsvetanov, and W. F. Welsh, 2014: Kepler-413b: A Slightly Misaligned, Neptune-size Transiting Circumbinary Planet. *ApJ*, **784**, 14.
- Kostov, V. B., P. R. McCullough, T. C. Hinse, Z. I. Tsvetanov, G. Hébrard, R. F. Díaz, M. Deleuil, and J. A. Valenti, 2013: A Gas Giant Circumbinary Planet Transiting the F Star Primary of the Eclipsing Binary Star KIC 4862625 and the Independent Discovery and Characterization of the Two Transiting Planets in the Kepler-47 System. *ApJ*, **770**, 52.
- Kozai, Y., 1962: Secular perturbations of asteroids with high inclination and eccentricity. *AJ*, **67**, 591–+.
- , 1979: Secular perturbations of asteroids and comets. In R. L. Duncombe, ed., *Dynamics of the Solar System*, vol. 81 of *IAU Symposium*, pp. 231–236.
- Kratter, K. M. and H. B. Perets, 2012: Star Hoppers: Planet Instability and Capture in Evolving Binary Systems. *ApJ*, **753**, 91.
- Kulkarni, G. and A. Loeb, 2012: Formation of galactic nuclei with multiple supermassive black holes at high redshifts. *MNRAS*, **422**, 1306–1323.
- Kushnir, D., B. Katz, S. Dong, E. Livne, and R. Fernández, 2013: Head-on Collisions of White Dwarfs in Triple Systems Could Explain Type Ia Supernovae. *ApJ*, **778**, L37.
- Lanza, A. F. and E. L. Shkolnik, 2014: Secular orbital evolution of planetary systems and the

- dearth of close-in planets around fast rotators. *MNRAS*, **443**, 1451–1462.
- Levesque, E. M., P. Massey, A. N. Żytkow, and N. Morrell, 2014: Discovery of a Thorne-Żytkow object candidate in the Small Magellanic Cloud. *MNRAS*, **443**, L94–L98.
- Lévrad, B., A. C. M. Correia, G. Chabrier, I. Baraffe, F. Selsis, and J. Laskar, 2007: Tidal dissipation within hot Jupiters: a new appraisal. *A&A*, **462**, L5–L8.
- Li, G., S. Naoz, M. Holman, and A. Loeb, 2014a: Chaos in the Test Particle Eccentric Kozai-Lidov Mechanism. *ArXiv e-prints*.
- Li, G., S. Naoz, B. Kocsis, and A. Loeb, 2014b: Eccentricity Growth and Orbit Flip in Near-coplanar Hierarchical Three-body Systems. *ApJ*, **785**, 116.
- , 2015: Implications of the eccentric Kozai-Lidov mechanism for stars surrounding supermassive black hole binaries. *MNRAS*, **451**, 1341–1349.
- Li, G., S. Naoz, F. Valsecchi, J. A. Johnson, and F. A. Rasio, 2014c: The Dynamics of the Multi-planet System Orbiting Kepler-56. *ArXiv e-prints*.
- Lidov, M. L., 1962: The evolution of orbits of artificial satellites of planets under the action of gravitational perturbations of external bodies. *planss*, **9**, 719–759.
- Lidov, M. L. and S. L. Ziglin, 1974: The Analysis of Restricted Circular Twice-averaged Three Body Problem in the Case of Close Orbits. *Celestial Mechanics*, **9**, 151–173.
- , 1976: Non-restricted double-averaged three body problem in Hill’s case. *Celestial Mechanics*, **13**, 471–489.
- Lin, D. N. C. and J. Papaloizou, 1986: On the tidal interaction between protoplanets and the protoplanetary disk. III - Orbital migration of protoplanets. *ApJ*, **309**, 846–857.
- Lithwick, Y. and S. Naoz, 2011: The Eccentric Kozai Mechanism for a Test Particle. *ApJ*, **742**, 94.
- Lithwick, Y. and Y. Wu, 2012: Resonant Repulsion of Kepler Planet Pairs. *ApJ*, **756**, L11.
- Liu, B., D. J. Muñoz, and D. Lai, 2015: Suppression of extreme orbital evolution in triple systems with short-range forces. *MNRAS*, **447**, 747–764.
- Liu, S.-F., J. Guillochon, D. N. C. Lin, and E. Ramirez-Ruiz, 2013: On the Survivability and Metamorphism of Tidally Disrupted Giant Planets: The Role of Dense Cores. *ApJ*, **762**, 37.
- Luo, L., B. Katz, and S. Dong, 2016: Double-Averaging Can Fail to Characterize the Long-Term Evolution of Lidov-Kozai Cycles Derivation of an Analytical Correction. *ArXiv e-prints*.
- Madigan, A.-M. and Y. Levin, 2012: Secular Dynamical Anti-friction in Galactic Nuclei. *ApJ*, **754**, 42.
- Mandel, I., D. A. Brown, J. R. Gair, and M. C. Miller, 2008: Rates and Characteristics of Intermediate Mass Ratio Inspirals Detectable by Advanced LIGO. *ApJ*, **681**, 1431–1447.
- Maoz, D., F. Mannucci, and G. Nelemans, 2014: Observational Clues to the Progenitors of Type Ia Supernovae. *ARA&A*, **52**, 107–170.
- Marchal, C., 1990: *The three-body problem*.
- Mardling, R. A. and S. J. Aarseth, 2001: Tidal interactions in star cluster simulations. *MNRAS*, **321**, 398–420.
- Margot, J.-L., P. Pravec, P. Taylor, B. Carry, and S. Jacobson, 2015: Asteroid Systems: Binaries, Triples, and Pairs. *ArXiv e-prints*.
- Martin, D. V., T. Mazeh, and D. C. Fabrycky, 2015: No circumbinary planets transiting the tightest Kepler binaries - a possible fingerprint of a third star. *MNRAS*, **453**, 3554–3567.
- Martin, D. V. and A. H. M. J. Triaud, 2015a: Circumbinary planets - why they are so likely to transit. *MNRAS*, **449**, 781–793.
- , 2015b: Kozai-Lidov cycles towards the limit of circumbinary planets. *MNRAS*.
- Masset, F. S. and J. C. B. Papaloizou, 2003: Runaway Migration and the Formation of Hot Jupiters. *ApJ*, **588**, 494–508.
- Mazeh, T., Y. Krymolowski, and G. Rosenfeld, 1997: The High Eccentricity of the Planet Orbiting 16 Cygni B. *ApJ*, **477**, L103–L106.
- Mazeh, T. and J. Shaham, 1979: The orbital evolution of close triple systems - The binary eccentricity. *AA*, **77**, 145–151.

- McKenna, J. and A. G. Lyne, 1988: Timing measurements of the binary millisecond pulsar in the globular cluster M4. *Nature*, **336**, 226–+.
- Meiron, Y. and A. Laor, 2013: The kinematic signature of the inspiral phase of massive binary black holes. *MNRAS*, **433**, 2502–2510.
- Merritt, D., T. Alexander, S. Mikkola, and C. M. Will, 2010: Testing properties of the Galactic center black hole using stellar orbits. *Phys. Rev. D*, **81(6)**, 062002.
- Merritt, D. and E. Vasiliev, 2012: Spin evolution of supermassive black holes and galactic nuclei. *Phys. Rev. D*, **86(10)**, 102002.
- Michaely, E. and H. B. Perets, 2014: Secular Dynamics in Hierarchical Three-body Systems with Mass Loss and Mass Transfer. *ApJ*, **794**, 122.
- Miller, M. C. and D. P. Hamilton, 2002: Four-Body Effects in Globular Cluster Black Hole Coalescence. *ApJ*, **576**, 894–898.
- Milosavljević, M. and D. Merritt, 2001: Formation of Galactic Nuclei. *ApJ*, **563**, 34–62.
- Misner, C. W., K. S. Thorne, and J. A. Wheeler, 1973: *Gravitation*.
- Moeckel, N. and D. Veras, 2012: Exoplanets bouncing between binary stars. *MNRAS*, **422**, 831–840.
- Morbidelli, A., 2002: *Modern celestial mechanics : aspects of solar system dynamics*.
- Morton, T. D. and J. A. Johnson, 2011: Discerning Exoplanet Migration Models Using Spin-Orbit Measurements. *ApJ*, **729**, 138.
- Muñoz, D. J. and D. Lai, 2015: Survival of planets around shrinking stellar binaries. *Proceedings of the National Academy of Science*, **112**, 9264–9269.
- Murray, C. D. and S. F. Dermott, 2000: *Solar System Dynamics*.
- Murray, N. and M. Holman, 1997: Diffusive chaos in the outer asteroid belt. *AJ*, **114**, 1246–1259.
- Nagasawa, M. and S. Ida, 2011: Orbital Distributions of Close-in Planets and Distant Planets Formed by Scattering and Dynamical Tides. *ApJ*, **742**, 72.
- Nagasawa, M., S. Ida, and T. Bessho, 2008: Formation of Hot Planets by a Combination of Planet Scattering, Tidal Circularization, and the Kozai Mechanism. *ApJ*, **678**, 498–508.
- Naoz, S. and D. C. Fabrycky, 2014: Mergers and Obliquities in Stellar Triples. *ApJ*, **793**, 137.
- Naoz, S., W. M. Farr, Y. Lithwick, F. A. Rasio, and J. Teyssandier, 2011: Hot Jupiters from secular planet-planet interactions. *Nature*, **473**, 187–189.
- , 2013a: Secular dynamics in hierarchical three-body systems. *MNRAS*, **431**, 2155–2171.
- Naoz, S., W. M. Farr, and F. A. Rasio, 2012: On the Formation of Hot Jupiters in Stellar Binaries. *ApJ*, **754**, L36.
- Naoz, S., T. Fragos, A. Geller, S. P. Stephan, and F. A. Rasio, 2015: .
- Naoz, S., B. Kocsis, A. Loeb, and N. Yunes, 2013b: Resonant Post-Newtonian Eccentricity Excitation in Hierarchical Three-body Systems. *ApJ*, **773**, 187.
- Naoz, S., H. B. Perets, and D. Ragozzine, 2010: The Observed Orbital Properties of Binary Minor Planets. *ApJ*, **719**, 1775–1783.
- Naoz, S. and J. Silk, 2014: Formation of Dark Matter Tori around Supermassive Black Holes via the Eccentric Kozai-Lidov Mechanism. *ApJ*, **795**, 102.
- Nesvorný, D., J. L. A. Alvarelos, L. Dones, and H. F. Levison, 2003: Orbital and Collisional Evolution of the Irregular Satellites. *AJ*, **126**, 398–429.
- Nesvorný, D., D. Vokrouhlický, W. F. Bottke, K. Noll, and H. F. Levison, 2011: Observed Binary Fraction Sets Limits on the Extent of Collisional Grinding in the Kuiper Belt. *AJ*, **141**, 159.
- Ngo, H., H. A. Knutson, S. Hinkley, J. R. Crepp, E. B. Bechter, K. Batygin, A. W. Howard, J. A. Johnson, T. D. Morton, and P. S. Muirhead, 2015: Friends of Hot Jupiters. II. No Correspondence between Hot-jupiter Spin-Orbit Misalignment and the Incidence of Directly Imaged Stellar Companions. *ApJ*, **800**, 138.
- O’Leary, R. M., F. A. Rasio, J. M. Fregeau, N. Ivanova, and R. O’Shaughnessy, 2006: Binary Mergers and Growth of Black Holes in Dense Star Clusters. *ApJ*, **637**, 937–951.
- Orosz, J. A., W. F. Welsh, J. A. Carter, E. Brugamyer, L. A. Buchhave, W. D. Cochran, M. Endl, E. B. Ford, P. MacQueen, D. R. Short, G. Torres, G. Windmiller, E. Agol, T. Barclay, D. A.

- Caldwell, B. D. Clarke, L. R. Doyle, D. C. Fabrycky, J. C. Geary, N. Haghighipour, M. J. Holman, K. A. Ibrahim, J. M. Jenkins, K. Kinemuchi, J. Li, J. J. Lissauer, A. Prša, D. Ragozzine, A. Shporer, M. Still, and R. A. Wade, 2012a: The Neptune-sized Circumbinary Planet Kepler-38b. *ApJ*, **758**, 87.
- Orosz, J. A., W. F. Welsh, J. A. Carter, D. C. Fabrycky, W. D. Cochran, M. Endl, E. B. Ford, N. Haghighipour, P. J. MacQueen, T. Mazeh, R. Sanchis-Ojeda, D. R. Short, G. Torres, E. Agol, L. A. Buchhave, L. R. Doyle, H. Isaacson, J. J. Lissauer, G. W. Marcy, A. Shporer, G. Windmiller, T. Barclay, A. P. Boss, B. D. Clarke, J. Fortney, J. C. Geary, M. J. Holman, D. Huber, J. M. Jenkins, K. Kinemuchi, E. Kruse, D. Ragozzine, D. Sasselov, M. Still, P. Tenenbaum, K. Uddin, J. N. Winn, D. G. Koch, and W. J. Borucki, 2012b: Kepler-47: A Transiting Circumbinary Multiplanet System. *Science*, **337**, 1511–.
- Pejcha, O., J. M. Antognini, B. J. Shappee, and T. A. Thompson, 2013: Greatly enhanced eccentricity oscillations in quadruple systems composed of two binaries: implications for stars, planets and transients. *MNRAS*, **435**, 943–951.
- Perets, H. B. and D. C. Fabrycky, 2009: On the Triple Origin of Blue Stragglers. *ApJ*, **697**, 1048–1056.
- Perets, H. B. and K. M. Kratter, 2012: The triple evolution dynamical instability: Stellar collisions in the field and the formation of exotic binaries. *ArXiv e-prints*.
- Perets, H. B. and S. Naoz, 2009: Kozai Cycles, Tidal Friction, and the Dynamical Evolution of Binary Minor Planets. *ApJ*, **699**, L17–L21.
- Petrovich, C., 2015a: Hot Jupiters from Coplanar High-eccentricity Migration. *ApJ*, **805**, 75.
- , 2015b: Steady-state Planet Migration by the Kozai-Lidov Mechanism in Stellar Binaries. *ApJ*, **799**, 27.
- , 2015c: The Stability and Fates of Hierarchical Two-planet Systems. *ApJ*, **808**, 120.
- Podsiadlowski, P., S. Rappaport, and Z. Han, 2003: On the formation and evolution of black hole binaries. *MNRAS*, **341**, 385–404.
- Polishook, D. and N. Brosch, 2006: Many binaries among NEAs. *ArXiv Astrophysics e-prints*.
- , 2009: Photometry and spin rate distribution of small-sized main belt asteroids. *Icarus*, **199**, 319–332.
- Pravec, P., P. Scheirich, P. Kušnirák, L. Šarounová, S. Mottola, G. Hahn, P. Brown, G. Esquerdo, N. Kaiser, Z. Krzeminski, D. P. Pray, B. D. Warner, A. W. Harris, M. C. Nolan, E. S. Howell, L. A. M. Benner, J.-L. Margot, A. Galád, W. Holliday, M. D. Hicks, Y. N. Krugly, D. Tholen, R. Whiteley, F. Marchis, D. R. DeGraff, A. Grauer, S. Larson, F. P. Velichko, W. R. Cooney, R. Stephens, J. Zhu, K. Kirsch, R. Dyvig, L. Snyder, V. Reddy, S. Moore, Š. Gajdoš, J. Világi, G. Masi, D. Higgins, G. Funkhouser, B. Knight, S. Slivan, R. Behrend, M. Grenon, G. Burki, R. Roy, C. Demeautis, D. Matter, N. Waelchli, Y. Revaz, A. Klotz, M. Rieugn e, P. Thierry, V. Cotrez, L. Brunetto, and G. Kober, 2006: Photometric survey of binary near-Earth asteroids. *Icarus*, **181**, 63–93.
- Pribulla, T. and S. M. Rucinski, 2006: Contact Binaries with Additional Components. I. The Extant Data. *AJ*, **131**, 2986–3007.
- Prodan, S., F. Antonini, and H. B. Perets, 2015: Secular Evolution of Binaries near Massive Black Holes: Formation of Compact Binaries, Merger/Collision Products and G2-like Objects. *ApJ*, **799**, 118.
- Prodan, S. and N. Murray, 2012: ON THE DYNAMICS AND TIDAL DISSIPATION RATE OF THE WHITE DWARF IN 4U 1820-30. *The Astrophysical Journal*, **747(1)**, 4.
- Prodan, S., N. Murray, and T. A. Thompson, 2013: On WD-WD Mergers in Triple Systems: The Role of Kozai Resonance with Tidal Friction. *ArXiv e-prints*.
- Quinn, T., S. Tremaine, and M. Duncan, 1990: Planetary perturbations and the origins of short-period comets. *ApJ*, **355**, 667–679.
- Raghavan, D., T. J. Henry, B. D. Mason, J. P. Subasavage, W.-C. Jao, T. D. Beaulieu, and N. C. Hambly, 2006: Two Suns in The Sky: Stellar Multiplicity in Exoplanet Systems. *ApJ*, **646**, 523–542.

- Raghavan, D., H. A. McAlister, T. J. Henry, D. W. Latham, G. W. Marcy, B. D. Mason, D. R. Gies, R. J. White, and T. A. ten Brummelaar, 2010: A Survey of Stellar Families: Multiplicity of Solar-type Stars. *ApJS*, **190**, 1–42.
- Rasio, F. A., 2001: A Hierarchical Triple Star System in M4. *Evolution of Binary and Multiple Star Systems; A Meeting in Celebration of Peter Eggleton's 60th Birthday. ASP Conference Series*, **229**, 117.
- Rasio, F. A. and E. B. Ford, 1996a: Dynamical instabilities and the formation of extrasolar planetary systems. *Science*, **274**, 954–956.
- , 1996b: Dynamical instabilities and the formation of extrasolar planetary systems. *Science*, **274**, 954–956.
- Rice, K., 2015: Can Kozai-Lidov cycles explain Kepler-78b? *MNRAS*, **448**, 1729–1737.
- Schwamb, M. E., J. A. Orosz, J. A. Carter, W. F. Welsh, D. A. Fischer, G. Torres, A. W. Howard, J. R. Crepp, W. C. Keel, C. J. Lintott, N. A. Kaib, D. Terrell, R. Gagliano, K. J. Jek, M. Parrish, A. M. Smith, S. Lynn, R. J. Simpson, M. J. Giguere, and K. Schawinski, 2013: Planet Hunters: A Transiting Circumbinary Planet in a Quadruple Star System. *ApJ*, **768**, 127.
- Sesana, A., A. Gualandris, and M. Dotti, 2011: Massive black hole binary eccentricity in rotating stellar systems. *MNRAS*, **415**, L35–L39.
- Seto, N., 2013: Highly Eccentric Kozai Mechanism and Gravitational-Wave Observation for Neutron-Star Binaries. *Physical Review Letters*, **111**(6), 061106.
- Shappee, B. J., K. Z. Stanek, R. W. Pogge, and P. M. Garnavich, 2013: No Stripped Hydrogen in the Nebular Spectra of Nearby Type Ia Supernova 2011fe. *ApJ*, **762**, L5.
- Shappee, B. J. and T. A. Thompson, 2013: The Mass-loss-induced Eccentric Kozai Mechanism: A New Channel for the Production of Close Compact Object-Stellar Binaries. *ApJ*, **766**, 64.
- Sigurðsson, S., H. B. Richer, B. M. Hansen, I. H. Stairs, and S. E. Thorsett, 2003: A Young White Dwarf Companion to Pulsar B1620-26: Evidence for Early Planet Formation. *Science*, **301**(5), 193–196.
- Söderhjelm, S., 1975: The three-body problem and eclipsing binaries - Application to algol and lambda Tauri. *A&A*, **42**, 229–236.
- Soderhjelm, S., 1982: Studies of the stellar three-body problem. *A&A*, **107**, 54–60.
- Söderhjelm, S., 1984: Third-order and tidal effects in the stellar three-body problem. *A&A*, **141**, 232–240.
- Stephan, A. P., N. S., A. M. Ghez, M. R. Morris, , W. G., B. N. Sitarski, and T. Do, 2016: The Decisive Role of Binaries in the Galactic Center: The eccentric Kozai-Lidov mechanism with stellar evolution. *ApJ*.
- Storch, N. I., K. R. Anderson, and D. Lai, 2014: Chaotic dynamics of stellar spin in binaries and the production of misaligned hot Jupiters. *Science*, **345**, 1317–1321.
- Storch, N. I. and D. Lai, 2015: Chaotic dynamics of stellar spin driven by planets undergoing Lidov-Kozai oscillations: resonances and origin of chaos. *MNRAS*, **448**, 1821–1834.
- Takeda, G., R. Kita, and F. A. Rasio, 2008: Planetary Systems in Binaries. I. Dynamical Classification. *ApJ*, **683**, 1063–1075.
- Tamayo, D., J. A. Burns, and D. P. Hamilton, 2013: Chaotic dust dynamics and implications for the hemispherical color asymmetries of the Uranian satellites. *Icarus*, **226**, 655–662.
- Teyssandier, J., S. Naoz, I. Lizarraga, and F. A. Rasio, 2013: Extreme Orbital Evolution from Hierarchical Secular Coupling of Two Giant Planets. *ApJ*, **779**, 166.
- Thomas, F. and A. Morbidelli, 1996: The Kozai Resonance in the Outer Solar System and the Dynamics of Long-Period Comets. *Celestial Mechanics and Dynamical Astronomy*, **64**, 209–229.
- Thompson, T. A., 2011: Accelerating Compact Object Mergers in Triple Systems with the Kozai Resonance: A Mechanism for "Prompt" Type Ia Supernovae, Gamma-Ray Bursts, and Other Exotica. *ApJ*, **741**, 82.
- Thorne, K. S. and A. N. Zytkov, 1975: Red giants and supergiants with degenerate neutron cores. *ApJ*, **199**, L19–L24.

- Thorsett, S. E., Z. Arzoumanian, F. Camilo, and A. G. Lyne, 1999: The Triple Pulsar System PSR B1620-26 in M4. *The Astrophysical Journal*, **523(2)**, 763–770.
- Tokovinin, A., 2008: Comparative statistics and origin of triple and quadruple stars. *MNRAS*, **389**, 925–938.
- , 2014a: From binaries to multiples I: Data on F and G dwarfs within 67 pc of the Sun. *AJ*, **147**, 86.
- , 2014b: From binaries to multiples II: hierarchical multiplicity of F and G dwarfs. *AJ*, **147**, 87.
- Tokovinin, A. A., 1997: On the multiplicity of spectroscopic binary stars. *Astronomy Letters*, **23**, 727–730.
- Tokovinin, A. A. and M. G. Smekhov, 2002: Statistics of spectroscopic sub-systems in visual multiple stars. *A&A*, **382**, 118–123.
- Touma, J. R., S. Tremaine, and M. V. Kazandjian, 2009: Gauss’s method for secular dynamics, softened. *MNRAS*, **394**, 1085–1108.
- Triaud, A. H. M. J., A. Collier Cameron, D. Queloz, D. R. Anderson, M. Gillon, L. Hebb, C. Hellier, B. Loeillet, P. F. L. Maxted, M. Mayor, F. Pepe, D. Pollacco, D. Ségransan, B. Smalley, S. Udry, R. G. West, and P. J. Wheatley, 2010: Spin-orbit angle measurements for six southern transiting planets. New insights into the dynamical origins of hot Jupiters. *A&A*, **524**, A25+.
- Triaud, A. H. M. J., L. Hebb, D. R. Anderson, P. Cargile, A. Collier Cameron, A. P. Doyle, F. Faedi, M. Gillon, Y. Gomez Maqueo Chew, C. Hellier, E. Jehin, P. Maxted, D. Naef, F. Pepe, D. Pollacco, D. Queloz, D. Ségransan, B. Smalley, K. Stassun, S. Udry, and R. G. West, 2013: The EBLM project. I. Physical and orbital parameters, including spin-orbit angles, of two low-mass eclipsing binaries on opposite sides of the brown dwarf limit. *A&A*, **549**, A18.
- Valtonen, M. and H. Karttunen, 2006: *The Three-Body Problem*.
- Valtonen, M. J., 1996: Triple black hole systems formed in mergers of galaxies. *MNRAS*, **278**, 186–190.
- Vashkov’yak, M. A., 1999: Evolution of the orbits of distant satellites of Uranus. *Astronomy Letters*, **25**, 476–481.
- Veras, D., N. W. Evans, M. C. Wyatt, and C. A. Tout, 2014: The great escape - III. Placing post-main-sequence evolution of planetary and binary systems in a Galactic context. *MNRAS*, **437**, 1127–1140.
- Veras, D. and E. B. Ford, 2010: Secular Orbital Dynamics of Hierarchical Two-planet Systems. *ApJ*, **715**, 803–822.
- Veras, D., A. J. Mustill, A. Bonsor, and M. C. Wyatt, 2013: Simulations of two-planet systems through all phases of stellar evolution: implications for the instability boundary and white dwarf pollution. *MNRAS*, **431**, 1686–1708.
- Veras, D. and C. A. Tout, 2012: The great escape - II. Exoplanet ejection from dying multiple-star systems. *MNRAS*, **422**, 1648–1664.
- Wang, J., D. A. Fischer, E. P. Horch, and J.-W. Xie, 2015: Influence of Stellar Multiplicity On Planet Formation. III. Adaptive Optics Imaging of Kepler Stars With Gas Giant Planets. *ApJ*, **806**, 248.
- Wang, L., P. Berczik, R. Spurzem, and M. B. N. Kouwenhoven, 2014: The Link between Ejected Stars, Hardening and Eccentricity Growth of Super Massive Black Holes in Galactic Nuclei. *ApJ*, **780**, 164.
- Welsh, W. F., J. A. Orosz, J. A. Carter, D. C. Fabrycky, E. B. Ford, J. J. Lissauer, A. Prša, S. N. Quinn, D. Ragozzine, D. R. Short, G. Torres, J. N. Winn, L. R. Doyle, T. Barclay, N. Batalha, S. Bloemen, E. Brugamyer, L. A. Buchhave, C. Caldwell, D. A. Caldwell, J. L. Christiansen, D. R. Ciardi, W. D. Cochran, M. Endl, J. J. Fortney, T. N. Gautier, III, R. L. Gilliland, M. R. Haas, J. R. Hall, M. J. Holman, A. W. Howard, S. B. Howell, H. Isaacson, J. M. Jenkins, T. C. Klaus, D. W. Latham, J. Li, G. W. Marcy, T. Mazeh, E. V. Quintana, P. Robertson, A. Shporer, J. H. Steffen, G. Windmiller, D. G. Koch, and W. J. Borucki, 2012: Transiting circumbinary planets Kepler-34 b and Kepler-35 b. *Nature*, **481**, 475–479.
- Welsh, W. F., J. A. Orosz, D. R. Short, W. D. Cochran, M. Endl, E. Brugamyer, N. Haghighipour,

- L. A. Buchhave, L. R. Doyle, D. C. Fabrycky, T. C. Hinse, S. R. Kane, V. Kostov, T. Mazeh, S. M. Mills, T. W. A. Müller, B. Quarles, S. N. Quinn, D. Ragozzine, A. Shporer, J. H. Steffen, L. Tal-Or, G. Torres, G. Windmiller, and W. J. Borucki, 2015: Kepler 453 b - The 10th Kepler Transiting Circumbinary Planet. *ApJ*, **809**, 26.
- Wen, L., 2003: On the Eccentricity Distribution of Coalescing Black Hole Binaries Driven by the Kozai Mechanism in Globular Clusters. *ApJ*, **598**, 419–430.
- Will, C. M., 2014a: Incorporating post-Newtonian effects in N-body dynamics. *Phys. Rev. D*, **89(4)**, 044043.
- , 2014b: Post-Newtonian effects in N-body dynamics: conserved quantities in hierarchical triple systems. *Classical and Quantum Gravity*, **31(24)**, 244001.
- Winn, J. N., D. Fabrycky, S. Albrecht, and J. A. Johnson, 2010: Hot Stars with Hot Jupiters Have High Obliquities. *ApJ*, **718**, L145–L149.
- Wisdom, J. and M. Holman, 1991: Symplectic maps for the n-body problem. *AJ*, **102**, 1528–1538.
- Witzel, G., A. M. Ghez, M. R. Morris, B. N. Sitarski, A. Boehle, S. Naoz, R. Campbell, E. E. Becklin, G. Canalizo, S. Chappell, T. Do, J. R. Lu, K. Matthews, L. Meyer, A. Stockton, P. Wizinowich, and S. Yelda, 2014: Detection of Galactic Center Source G2 at 3.8 μm during Periapse Passage. *ApJ*, **796**, L8.
- Wu, Y. and N. Murray, 2003: Planet Migration and Binary Companions: The Case of HD 80606b. *ApJ*, **589**, 605–614.
- Wu, Y., N. W. Murray, and J. M. Ramsahai, 2007: Hot Jupiters in Binary Star Systems. *ApJ*, **670**, 820–825.
- Yokoyama, T., M. T. Santos, G. Cardin, and O. C. Winter, 2003: On the orbits of the outer satellites of Jupiter. *A&A*, **401**, 763–772.
- Yu, Q., 2002: Evolution of massive binary black holes. *MNRAS*, **331**, 935–958.
- Yunes, N., M. C. Miller, and J. Thornburg, 2011: Effect of massive perturbers on extreme mass-ratio inspiral waveforms. *Phys. Rev. D*, **83(4)**, 044030.
- Zdziarski, A. A., L. Wen, and M. Gierliński, 2007: The superorbital variability and triple nature of the X-ray source 4U 1820-303. *MNRAS*, **377(3)**, 1006–1016.
- Zhou, G. and C. X. Huang, 2013: A highly inclined orbit for the 110-day period M-dwarf companion KOI-368.01. *ArXiv e-prints*.